

Putting pressure on the spine : an osmviscoelastic FE model of the intervertebral disc

Citation for published version (APA):

Schroder, Y. (2008). *Putting pressure on the spine : an osmviscoelastic FE model of the intervertebral disc*. [Phd Thesis 1 (Research TU/e / Graduation TU/e), Biomedical Engineering]. Technische Universiteit Eindhoven. <https://doi.org/10.6100/IR631918>

DOI:

[10.6100/IR631918](https://doi.org/10.6100/IR631918)

Document status and date:

Published: 01/01/2008

Document Version:

Publisher's PDF, also known as Version of Record (includes final page, issue and volume numbers)

Please check the document version of this publication:

- A submitted manuscript is the version of the article upon submission and before peer-review. There can be important differences between the submitted version and the official published version of record. People interested in the research are advised to contact the author for the final version of the publication, or visit the DOI to the publisher's website.
- The final author version and the galley proof are versions of the publication after peer review.
- The final published version features the final layout of the paper including the volume, issue and page numbers.

[Link to publication](#)

General rights

Copyright and moral rights for the publications made accessible in the public portal are retained by the authors and/or other copyright owners and it is a condition of accessing publications that users recognise and abide by the legal requirements associated with these rights.

- Users may download and print one copy of any publication from the public portal for the purpose of private study or research.
- You may not further distribute the material or use it for any profit-making activity or commercial gain
- You may freely distribute the URL identifying the publication in the public portal.

If the publication is distributed under the terms of Article 25fa of the Dutch Copyright Act, indicated by the "Taverne" license above, please follow below link for the End User Agreement:

www.tue.nl/taverne

Take down policy

If you believe that this document breaches copyright please contact us at:

openaccess@tue.nl

providing details and we will investigate your claim.

Putting pressure on the spine

An osmotic viscoelastic FE model of the intervertebral disc

A catalogue record is available from the Eindhoven University of Technology Library

ISBN: 978-90-386-1187-7

Copyright © 2007 by Y. Schröder

All rights reserved. No part of this book may be reproduced, stored in a database or retrieval system, or published, in any form or in any way, electronically, mechanically, by print, photo print, microfilm or any other means without prior written permission of the author.

Cover Design: Karin Obertreis, oberka@web.de

Printed by PrintPartners Ipskamp, The Netherlands.

The financial support from the following institutions is gratefully acknowledged:

❖ Zimmer Spine



❖ Abaqus, Simulia Benelux



❖ Medtronic

❖ Stryker

Um das Herz und den Verstand eines Menschen zu verstehen,
schaue nicht darauf, was er erreicht hat,
sondern wonach er sich sehnt.

Khalil Gibran



Es gibt immer nur einen richtigen Weg: Deinen eigenen!
Danke Mutti,
dass ich dabei immer
deine Liebe und Unterstützung hatte.

Putting pressure on the spine

An osmovoiscoelastic FE model of the intervertebral disc

PROEFSCHRIFT

ter verkrijging van de graad van doctor
aan de Technische Universiteit Eindhoven,
op gezag van de Rector Magnificus, prof.dr.ir. C.J. van Duijn,
voor een commissie aangewezen door het College
voor Promoties in het openbaar te verdedigen
op donderdag 10 januari 2008 om 16.00 uur

door

Yvonne Schröder

geboren te Rostock, Duitsland

Dit proefschrift is goedgekeurd door de promotor:

prof.dr.ir. F.P.T. Baaijens

en

prof.dr.ir. K. Ito

Copromotor:

dr.ir. J.M. Huyghe

Contents

Contents	vii
Summary	ix
Samenvatting.....	xi
1 General Introduction	1
1.1 Clinical relevance and background	2
1.2 Objectives of the EURODISC project	4
1.3 Objectives of this thesis	5
1.4 Outline	7
2 Introduction to the spine - with special emphasis on the disc.....	9
2.1 Anatomical perspective	10
2.2 Biomechanical perspective	11
2.3 Composition and structure of the intervertebral disc	11
2.3.1 Main biochemical components	12
2.3.2 Disc structure and properties	14
2.4 Load bearing and distribution within the disc	16
2.4.1 Compressive and tensile properties	16
2.4.2 Osmotic forces	17
2.4.3 Stress distribution and profiles	17
2.5 Intervertebral disc ageing and degeneration	18
2.5.1 Changes with age and degeneration	19
2.5.2 Effects of degenerative changes on disc function and pathology	19
2.5.3 Degenerative disc diseases	20
3 Initial development of a 3D FE model of the disc	21
3.1 Overview of finite element approaches for the disc	22
3.2 Aim of study	23
3.3 Material and Methods.....	24
3.3.1 Finite Element model	24
3.3.2 Boundary conditions	27
3.3.3 Material properties	29
3.4 Results	30
3.5 Discussion.....	33
4 Intra and extrafibrillar fluid exchange in the disc.....	37
4.1 Introduction.....	38
4.2 Material and Methods.....	40
4.2.1 Rule of Mixtures.....	40
4.2.2 Osmotic swelling	41
4.2.3 Finite element model	43
4.3 Results	45
4.4 Discussion.....	47

5	Material properties and osmoviscoelastic constitutive law	49
5.1	Introduction	50
5.2	Material and Method.....	51
5.2.1	Experiment.....	51
5.2.2	Finite element Model.....	52
5.2.3	Determination of the material properties	54
5.2.4	Curve fitting procedure	55
5.3	Results.....	57
5.4	Discussion	59
6	Evaluation of the 3D FE osmoviscoelastic disc model with experimental data from literature.....	61
6.1	Introduction	62
6.2	Material and Methods	63
6.2.1	Finite element model.....	63
6.2.2	Material properties.....	65
6.2.3	Boundary conditions	66
6.2.4	Model adaptations	67
6.3	Results.....	68
6.4	Discussion	72
7	General discussion & conclusion	75
7.1	Introduction	76
7.2	Development of a 3D osmoviscoelastic FE model of the disc.....	76
7.2.1	Constitutive law and material parameter determination.....	77
7.2.2	Evaluation of the full 3D osmoviscoelastic FE model.....	78
7.3	Relevance of this FE model and future adaptations.....	79
7.3.1	Applications through collaborations with other ‘disc groups’	80
7.3.2	Future adaptations to improve the model application	82
7.4	Conclusion.....	82
	Reference	83
	Appendix	91
	Acknowledgment.....	93
	Curriculum Vitae.....	97

Summary

Putting pressure on the spine An osmoviscoelastic FE model of the intervertebral disc

Back pain is a frequently occurring complaint in adults, having a relatively large impact on the European economy due to the fact that it often partially incapacitates the patient. Intervertebral discs are believed to be a key element of back pain. Apart from providing flexibility to the spine, intervertebral discs have a mechanical role in absorbing and transmitting loads through the spine. As measurements in living humans are complex, finite element (FE) models have become an important tool to study load distribution in healthy and degenerated discs. The disc is subjected to a combination of elastic, viscous and osmotic forces, but the latter has mostly been neglected in previous 3D FE models. To illustrate, in the fiber-reinforced disc tissue, there is interdependency between swelling of its proteoglycan (PG) rich ground substance and the tensile stresses in its collagen structure, which has not been accounted for previously. Furthermore, the total amount of water in the tissue is divided into intrafibrillar water (IFW) and extrafibrillar water (EFW). IFW is present in the intrafibrillar space within the collagen fibers and is therefore not accessible to the PG's that reside in the extrafibrillar compartment. Experimental results have shown that both gene expression of cells in the intervertebral disc and propagation of cracks are affected by changes in osmotic pressure which must be determined on the basis of the extrafibrillar water (EFW) only. Hence, quantification of intra- and extrafibrillar fluid exchange and its effect on osmolarity of disc tissue is important for determining the physical conditions of disc tissue and its role in disc degeneration and failure.

In an initial osmoviscoelastic FE model (chapter 3), the interdependency of swelling and collagen pre-stressing was modeled. It predicted intradiscal pressures within unloaded discs to the order of 0.1-0.2MPa, which is in agreement with *in vivo* experimental measurements published by Wilke et al. In the initial model, a correction factor was used to account for the influence of IFW based on the seminal work of Urban and McMullin for tissue containing a low collagen content such as the nucleus pulposus. However, this was recently not shown to be the case for the annulus which has much higher collagen content. A study by Sivan et al. demonstrated that IFW was sensitive to the applied load which can alter significantly the fixed charged density. Consequently, the initial FE model of the disc in this thesis was extended to include the intra and extrafibrillar water differentiation (chapter 4) and exhibited that the intradiscal pressure profile was clearly influenced by the IFW content. Unfortunately, lack of experimental data to determine some of the model parameters limited the applicability of the model.

In addition to osmotic effects, mechanical properties of the intervertebral disc are complex. The composite behavior of disc tissue is regulated by its biochemical composition and fiber-reinforced structure. The anisotropic, nonlinear behavior of a multi-component material like the intervertebral disc can only be assessed through a variety of experiments. Hence, data from several different experiments was simultaneously fitted to

a simple FE model to calculate the material law for the disc (chapter 5). As part of this study experimental data for the material properties of the disc published in literature, was complemented with further tensile tests on human annulus fibrosus. Furthermore, the existing data on compression of non-degenerated human annulus and nucleus tissue together with the new tensile data was used to tune the osmoviscoelastic material constitutive law.

The osmoviscoelastic material law was implemented into the full 3D model. The bulging and creep behavior of the resulting disc model was confronted with experiments of whole discs from the literature. From this comparison, it appeared that a refinement of the osmoviscoelastic model was necessary. Thus, the simplified fiber structure from earlier studies was extended with a more complex secondary fiber structure, which reduced the deformability of the model, while maintaining a correct reproduction of the experiments in confined compression, relaxation and tensile stiffness. Furthermore, to ensure convergence of the highly non-linear simulations the shear stiffness of the elastic non-fibrillar matrix was increased slightly, which was still in reasonable agreement with the experimental data (chapter 6).

The evaluated 3D disc model may now be used to explore the biomechanical implications of disc degeneration on its function and integrity as well as to explore therapeutic mechanisms for repair and regeneration.

McNally et al. measured compressive stress profiles in human discs post mortem. The stresses in the nucleus were nearly constant, whereas high peaks of compressive stress were found on the posterior and anterior side of the annulus. The posterior side experienced the highest compressive stress peaks. These peaks may partly explain the prevalence of postero-lateral herniation in human intervertebral discs. The osmoviscoelastic disc model also predicted similar posterior and anterior stress peaks characterized by McNally et al. (chapter 7). The posterior peak was higher than the anterior peak, consistent with the experimental trend. Results of a primary sensitivity study showed that the development of these peaks depend partly on the amount of fixed charges, which influenced the swelling capacity of the disc tissue. Hence, an increase of the stress peaks was noticed when the swelling ability of the tissue was reduced; this indicated a load shift from nucleus towards the annulus. To further quantify parameters that influence the load distribution in the normal and degenerated disc, a degenerated human data set to describe the fiber and non-fiber properties is needed. Furthermore, the quantification of the stress and load distribution under different load cases (e.g. bending, torsion) is required.

Samenvatting

Rugpijn is een veel voorkomende aandoening bij volwassenen. Doordat een grote groep patiënten blijvend invalide raakt, kost rugpijn de Europese economie veel geld. Het wordt algemeen aangenomen dat de tussenwervelschijf (TWS) een belangrijke rol speelt in het ontstaan van rugpijn. De tussenwervelschijven geven niet alleen flexibiliteit aan de wervelkolom, maar zorgen ook voor schokabsorptie en overdracht van de belasting door de wervelkolom.

Metingen in het menselijk lichaam zijn zeer complex. Hierdoor is het gebruik van Eindige Elementen (EE) modellen een belangrijke onderzoeksmethode geworden in het onderzoek naar belastingsoverdracht in gezonde en gedegenererde tussenwervelschijven. De tussenwervelschijf is onderhevig aan een combinatie van elastische, viskeuze en osmotische krachten, waarvan de laatstgenoemde tot nu toe in 3D EE modellen buiten beschouwing zijn gelaten. Bijvoorbeeld, in de tussenwervelschijf is er sprake van een sterke relatie tussen het zwellen van de grondsubstantie, voornamelijk bestaande uit proteoglycanen (PGs), en de trekspanningen in de bundels collageen. Zo ook bestaat de totale waterinhoud in het weefsel uit intrafibrillair water (IFW) en extrafibrillair water (EFW) en het meenemen van dit onderscheid heeft een groot effect op de osmotische krachten. IFW bevindt zich in de ruimte in de collageenvezels waardoor geen interactie mogelijk is met de PGs, die zich in de ruimte buiten de collageenvezels bevinden. De osmotische druk moet worden bepaald, gebaseerd op alleen de hoeveelheid extrafibrillair water. Uit experimenten is gebleken dat veranderingen in de osmotische druk de genexpressie in de cellen van de TWS en ook groei van scheuren beïnvloeden. De kwantificering van de uitwisseling van intra- en extrafibrillair water en de gevolgen hiervan op de osmolariteit van de TWS is daarom van groot belang voor de bepaling van de fysische condities van de tussenwervelschijf en van de gevolgen voor TWS degeneratie en schadegedrag.

De relatie tussen de zwelling en de voorspanning in het collageen is gemodelleerd in een osmoviscoelastisch EE model (hfst. 3). De door dit model voorspelde waarden voor inwendige druk lagen in de orde van 0.1-0.2MPa in de onbelaste TWS. Dit komt overeen met waarden uit de *in vivo* experimenten van Wilke et al. In het model is een correctiefactor voor de invloed van IFW gebruikt gebaseerd op het werk van Urban en McMullin voor een weefsel met een lage collageenconcentratie, zoals de nucleus pulposus. Recentelijk bleek echter, dat dit niet opging voor de annulus, welke een veel hogere collageen concentratie heeft. De resultaten van Sivan et al. tonen dat de hoeveelheid IFW afhankelijk van de opgelegde belasting, waardoor de vaste-lading-concentratie significant kan veranderen. Daarom is het model uitgebreid met de scheiding tussen intra- en extrafibrillair water (hfst. 4). Hierdoor kon aangetoond worden dat het profiel van de inwendige druk in de schijf wordt beïnvloed door de hoeveelheid IFW. Helaas werd de toepasbaarheid van het model beperkt doordat een aantal modelparameters niet bepaald kon worden door gebrek aan experimentele resultaten.

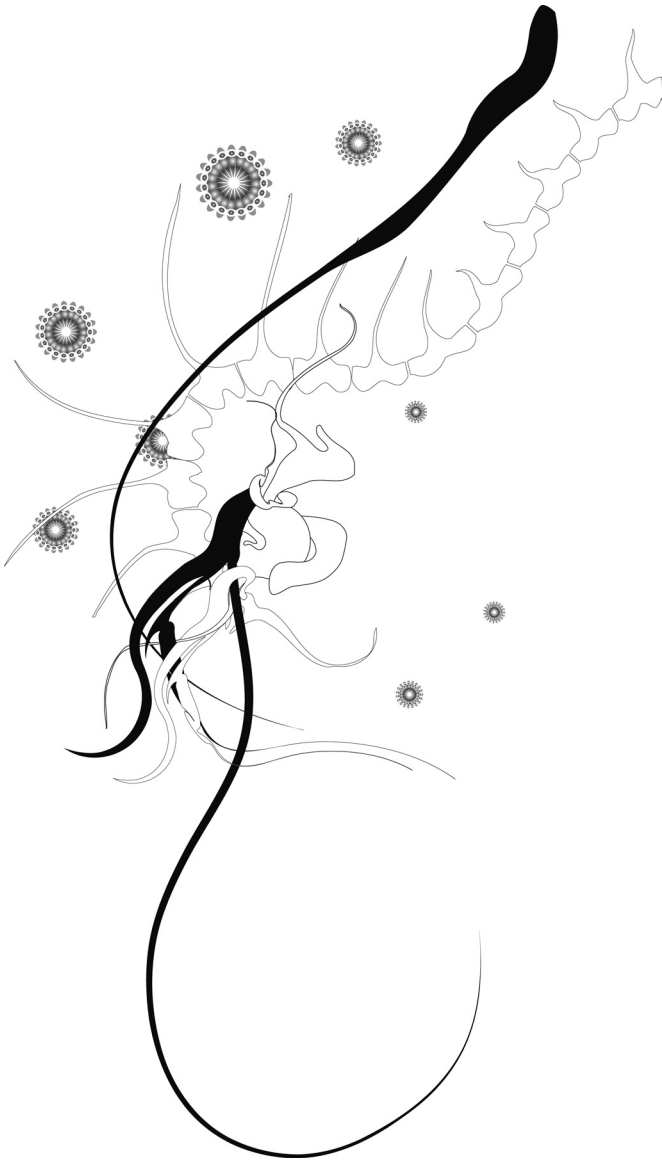
Naast osmotische effecten zijn ook de andere mechanische eigenschappen van de tussenwervelschijf complex. Het constitutieve gedrag van het weefsel wordt voornamelijk bepaald door de biochemische samenstelling en de vezelversterkte structuur. Het

anisotrope, niet-lineaire gedrag van een samengesteld materiaal als de tussenwervelschijf kan alleen door een verscheidenheid aan experimenten worden bepaald. Daarom zijn voor het verkrijgen van een materiaalwet voor de TWS meerdere experimenten tegelijk op het model gelegd (hfst. 5). De resultaten uit de literatuur werden aangevuld met trekproeven op weefsel uit de annulus fibrosus van de mens. De resultaten uit de literatuur van compressie experimenten met niet-gedegeneerde humaan annulus and nucleus en de nieuwe resultaten uit trekproeven werden gezamenlijk gebruikt om het osmoviscoelastische gedrag van het model te beschrijven.

Deze osmoviscoelastische materiaalwet werd geïmplementeerd in het 3D model. Het model werd geëvalueerd door zwelgedrag en kruip van het model te vergelijken met experimenten op de hele tussenwervelschijf. De overeenkomsten waren voldoende om met het model de implicaties van de biomechanica van degeneratie te onderzoeken voor functie en integriteit van de tussenwervelschijf en voor therapeutische mechanismen voor herstel en regeneratie.

McNally et al. hebben spanningsprofielen gemeten onder compressie in post-mortem humane TWS. De spanningen in de nucleus waren bij benadering constant, terwijl in de posterieure en anterieure zijde van de annulus hoge pieken in de drukspanning werden gevonden. De posterieure annulus is onderhevig aan de hoogste piekspanningen. Deze pieken kunnen gedeeltelijk de prevalentie van een postero-laterale hernia in de menselijke tussenwervelschijf verklaren. Het osmoviscoelastische model voorspelde deze karakteristieke piekspanningen aan de posterieure en anterieure zijde, gemeten door McNally et al. De posterieure piek was hoger dan de anterieure piek, overeenkomstig de experimentele trend. De eerste resultaten van een gevoeligheidsstudie toonden dat het ontstaan van deze pieken gedeeltelijk afhing van de hoeveelheid vaste lading. Deze vaste lading beïnvloedde de zwelcapaciteit van het TWS weefsel. Er werd een stijging van de piekwaarden gevonden wanneer de zwelcapaciteit werd verlaagd; dit weerspiegelt een belastingsverschuiving van de nucleus naar de annulus.

Om verder kwantificering mogelijk te maken van de parameters, die de belasting in de normale en gedegeneerde schijf beïnvloeden, is er ook een data set nodig van de gedegeneerde humane schijf om de vezel en matrix eigenschappen te beschrijven. Verder is een kwantificering wenselijk van de spannings- en belastingsverdeling onder verschillende belastingscondities (bijv. buiging of torsie).



Chapter 1

General Introduction

1.1 Clinical relevance and background

Recent studies of low back pain disorder demonstrate that back pain is a major health problem within Europe, resulting in large economic losses. The report of the European agency for safety and health at work [83] indicates that the number of people who suffer from back pain during their lifetime lies between 60% and 90%.

The intervertebral disc is always exposed to mechanical loads – even when the body is at rest; slight activities such as breathing is known to cause measurable changes in intradiscal pressure [79,122]. The mechanics of load transfer in the spine, and particularly the intervertebral disc, are an important factor in understanding the patterns and mechanisms of back pain. Degeneration in the disc, which in some cases is associated with back pain, occurs much earlier than in other tissues for reasons that are still unclear [13,110]. Chapter 2 focuses on clarifying the clinical background a little more in detail.

During degenerative changes the disc may herniate and possibly lead to sciatica and low back pain. This severely incapacitates the patient. Costs are high due to the intense level of care patients require and the fact that they often cannot participate in work processes for prolonged periods. Disc degeneration is a multifactorial and heterogeneous disease that is hugely detrimental to both individuals and populations. It is significant in around 10% of teenagers and more than 70% of people over 50 years. 5-10% of disc-degeneration-related cases lead to chronic disability. This is often coupled with depressive illness, which further decreases the quality of life for the patient and his/her family.

Because of poor knowledge of the aetiopathogenesis of these disorders, there is no clinical consensus on indications or methods of treatment. Thus, treatments vary widely with surgery the only medical intervention on offer.

The complex nature of disc degeneration-related disorders requires a multidisciplinary approach to identify the cause of initiation and progression of degenerative changes. Researchers from different fields, such as biochemistry, genetics, biology, histology, pathology and biomechanics are collaborating in a European Union financed project (EURODISC) to study disc degeneration. The close network within this project firstly allows questions to be addressed from different perspectives and subsequently to study key aspects in disc degeneration by correlating the findings.

To improve the conclusiveness of the results, experimental studies are carried out on the same specimens (biochemistry, histology studies and cell biology). Furthermore, blood samples are collected to study the genetic variations and then compared to the experimental data to study the correlations between tissue behavior and genetic polymorphisms.

In parallel to the analysis of disc tissue, cells, and blood samples, the biomechanical aspects of the degenerative process are addressed through an experimental and numerical approach. The latter is a mathematical approximation method used to address a complex problem through many smaller and simpler, solvable problems. In recent years, finite element models have proven to be a supporting tool to study biological problems. The main drawbacks of *in vivo* and *in vitro* studies are inter-subject variations, the limitations of results from animal models, ethical concerns, financial costs and practical limitations that hinder detailed knowledge about the stress distribution within

the tissue. Through finite element (FE) studies some of these issues may be overcome to study the biomechanical behaviour of the disc. As recently highlighted in a review by Bowden on finite element modelling of the spine [14], a good FE model is the outcome of a long developing process that requires verification and validation of the model with experimental data. As for the disc, Bowden suggests that the main criterion for a good disc model is the choice of the constitutive law, rather than accounting for the geometric features.

To summarize, degenerative changes in the disc are a result of interactions between genetics, age and increasing exposure to environmental factors [8,9,88,114]. Therefore, a 3D finite element model of the disc was developed in association with the EURODISC project to complement and improve the understanding of experimental findings and to further study the load distribution in the disc, which is the main focus of this thesis. The overall aim of this thesis is to investigate key parameters that are believed to be of importance in understanding disc biomechanics with regards to degeneration.

1.2 Objectives of the EURODISC project

The work presented in this thesis, in part, contributes towards the aims and objectives of the EURODISC project. The aim of the EURODISC project is to examine the interplay of ageing, genotype and environmental factors in disc tissue degeneration. Whether these factors occur by altered synthesis, accumulation, or breakdown of matrix macromolecules are addressed by our partners in the project. The partners determine whether the altered matrix allows ingrowths of blood vessels and nerves and isolate matrix components which are responsible for this. The experimental work and mathematical model presented in this thesis works towards addressing how the altered matrix affects aspects of mechanical function and the mechanical environment of the cells. This work also fit in with our partners study on how environmental stresses arising from changes in mechanical load and nutrient supply affect disc cell metabolism and their capacity to promote tissue repair. Our EURODISC partners (Figure 1.1) are also investigating the signaling pathways involved; the role of age and of genotype in mediating all these cell-induced changes, and are also examining a population-based twin data base for age-gene-environmental associations with disc degeneration and relate results from this study with those obtained at a tissue-cell level.

The aetiopathogenesis including genetic determinants for disc degeneration are unknown. Only after these are clarified, can we have knowledge-based diagnosis and rational prevention and treatments. The EURODISC project hopes to provide an essential basis for effective diagnosis of the disorders associated with the intervertebral disc. The partners in the project utilize the combined data sets to develop a knowledge-based classification scheme for clinical diagnosis.

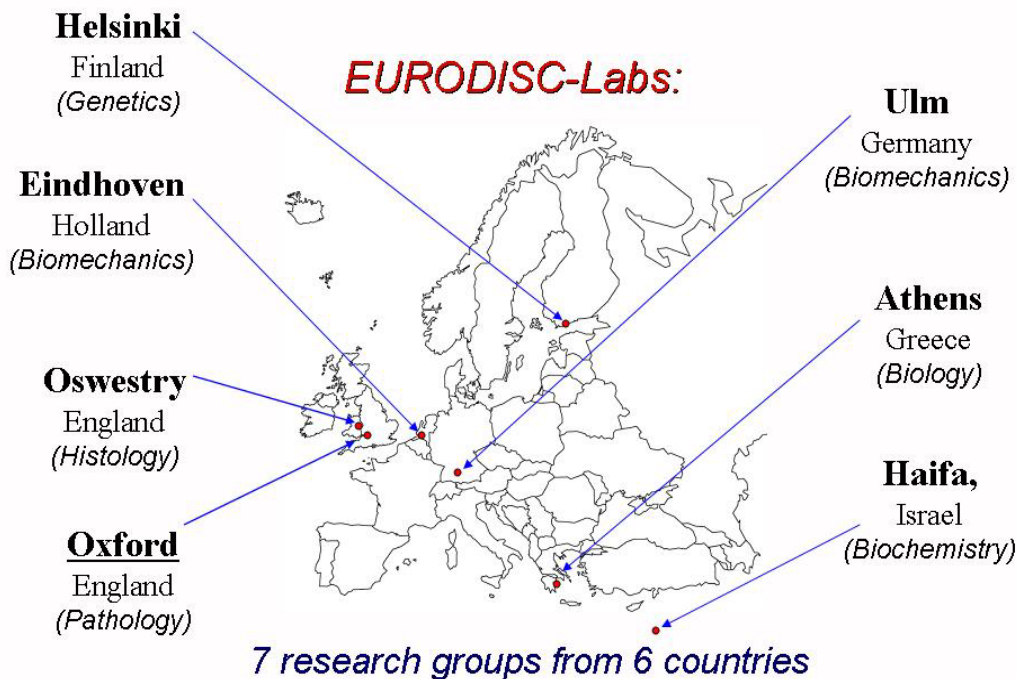


Figure 1.1: Overview of EURODISC-Labs (adapted from Neidlinger-Wilke, personal communication).

1.3 Objectives of this thesis

The development and improvement of the finite element model in this thesis was steered by specific research questions and important experimental findings from the EURODISC project. Therefore, the objectives are presented in their context.

The disc is subjected to a combination of elastic, viscous and osmotic forces; the latter being mostly neglected in previous 3D FE models. The interdependency between the swelling tendency of the disc tissue and the tensile stresses in its collagen structure has not been accounted for.

➡ To overcome this problem we present a model, which takes the interdependency of the swelling and the collagen structure of the intervertebral disc into account. Because intervertebral disc cells are sensitive to osmotic pressure and hydrostatic pressure changes, the primary aim of this study was to predict these quantities in the disc.

Experimental results show that both gene expression of cells in the intervertebral disc and propagation of cracks are affected by changes in extrafibrillar osmolarity. This makes quantification of intra- and extrafibrillar fluid exchange physiologically relevant.

➡ As the stress state of the intervertebral disc is essentially triaxial, a 3D FE model was mandatory for this study. Hence, we extended the initial 3D osmovoelasticoelastic FE model of the disc to account for the intrafibrillar water content and for the solid fraction dependency, to study the effects of water differentiation on the intradiscal pressure and stress distribution throughout the tissue.

Finite element (FE) models have become an important tool to study load distribution in the healthy and degenerated disc. However, model predictions require accurate constitutive models and material properties. In addition to osmotic effects, other mechanical properties of the intervertebral disc are complex. The complex constitutive behavior of the tissue is regulated by its biochemical composition and fiber-reinforced structure [14,51] and the anisotropic, nonlinear behavior of a multi-component material like the intervertebral disc can only be assessed through a variety of experiments.

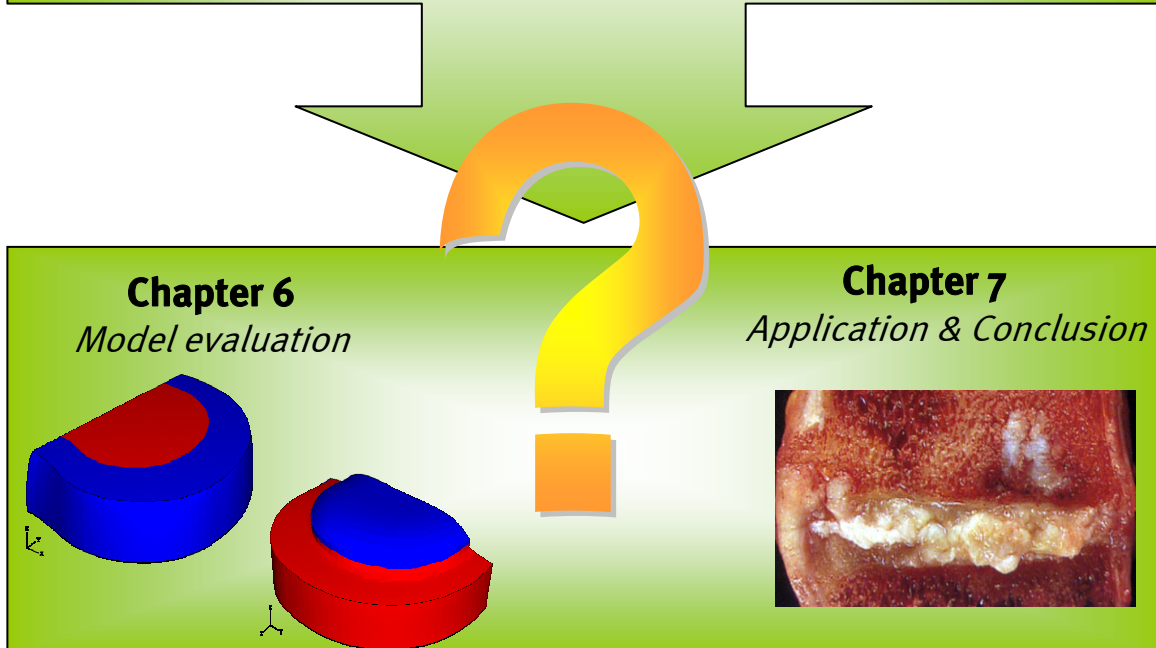
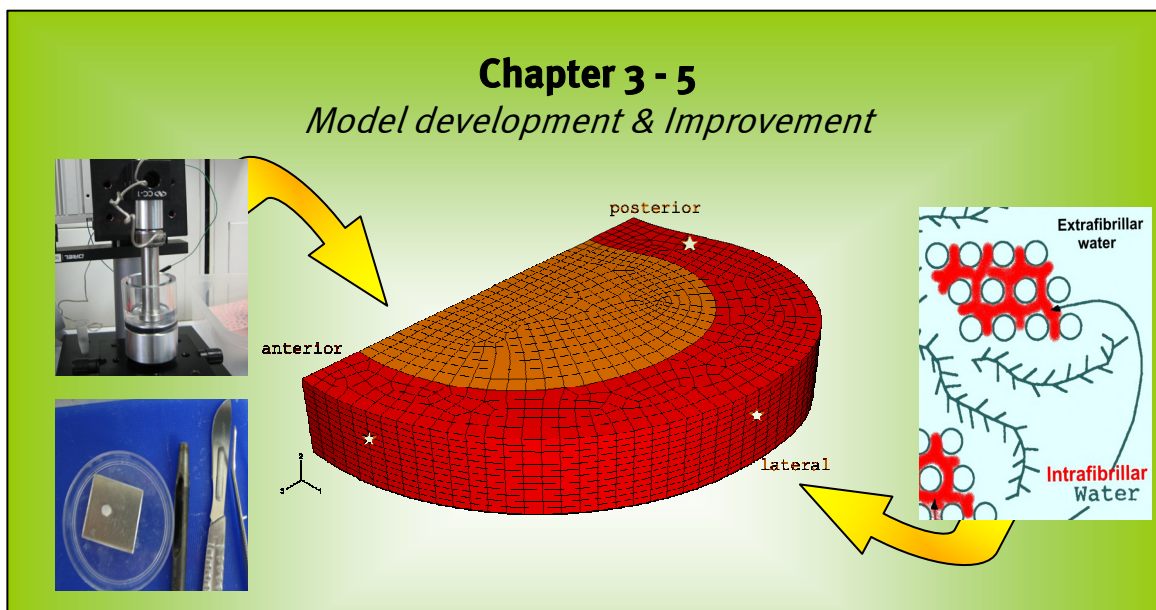
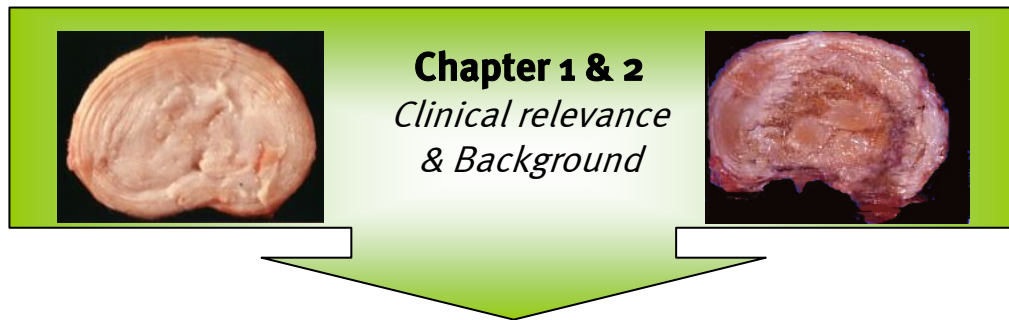
➡ Therefore, an objective of this study was (1) to complement the existing material testing in literature with confined compression and tensile stress-relaxation tests on isolated human annulus fibrosus samples and (2) to use this data, together with existing nucleus pulposus compression data to tune an osmovoelasticoelastic material constitutive law.

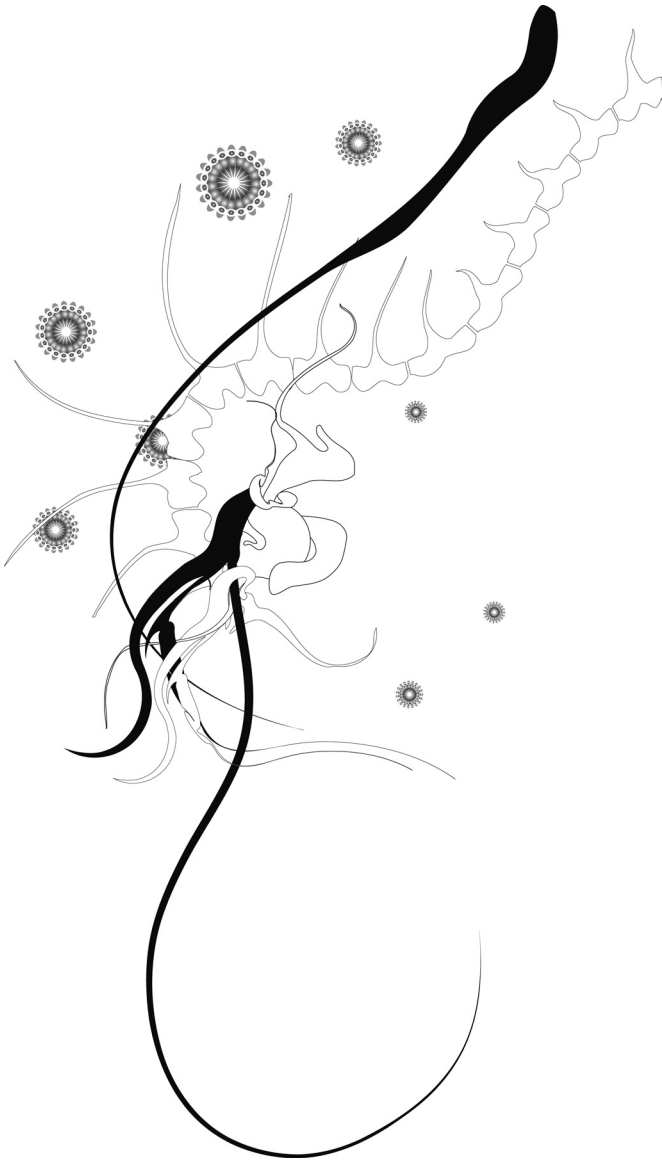
Natarajan and coworkers [80] compared analytical models which have been used to study disc degeneration. They found that the implementation of the osmotic pressure into poroelastic FE models is an essential factor for understanding disc degeneration. Experimental validation of the analytical model is an additional requirement; it implies that the finite element model reproduces experimental behavior.



The aim of the study was to introduce an osmoviscoelastic constitutive law and the obtained material properties in to the full 3D FE disc model. The aim was also to validate the model on the basis of experimental data of whole discs (bulging, height change and intradiscal pressure) from literature.

1.4 Outline





Chapter 2

**Introduction to the spine - with
special emphasis on the disc**

2.1 Anatomical perspective

The human spine is a complex structure with regard to anatomy and physiology, consisting of hard and soft tissues (Figure 2.1). Different regions of the spine have varying functions and structures, accordingly. For example the cervical spine allows maximum movement and flexibility of the neck, while the thoracic spine supports the thorax and organs within. In general the 24 vertebrae (Figure 2.2) consist of a massive vertebral body and the posterior elements that enclose the vertebral foramen. The vertebral canal, in which the spinal cord is situated, is formed via the longitudinal alignment of all the vertebral foramen. Intervertebral disc tissue is a cartilaginous structure connecting adjacent vertebral bodies. The size and the shape of the intervertebral discs varies with the spinal level, while the general composition and structure is fairly constant along the spine. The composition and structure of the disc is explained in detail in Section 2.3.

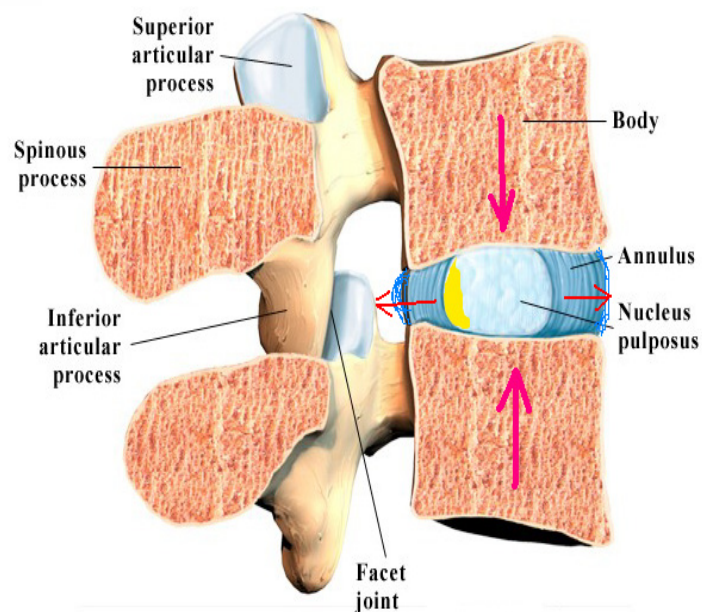
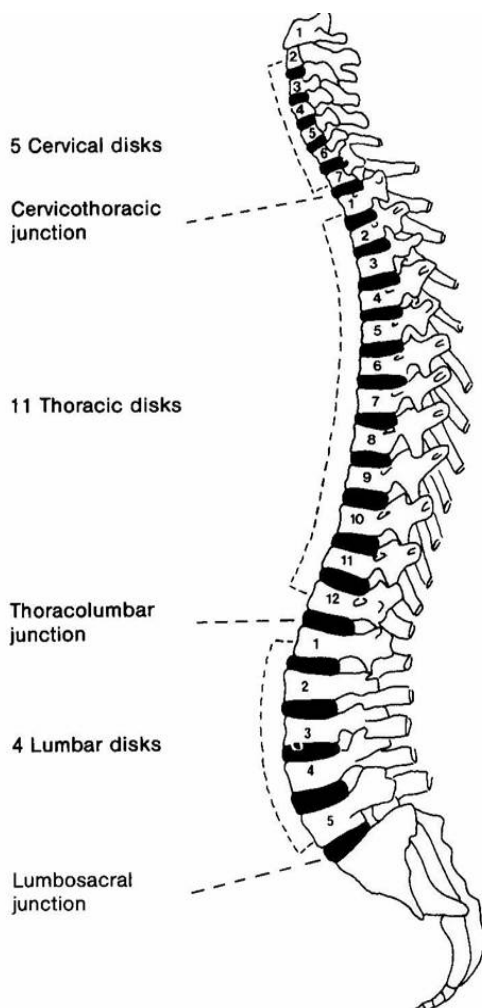


Figure 2.1: Schematic drawing of spinal Colum and disc (adapted from Kramer 1981).

Figure 2.2: Motion segment, 2 adjacent vertebrae connected through the intervertebral disc (www.apmsurgery.com/images).

2.2 Biomechanical perspective

The primary function of the spine is to protect the spinal cord and to provide support for the upper body; the fundamental mechanical functions are to assist in articulation and provide flexibility of the upper body and to distribute the forces acting on the spine from upper body activities. The smallest unit of the spine is called a 'motion segment', consists of two adjacent vertebra, the connecting disc and ligaments (Figure 2.2). Each motion segment works as a single joint, though the flexibility is very limited.

The kinematical motions of the spine are:

- extension/ flexion,
- lateral bending,
- axial torsion and distraction

While the soft tissues anchor the adjacent vertebrae they also allow the movement of the spine. In engineering terms the spine works like a segmented beam. The vertebrae are stiff elements that are connected through flexible elements (disc and ligaments). The ligaments add to the stability of the spine. These are permanently under tension, and this is counteracted by the swelling ability of the intervertebral disc. Hence, the intervertebral disc is always under compression.

2.3 Composition and structure of the intervertebral disc

The following sections focus on the clarification of biochemistry with special emphasis on relevant terms with regard to finite element modeling of the disc.

The disc consists of a gelatinous core known as the nucleus pulposus, which is surrounded by a fibrous ring (the annulus fibrosus), and two cartilaginous endplates. These lie above and below the disc and help the disc to attach to the adjacent vertebrae (Figure 2.3). The intervertebral discs are the largest (4-10mm thick) avascular and virtually aneural structures in the human body. In comparison to any other tissue the mean cell density of the disc is very low ($5800\text{cells}/\text{mm}^3$), making up approximately only 1% of the total tissue volume [110, 88].

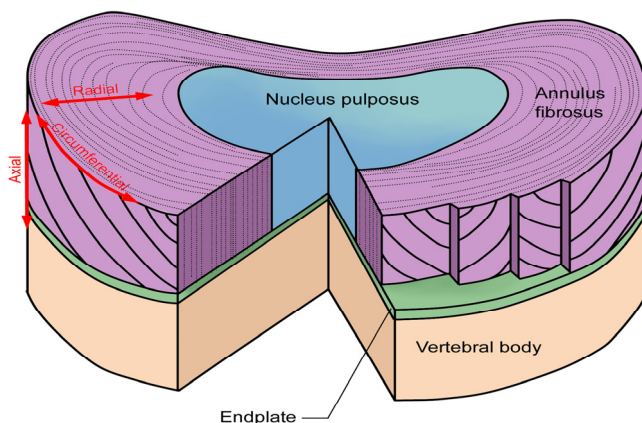


Figure 2.3: Schematic view of the intervertebral disc components; nucleus, annulus, endplate. Also showing the annulus structure; concentric layers of collagen (reprinted from Kurtz & Edidin 2006 [61] with permission from Elsevier).

2.3.1 Main biochemical components

The extracellular matrix (ECM) is a dynamic structure and its integrity (resulting from the balance of synthesis, breakdown and accumulation of macromolecules) is important for the mechanical behavior of the disc [110]. The matrix of the disc consists mainly of two major biochemical structures, proteoglycans and collagen [106].

Proteoglycans

Proteoglycans (PG's) are large complex biomolecules composed of many glycosaminoglycan (GAG) molecules that are attached to a core protein. The main PG in the disc tissue is aggrecan recognizable by its typical brush like structure. The GAG side chains contain fixed negative charges and are hydrophilic. The total concentration of negatively charged groups (carboxyl and sulfonate) present in the GAG is the fixed charge density (FCD). FCD determines the concentration difference between counter- and coions in the disc tissue. The positive counter ions and negative coions distribute themselves in the matrix to maintain electro neutrality. As a consequence the ion concentration in the tissue is higher than the surrounding synovial fluid, which causes a pressure difference. The osmotic pressure leads to a swelling pressure of the tissue [106,110].

Collagen

A broad range of collagen types (e.g. I, II, III, V, VI) are distributed in the extracellular matrix of the disc tissue, more than in any other connective tissue [31]. The main types found in the tissue are collagen type I and type II, their distribution depending on the location in the disc. For example, the proportion of type I:II decreases from outer annulus towards nucleus. The nucleus consists primarily of collagen type II randomly distributed in a loose meshwork of fibers. The collagen fibers (type I) in the annulus are highly oriented in concentric layers with alternating angles (± 30 degrees) towards the transversal plane (Figure 2.3) [21,31].

Table 2.1 Overview of the biochemical composition of the disc [18,89]

Components	Nucleus	Annulus	Endplate
Proteoglycans [% dry weight]	30-50	10	36-48
Collagen [% dry weight]	20	60-70	62
Water [%wet weight]	70-80	70	55

Water- intrafibrillar and extrafibrillar water

The hydration in the tissue is not constant as the disc is always under load in vivo. Thus, the disc experiences a diurnal cycle of fluid loss, (up to 25% during the day) to restore osmotic equilibrium when loaded, followed by regaining the fluid when the loads are reduced (resting period). Hydration of the tissue is maintained through the osmotic properties of the PG, as they imbibe fluid and as a result maintain the tissue turgor. Depending on the location in the tissue the total water content differs between the nucleus and the annulus (Table 2.1). Moreover, changes in water content of the disc are controlled primarily by the difference between the externally applied pressure and the disc swelling pressure. The latter depends mainly on the effective stress and the FCD, which in turn depends on PG content. This swelling tendency is magnified by the partial shielding of some of the water within the collagen fibrils (the intrafibrillar water) [107,108]. Indeed the scatter on the data of swelling pressure versus fixed charge density is less when extrafibrillar fixed charge density is used rather than total fixed charge density based of total water volume (Figure 2.4).

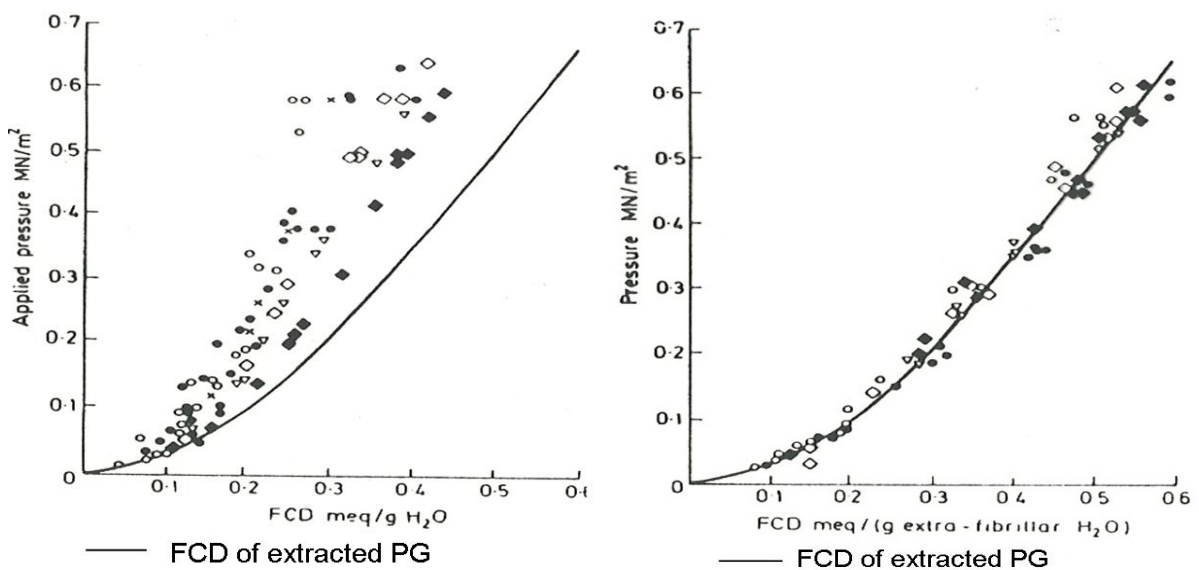


Figure 2.4: The continuous line represents the swelling pressure of extracted proteoglycan gel as a function of fixed charge density, both in the left as in the right graph. Symbols in left graph: The swelling pressure of human nucleus tissue as a function of fixed charge density expressed per unit total water volume. Symbols in right graph: The swelling pressure of human nucleus tissue as a function of fixed charge density expressed per unit extrafibrillar water volume. The extrafibrillar water content in the right graph is evaluated per sample assuming intrafibrillar water content proportional to the measured collagen content of the sample. The shielding of water by the collagen accounted for in the right graph results in a better prediction of the nucleus swelling pressure from the proteoglycan gel data and a smaller scatter on the data. (adapted from Urban & McMullin [108], personal communication).

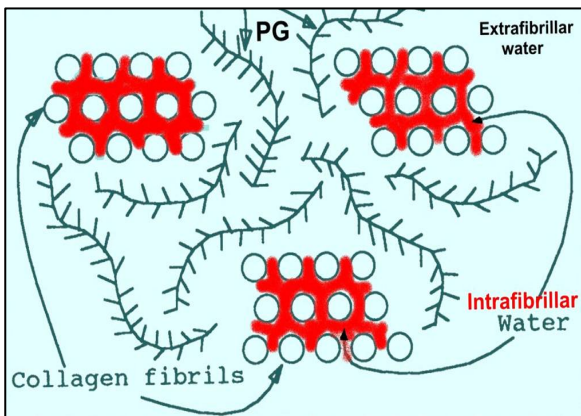


Figure 2.5: Schematic drawing of extracellular matrix with differentiating the total water content of the tissue into intrafibrillar and extrafibrillar water (adapted from Urban & McMullin [108], personal communication).

In detail, the total amount of water is divided into intrafibrillar water (IFW) and extrafibrillar water (EFW) (Figure 2.5). IFW is present in the intrafibrillar space of the collagen fibers and is therefore not accessible to the PG's, which due to their size are only present in the extrafibrillar component. Hence, to predict the osmotic pressure of the disc from its PG content, the latter must be determined on the basis of the extrafibrillar water (EFW) only [100,108]. The importance of this topic with regard to the finite element model is discussed in more detail in chapter 4.

2.3.2 Disc structure and properties

The mechanical properties and physical function of the disc are regulated by its biochemical composition and organization. The unique material properties of the nucleus are the outcome of a high swelling propensity of proteoglycans and a loose collagen network. The annulus fibrosus on the other hand consists mainly of a highly oriented and a dense collagen network (providing tensile strength and anchors the tissue to the bone), embedded in a proteoglycan gel; the proteoglycans, due to their strong swelling ability [41,107,110] assure the tissue hydration.



Figure 2.6: Unconstrained swelling (in vitro) of a bovine disc, showing clearly the high swelling propensity of the nucleus tissue.

Nucleus

The composition of the nucleus as given in Table 2.1 shows that it has a very high water content, which from a mechanical point of view would describe the tissue as a fluid instead of a solid [51]. However, the behavior of the nucleus tissue is more gel like, the swelling of which is restrained by the collagen network. The high water content in the nucleus is due to the hydrophilic PG which results in the swelling ability of the tissue (Figure 2.6). To ensure electro neutrality in the tissue, mobile ions in water are attracted to the PG by means of osmosis. Consequently, this high water content in the nucleus causes it to be highly pressurized.

Annulus

The annulus is often described as a fiber reinforced poroviscoelastic material from the mechanical point of view - why so? The highly organized collagen structure of the annulus, e.g. 15-25 concentric lamellae which contain most of the fiber bundles arranged in alternating directions [67], resembles a fiber reinforced composite material. One of the main advantages of this structure is the ability to withstand large and complex loads in multiple directions with optimized material proportions. Furthermore, the PGs intertwined in the collagen structure that attract water, contribute also to the overall stiffness of the annulus as well as the smaller fibrils structures also present in the annulus, e.g. minor collagen, elastin or collagen crosslinks [21,39,70,91,103,131]. From here on, the smaller fibril structures are referred to as secondary fibers and the larger collagen fibers are referred to as primary fibers.

Lanir describes cartilaginous tissue through a biphasic material law [63,64], consisting of a solid matrix saturated with a osmotically prestressed water. The solid matrix is further defined as a porous structure, indicating the fluid flow through tiny pores within the tissue when loaded or unloaded. The fluid flow causes the tissue to exhibit time-dependent material behavior [11,26]. In addition to this, the time dependent behavior is induced by the intrinsic viscoelasticity of the collagen fibers [98,119].

Endplates

Although the biochemical composition of the cartilage end plates is similar to the rest of the disc tissue, the varying proportions of water, proteoglycans and collagen and its structural organization give it different material and physical properties (Table 2.1). The endplates are thinnest in the middle, with a higher percentage of PG's and water than the peripheral regions of the endplates. The peripheral regions are thicker and have a higher percentage of collagen, but lower water and PG than centrally; therefore, are stiffer possibly due to the difference in this composition [89,110]. The endplates are divided in a calcified layer of cartilage closest to the vertebra and a hyaline layer of cartilage closer to the disc itself. The endplates are considered as the main route for fluid flow, e.g. nutrient and waste transport in and out of the disc, as the blood vessels and marrow in the adjacent vertebrae are in close proximity to the nucleus [110].

However, no compelled experimental evidence for this flow exists. These channels and vessels enter only halfway through the endplate (calcified layer) and do not penetrate into the disc. As the interface between the intervertebral disc and vertebra, the

endplate contribute to the load distribution and assist in maintaining the water content and the intradiscal pressure of the disc.

2.4 Load bearing and distribution within the disc

The intervertebral disc is always exposed to mechanical loads [79,122]. Loading of the disc causes multiple physical stimuli that influence disc cell behavior by means of tensile forces, compressive and osmotic forces [41,81,82].

2.4.1 Compressive and tensile properties

A high intradiscal pressure in the nucleus is the consequence of the swelling propensity and the confinement between the vertebra and the annulus. This is counteracted by the dense collagen fiber structure of the annulus and the external load which is transformed by the intradiscal pressure to a tensile stress in the collagen fiber structure of the annulus.

Compressive properties

The disc has a higher compressive strength than the adjacent vertebrae. Compression of the disc results in outward bulging of the annulus and bulging of the endplates into the vertebra [15,17]. To balance the compressive forces a volumetric change occurs in the tissue due to the fluid flow. The effective stiffness of the tissue increases with a decreasing volume, as the tissue stress-strain relationship leaves the toe region and FCD rises. As the nucleus swelling ability is restrained by the annulus and the adjacent endplates, a high intradiscal pressure is maintained.

Tensile properties

The gradual increase of both collagen content and collagen orientation from anterior to posterior and from outer to inner annulus contributes to the anisotropic and non-homogenous material properties of the annulus.

The tensile properties of the annulus are highly nonlinear and depend on the collagen fibril density and orientation [30,34,38]. Experimental data shows that when annulus fibers are tested in tension, first a toe region (small strain → small stresses) is seen followed by a stiffer linear region (high strain → high stresses) and finally failure of the tissue in the stress-strain curve (Figure 2.7). This can be explained firstly through the fact that the collagen fibers align along the loading direction (toe region) before being stretched and thus generating low tensile stresses. However, higher strains result in stretching of the collagen fibrils and consequently in higher tensile stresses (linear region) [38,39].

The collagen fibers in the annulus are prestressed even in a supine position [95]. A reason for this is the swelling propensity of the tissue due to the hydrophilic nature of the PG's intertwined in the collagen network. This also contributes to the tensile properties of the tissue.

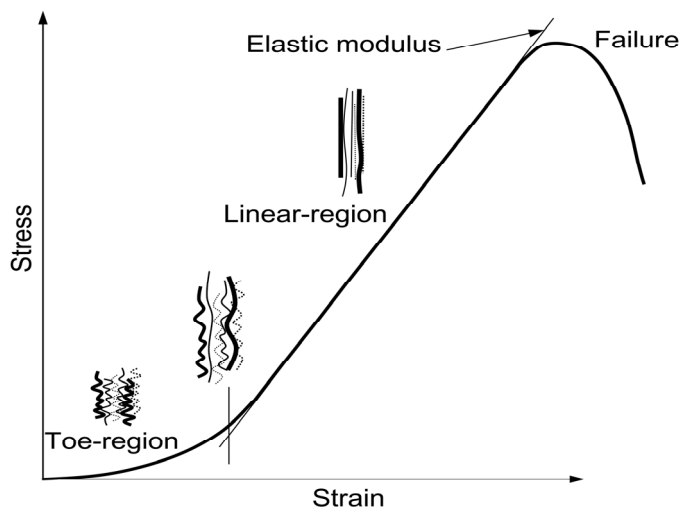


Figure 2.7: Schematic view of the tensile behavior of the collagen fibrils in the annulus (reprinted from Kurtz & Edidin 2006 [61] with permission from Elsevier).

2.4.2 Osmotic forces

Fissures in the degenerating disc are poorly related to external mechanical load [115]. This suggests that mechanical load may not be the primary determinant of crack propagation in the disc. Physical and numerical models of disc degeneration [129], suggest that osmotic forces have a major impact on crack opening and propagation.

Although osmotic pressures are an order of magnitude lower than external mechanical load, decreasing osmosis in the degenerated disc may cause local stress concentration resulting in crack propagation [47]. The mechanism underlying this protective effect is best understood in the context of Starling's law. This law states that the driving force of fluid flow from the crack to the medium is governed by the gradient of the chemical potential of water. The chemical potential is the difference between hydrostatic pressure and osmotic pressure (this is equivalent to the gas constant multiplied by the absolute temperature and osmolarity).

A crack in a healthy young disc is surrounded by high osmotic pressure tissue, causing the fluid to leave the crack and the crack to close. Degeneration of the tissue causes the osmotic pressure of the tissue to decrease, due to loss of (PG's), leading the fluid into the crack, causing patency of the crack, stress concentration at the crack tip and crack propagation. Experimental results [22,82,97] demonstrate that cellular responses are affected by osmotic forces.

2.4.3 Stress distribution and profiles

Experimental measurements of in vivo intradiscal stresses are difficult. However, through stress profilometry, it is possible to measure directly the compressive stress distribution within the matrix of the discs [71]. Briefly, during the experiment, a miniature stress transducer mounted on a long needle is drawn through the disc from posterior to anterior along its mid-sagittal plane. Thus, it is possible to obtain a stress profile depending on the position within the disc [72]. As mechanical properties vary with direction (anisotropic

material) stress profilometries in two perpendicular directions are measured. Experimental data has shown that within normal (young) discs the stresses are distributed evenly. However, with increasing age and fluid loss, stress peaks are noticed in the annulus. The appearance of these peaks is still unclear. Nevertheless, from a mechanical perspective, the peaks suggest a change in load distribution [74] and therefore need to be examined further.

2.5 Intervertebral disc ageing and degeneration

The mechanics of load transfer in the spine, and particularly the intervertebral disc, are an essential factor in understanding the patterns and mechanisms of back pain. Degeneration in the disc, which in some cases is associated with back pain, occurs much earlier than in other tissues for reasons that are still unclear. However, the low renewal rate of disc tissue as opposed to the renewal rate of other tissues may play a role [13,110].

The focus of current research is aimed at clarifying and differentiating between the degenerative process due to ageing effects and degeneration that occurs as part of a pathological process [13,88,110]. Adams and coworkers [2], for example give a definition for both processes. According to Adams et al. [2], degeneration implies specific and deleterious changes in disc composition, structure and function. While aging is a life long process, it starts right after birth and involves structural biochemical and functional changes noticeable in any connective tissue, but particularly in the intervertebral disc [13].

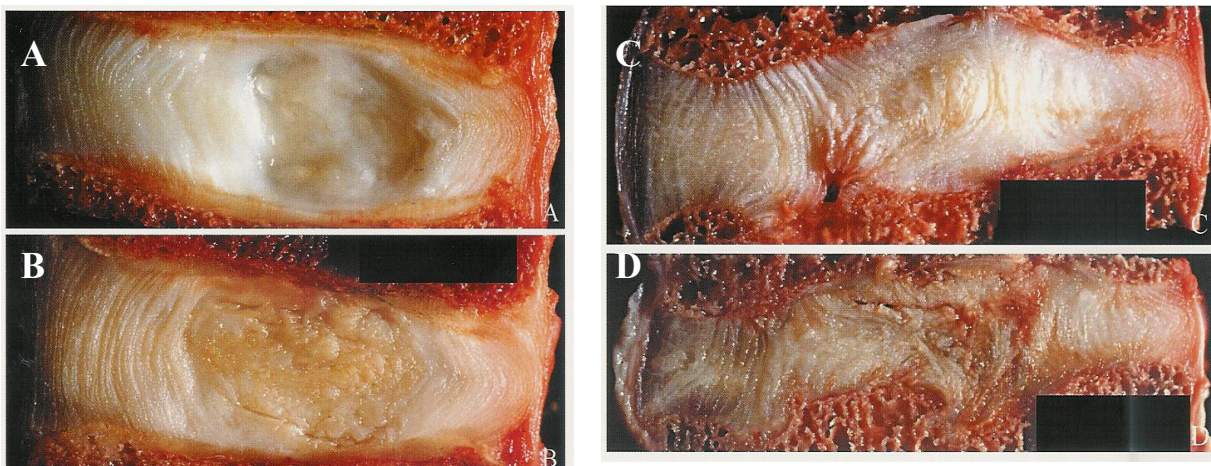


Figure 2.8: Lumbar intervertebral disc sectioned in the mid-sagittal plane, from anterior to posterior side (A) Grade 1 disc, typical of ages 15-40 years; (B) Grade 2 disc, typical of ages 35-70 years; (C) Grade 3, showing moderate degenerative changes; (D) Grade 4 disc, showing severe degenerative changes (reprinted from Adams, Bogduk, et al. 2004 [2] with permission from Elsevier).

2.5.1 Changes with age and degeneration

Structural changes associated with degeneration are often the decrease of disc height, inward buckling of the inner annulus, increase of radial disc bulging or tears in the annulus. Morphological changes, such as disorganization of the collagen and elastin structures (e.g. annular lamellae become irregular, bifurcating) are noticeable with increasing age and degeneration [13,110]. Also, the difference between nucleus and annulus decreases with increasing age (Figure 2.8) [18].

The ingrowths of blood vessels and nerves into the disc is observable with degenerative changes [55, 60,76]. A possible explanation could be the loss of osmolarity in the nucleus; a high osmolarity would draw the fluid out of the hollow vessels, explaining why the young disc is unperfused. As the FCD decreases with age, the osmolarity decreases and the blood vessels have a chance to grow. Hence, loss of osmolarity and hydration is the consequence of the most significant biochemical change, the degradation and leaching of PG's [35,36]. This loss of PGs appears to allow nerve and endothelial cells to grow into the PG-depleted disc tissue [58]. Also noticeable, but not as significant, are changes in the collagen distribution and alterations in the proportions of the different collagen types [5]. Degeneration also effects the cell metabolism, e.g. imbalance of PG synthesis and degradation and nutrient supply, as well as an increased incidence of cell clustering [57,87]. However, the exact pathogenesis of the degenerative process is still unclear.

2.5.2 Effects of degenerative changes on disc function and pathology

Thus, with age and degeneration the load distribution between annulus and nucleus changes: as the nucleus hydration decreases the compressive load bearing capacity of the annulus increases [4]. This behavior is often referred to as a 'flat tyre' [2,17]; consequently with a reduced intradiscal pressure the annulus fibers are no longer loaded in tension and therefore have to take up more compressive forces than in normal discs. A study by McNally et al. [75] showed that alterations of the stress distribution in the disc under loading can be associated with discogenic pain in the posterolateral annulus.

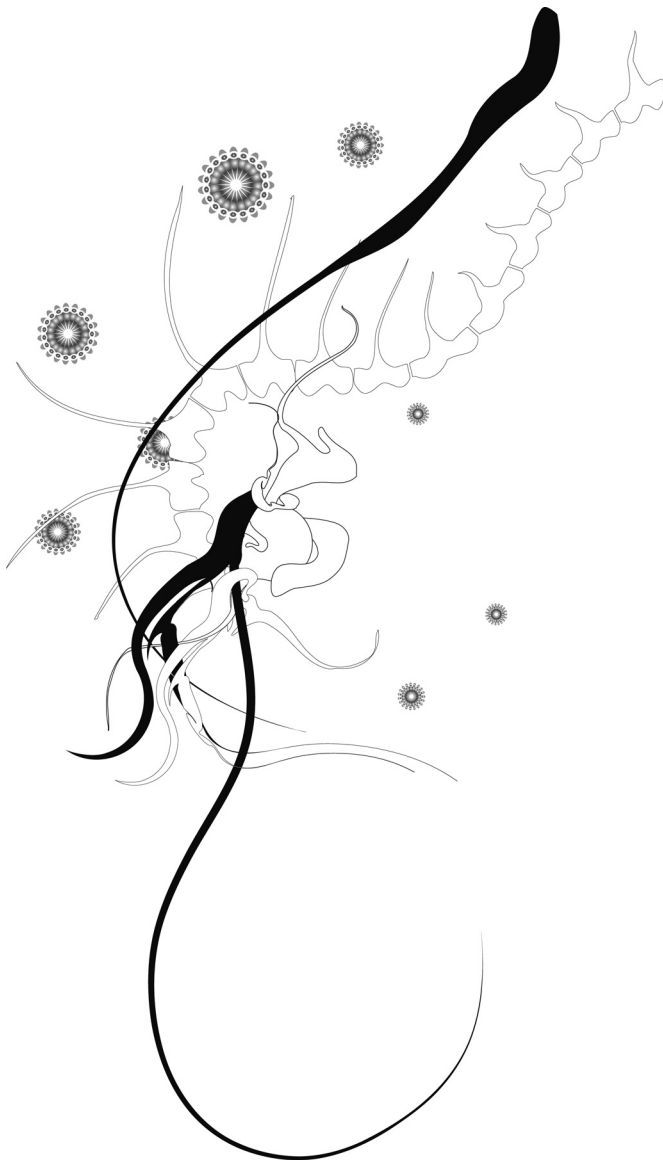
Loss of disc substance including PG's also influences the ability of the disc to regain disc height and fluid when the load is decreased. Decrease of disc height and changes in the load bearing behavior of the disc also affect other spinal structures. For instance, the adjacent vertebrae are directly influenced by the change in the load distribution (load shift from nucleus to annulus) and disc height loss. The spongiosa of the adjacent vertebrae tend toward osteopenia and facet joint may be overloaded [3,85,86]. Consequently, adaptation of the muscles will follow to assure spinal stability. The whole adaptation process may be painful and predispose the other spinal structures to injuries.

With an increasing degeneration process, the ingrowth of vessels and nerves increases. The nerve ingrowths has been associated with chronic back pain and loss of PG [32,56,58].

2.5.3 Degenerative disc diseases

A common disc disease is disc herniation (or prolapse) which occurs most frequently at lower lumbar levels. The disc prolapse involves a relative displacement between annulus and nucleus, for example the annulus can bulge intensively but remain intact or nucleus tissue can extrude through the ruptured collagen layers of the annulus [2]. This can cause neurological symptoms, e.g. sciatica, and sometimes back pain. Structural changes, such as reduction of disc height and/or calcification of the endplates may contribute to spinal stenosis, which leads to low back pain and neurological problems.

The diagnosis and treatment of painful degenerative disc disease remains one of the most controversial topics in the spine literature. The amount of research conducted on the disc does not stand in relation to the economical burden on the society [110].



Chapter 3

Initial development of a 3D FE model of the disc

The content of this chapter is based on an article in
European Spine Journal 15 Suppl 15: 361-71
“Osmoviscoelastic finite element model of the
intervertebral disc.”

Y. Schroeder
W. Wilson
J. M. Huyghe
F. P.T. Baaijens

3.1 Overview of finite element approaches for the disc

Degeneration in the disc, which is closely associated with back pain, occurs much earlier than in other tissues for reasons that are still unclear, but daily loads may play a role [110]. The environment of the disc cells, which manufacture and maintain the disc's composition and integrity, is influenced through loading. The degree of change in the extra cellular environment depends on the magnitude, duration and type of loading [110]. Because the cells in the intervertebral discs are sensitive to hydrostatic and osmotic pressure, quantification of these pressures and stresses with regard to disc degeneration is important.

Experimental measurements of *in vivo* intradiscal stresses are difficult. Therefore, different finite element approaches have been made in recent years to gain a better understanding of the load distribution in the spine and especially in the disc. In recent studies a poroelastic model has been widely used. A major problem associated with this type of model is that intradiscal pressure tends ultimately to zero under constant load, which does not mirror physiological reality [122].

Different approaches for the implementation (e.g. stresses) of collagen fibers have been made [23,130]. Elliott et al. [29] recommend applying a linear fiber-induced anisotropic model to the annulus fibrosus. Wagner et al. [117] developed a theoretical model for the nonlinear elastic behavior of the human annulus fibrosus. However, different material laws have been considered to explain the complex tissue behavior. Wang et al. [118] applied a viscoelastic material law that was also applied to our current study. All of these models assume that the *in vivo* disc is stress-free in the supine position. This assumption contradicts experimental results which show hydrostatic pressure in the order of 0.1MPa in an unloaded disc [79,122]. Few models calculate the distribution of osmolarity in the disc and to our knowledge no such FE-model is currently available in the literature. Osmolarity is vital as it regulates swelling pressure and disc hydration, hence, contributes to load-bearing [52] and also affects the cellular responses [81]. Furthermore, a recent study suggested an important role of osmolarity changes in the propagation of cracks in the disc [129]. Therefore, a finite element model, which accounts for both the collagen fibers and the swelling properties of the tissue, is a very useful tool to study stress distribution in the disc.

Several authors have proposed models of osmotic prestressing in cartilaginous tissues. However, few have been applied to the disc. Lanir [63,64] recommended a bicomponent fluid-solid model which includes the Donnan-osmotic pressure generated by the proteoglycan molecules that are entangled in the collagen network of articular cartilage. While neglecting the effect of the diffusion-convection of counter- and coions, which are responsible for the osmotic forces, Lanir [63,64] assumed that the ionic distribution is always in equilibrium with the surrounding physiological salt concentration of the blood. This simplification cannot be justified in unsteady state conditions where loading changes lead to fluid expression or imbibitions, as diffusion times of ions in cartilages are of the same order of magnitude as the diffusion or flow of the water.

Lai et al. [62] included a diffusing ionic component in a cartilage model, hence making it a triphasic model. Huyghe and Janssen [44] further generalized the model to finite deformation and showed that the full constitutive behavior of the swelling tissue can be

described by one free energy function and one frictional coefficient matrix. This electro-chemical model of Huyghe and Janssen [44] was used by Frijns et al. [33] to reproduce swelling and compression of canine annulus fibrosus. This finite deformation model was further extended by Van Loon et al. [113] in a 3D finite element study.

A detailed comparison of Lanir's two-component model [64] and the electro-chemo-mechanical models of Lai et al. [62] and Huyghe and Janssen [44] was carried out by Wilson et al. [125]. They showed that the bicomponent model is a reasonable approximation of the more complex electro-chemo-mechanical models under physiological conditions. Iatridis and coworkers [48] developed a 2D plane stress poroelastic and chemical (PEACE) model to study the influence of the fixed charge density magnitude and the distribution in a slice of disc material. Results showed that the influence of the fixed charge density on the mechanical, chemical and electrical behavior of the tissue should definitely be taken into account for finite element modeling of the disc. Sun and Leong [104] developed a nonlinear hyperelastic mixture theory model for the annulus fibrosus, which takes the anisotropy, transport, and swelling tendency into account. Unfortunately, to our knowledge their computations are not yet published. Wilson et al. [126] combined the bicomponent model [125] with their fibril-reinforced poroviscoelastic model [127]. This allows the inclusion of the fibril structure of articular cartilage. Natarajan and coworkers [80] compared analytical models which have been used to study disc degeneration. They found that the implementation of the osmotic pressure and the strain-dependent-permeability into poroelastic finite element models is an essential factor for simulations and understanding disc degeneration. Experimental validation of the analytical model is an additional requirement.

3.2 Aim of study

The swelling tendency of the disc tissue and the tensile stresses in the collagen structure are highly interdependent, as Urban and Maroudas [106] demonstrated experimentally. The swelling propensity is counteracted by the viscoelastic stiffness of the dense collagen fiber structure of the annulus, resulting in high hydrostatic pressure in the nucleus [99]. However, no published 3D finite element model of the disc includes osmotic prestressing. In our group, we have thought to overcome this problem by developing a 3D model that takes the interdependency of the swelling and the collagen structure into account. Because intervertebral disc cells are sensitive towards osmotic pressure and hydrostatic pressure changes, the primary aim of our work was to predict these quantities in the disc. This chapter describes the initial 3D model in detail and presents numerical results.

3.3 Material and Methods

A fibril-reinforced poroviscoelastic swelling model of Wilson et al. [126], based on the theory of Biot [12], Mow et al. [78] and Lanir [63,64], is used to describe the intervertebral disc; it consists of a swelling non-fibrillar part and a fibrillar part [126,127]. The model distinguishes between an elastic non-fibrillar solid matrix, a 3D viscoelastic collagen fiber structure and an osmotically prestressed extrafibrillar fluid. Because we assume no oriented collagen fiber structure in the nucleus pulposus, it only consists of an elastic non-fibrillar solid matrix and the osmotically prestressed fluid, while the annulus consists of all 3 parts.

Intrafibrillar water is water which is located in the collagen fibrils (chapter 2, Figure 2.5). We assume intrafibrillar water content to be constant in time and we deal with it as an integral part of the solid. Water located between the fibrils is extrafibrillar [116]. Literature [69,109, 116] shows that accounting for this difference has an amplifying effect on the swelling pressure of the tissue. The key equations of the main components are given here, for further details refer to Wilson et al. [126,127] and Appendix A.

3.3.1 Finite Element model

Non-fibrillar solid matrix

The extracellular matrix of the disc, consisting of many components, is a structure that continually renews itself. However, in our simulation we assume the matrix to be solid. The elastic material behavior of the non-fibrillar part of the extracellular matrix is accounted for through a compressible Neo-Hookean model [126].

$$\boldsymbol{\sigma}_{\text{non-fibrillar}} = K \frac{\ln(J)}{J} \mathbf{I} + \frac{G}{J} (\mathbf{F} \cdot \mathbf{F}^T - J^{2/3} \mathbf{I}), \quad (3.1)$$

where J is the determinant of the deformation tensor \mathbf{F} relative to the stress-free state of the tissue. \mathbf{I} is the unit tensor. K is the bulk modulus, and G is the shear modulus. The hydraulic permeability (k) is assumed to be fluid fraction-dependent [62], and is given by [112].

$$k = k_0 \left(\frac{1 + nf_{\text{eq}}}{1 + nf} \right)^M, \quad (3.2)$$

with k_0 the initial permeability, M a positive constant, nf and nf_{eq} the current and initial extrafibrillar fluid fraction, respectively.

Collagen fibers

The disc collagen fiber structure is a complex combination of larger collagen fibrils, arranged in concentric lamellae [21,67] with alternating fiber orientation and smaller fibrils structures, e.g. minor collagen, elastin or collagen crosslinks [21,39,70,91,103,131]. For simplicity in this study the fiber orientation is assumed to be ± 30 degrees to the transversal plane described through primary fibers only [93,95].

Experimental Data in the literature reveals the viscoelastic behavior of the extracellular matrix, especially for collagen [98,119]. Therefore, a viscoelastic material law [126] is used to describe the behavior of the collagen fibrils. Assuming that the fibrils only resist tension, the stresses in the viscoelastic fibrils are given by:

$$\begin{aligned} \sigma_f &= -\frac{\eta}{E_\varepsilon \varepsilon_f} \dot{\sigma}_f + E_0 \varepsilon_f + \left(\frac{\eta E_0}{E_\varepsilon \varepsilon_f} + \eta \right) \dot{\varepsilon}_f & \text{for } \varepsilon_f > 0 \\ \sigma_f &= 0 & \text{for } \varepsilon_f \leq 0, \end{aligned} \quad (3.3)$$

where σ_f and ε_f are the fibril stress and strain, respectively. E_0 and E_ε are stiffness constants and η is a damping coefficient. A more detailed description of this viscoelastic law can be found elsewhere [126, 128]. The strain is defined with respect to an initial stress-free state. The differential equations are numerically integrated using an implicit backward Euler scheme.

Osmotic swelling

The osmotic pressure ($\Delta\pi$) of the intervertebral disc tissue depends on the fixed charge concentration (c_f) of the proteoglycans [107]:

$$\Delta\pi = \phi_{int} RT \sqrt{c_{F,exf}^2 + 4 \frac{\gamma_{ext}^\pm}{\gamma_{int}^\pm} c_{ext}^2} - 2\phi_{ext} RT c_{ext} \quad (3.4)$$

The fixed charge density (c_f) is calculated per unit of extrafibrillar fluid volume. R is the universal gas constant, T is the absolute temperature and c_{ext} is the external salt concentration. The osmotic (ϕ_{int}, ϕ_{ext}) and activity coefficients ($\gamma_{int}, \gamma_{ext}$) are implemented as proposed by Huyghe and Janssen [44].

At each integration point the total stress is given by the sum of the stresses in the non-fibrillar matrix and the fibril stresses minus the intradiscal pressure:

$$\boldsymbol{\sigma}_{tot} = \boldsymbol{\sigma}_{non-fibrillar} + \rho_c \sum_{\text{all fibers } i} \sigma_f^i \vec{e}_f^i \vec{e}_f^i - p \mathbf{I} \quad (3.5)$$

where $\boldsymbol{\sigma}_{non-fibrillar}$ is the stresses in the non-fibrillar matrix, \mathbf{I} the unit tensor, ρ_c is collagen density, σ_f^i is the fibril stress and in each fibril \vec{e}_f^i is the unit vector pointing in the direction of the i^{th} fibril (Figure 3.1).

The intradiscal pressure p is defined through:

$$p = \mu^f + \Delta\pi, \quad (3.6)$$

with the chemical potential μ^f and the osmotic pressure ($\Delta\pi$).

The stress-free state is different from the unloaded state of the disc and defined as the state of the tissue when in contact with a saturated salt solution, i.e. the state of the tissue in which osmotic pressure ($\Delta\pi$) in Equation (3.4) approaches zero.

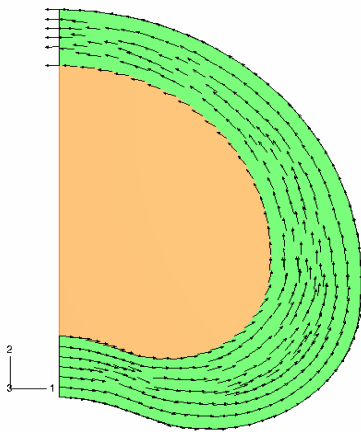


Figure 3.1: 2D fiber plot of one family of fibers in the disc model; the arrows show the projected fiber orientation in each integration point. The fiber density is uniformly distributed over the annulus (green). The fibers are oriented parallel to the outer curvature of the FE model at an angle of ± 30 degrees to the transversal plane. There are no fibers simulated in the nucleus (orange).

The model was implemented in ABAQUS v6.3 (ABAQUS Inc., Pawtucket, RI, USA). The subroutine UMAT was used to define the material behavior of the total solid matrix. An updated Lagrange procedure was used to account for geometric and physical nonlinearities of the model.

The element type, used for this computation a 3D 8-node brick element, has 8 integration points. Each node has 4 degrees of freedom: the 3 displacements plus the chemical potential of the fluid, which is the difference between the hydrostatic pressure and the osmotic pressure. To account for the fiber orientation independently from the discretisation of the finite element mesh, the fibril stresses are computed in each integration point of the element [126,127].

Disc mesh

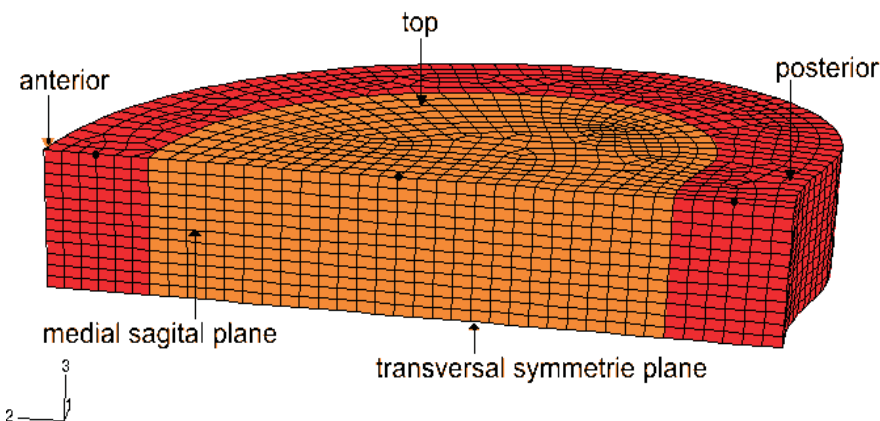


Figure 3.2: Finite Element mesh of $\frac{1}{4}$ of IVD with differentiation in the nucleus pulposus (orange) and the annulus fibrosus (red), in the stress-free state; black dots show node selection for Figure 3.3.

A simplified geometry of a human lumbar disc (L₄/L₅) is chosen (Figure 3.2). The model disc geometry is based on anatomical measurements of the typical geometry (outer curvature, bulging posterior, lateral) of a human lumbar vertebra. Because symmetry towards the transversal and sagittal plane is assumed, the whole disc geometry is reduced to 1/4 of the size. The mesh consists of 4776 3D 8-node elements for the nucleus pulposus and 4188 3D 8-node elements simulating the annulus fibrosus.

The upper (top) surface of the mesh is the interface between the vertebra and the disc. The lower surface of the mesh is the transversal symmetry plane of the disc. The vertical plane is the sagittal symmetry plane. The height of the finite element mesh is 6mm, the length from anterior to posterior is 36mm and the distance from medial to lateral is about 22mm, ensuing in a whole disc of 12mm height and a surface of 15cm² in total. In the analysis it is assumed that the interfaces between vertebrae and disc are flat surfaces parallel to each other. The initial mesh (Figure 3.2) is the shape of the tissue in equilibrium with a saturated salt solution.

The disc geometry, material parameters and boundary conditions are symmetric with respect to the medial and transversal plane. Across the interface between nucleus and annulus there is free fluid flow and no sliding.

3.3.2 Boundary conditions

Along the transversal symmetry plane, because of symmetry, we assume no axial displacement and no fluid flux across the plane. Along the sagittal symmetry plane, again because of symmetry, we assume the displacement normal to the plane and the fluid flux across the plane to vanish. Along the vertebra-disc interface we assume the anterior-posterior displacement and the lateral displacement to vanish because the bone is stiff relative to the disc. For the same reason we tie the axial displacement of all the nodes along the vertebra-disc interface to each other, allowing the distance between the 2 vertebrae to change. The fluid chemical potential along the interface is set equal to the chemical potential of the blood plasma (745kPa) in the vertebra. Along the outer boundary of the disc, we neglect the force exerted by the surrounding tissues and we assume the fluid chemical potential to be equal to the same value as along the vertebra-disc interface, i.e. that of physiological salt concentration.

The initial mesh is equilibrated with a hypertonic salt solution. First the stress, the pressure and the chemical potential are calculated for the physiological unloaded state of the disc by reducing the saturated external salt concentration to 0.15M. In other words, the disc is brought into its physiological unloaded state in equilibrium with a physiological salt solution (step 1), while the disc is gripped between the two vertebrae. This restrains the disc from swelling freely and allows the disc to develop its osmotic pressure. During the first step ions flow out of the mesh and water flows in, this causes the tissue to swell. Due to this the annulus bulges out (Figure 3.4 top). In steps 2 to 4, the disc is axially loaded and step 6 again simulates the physiological unloaded state (Table 3.1). The magnitudes of load have been chosen from frequently applied values in the literature.

Table 3.1: Different loading steps for the simulations and the salt concentration applied at the endplate and outer annulus.

Step	Loading	Salt concentration
1	constrained swelling, no axial loading	0.15 M
2	Increasing axial load from 0 to 500 N (3600s)	0.15 M
3	Constant axial load of 500 N	0.15 M
4	Increasing axial load from 500 to 1000 N (3600s)	0.15 M
5	Constant axial load of 1000 N	0.15 M
6	Decreasing axial load to 0	0.15 M

Table 3.2: A set of material parameters for finite element simulation with fibril-reinforced poroviscoelastic swelling model. Because the model is poroviscoelastic, the Poisson's ratio in the table relates to the porous solid, not to the solid filled with fluid. Therefore, the Poisson's ratio is very different from its incompressibility value of 0.5 [99].

Material parameters	Input value		References
	Nucleus	Annulus	
Young's modulus	0.15 MPa	1.5 MPa	[33, 41]
Extra-fibrillar fluid fraction [per wet weight]	70%	60%	[106]
Fixed charge density [mE/ml]	0.24	0.18	[33, 106]
Viscoelastic properties of collagen fibers	-	$E_o=3.337\text{MPa}$ $E_e=380.8\text{MPa}$ $\eta=1.53\times 10^3\text{MPa s}$	[98]
Poisson Ratio	0.17		[5,32,54,83]
Hydraulic Permeability	$5.0 \times 10^{-16}\text{ m}^4/\text{Ns}$		[26, 33, 41,54]

3.3.3 Material properties

The material properties include extrafibrillar fluid fraction, hydraulic permeability, fixed charge density, matrix stiffness, Poisson's ratio and viscoelastic properties of collagen fibers (Table 3.2). To account for the shielding of the intrafibrillar water by the collagen, the values of fixed charge density are the extrafibrillar values. During the simulation the gas constant is 8.31878×10^3 J/mol*K, the absolute temperature is 310K and the external salt concentration (c_{ext}) of 0.15 mmol/mm³ is kept constant during all loading steps.

The material parameters chosen from literature are mostly derived from measurements of tissue in an equilibrium state. This leads to a conflict with our assumption of a stress free state before starting the simulation. To account for this discrepancy between initial conditions in experiments and models, Wilson et al. [126] integrated an initial step into the simulation. During this first step the model is allowed to equilibrate to a physiological salt solution of 0.15M. The chosen material parameters, taken from literature, are derived from measurements of disc tissue in a swollen equilibrium, i.e. the state of the model at the *end* of the first step. Therefore, the initial material properties of the model (fixed charge density, fluid fraction) – i.e. the material properties at the *beginning* of the first step – were estimated recursively through an initial step. For more details the reader is referred to Wilson et al. [126].

3.4 Results

The extrafibrillar fluid content reaches about 70% for the nucleus at the beginning of step 2, while the fluid content for the annulus is about 10% lower. Thereafter, loading of the disc tissue decreases the water content of the disc. Applying an axial load of 1000N to the model decreased the fluid content in the annulus by about 8%, which is an average value between anterior and posterior side. A fluid decrease of about 6% was seen in the nucleus region after step 4. By the end of step 5 (loading disc with 1000N for 3600s) the fluid content decreased by about 11-12% for both nucleus and annulus. Following the load removal in step 6 the fluid content of the disc model reached the same condition subsequent to step 2 (Figure 3.3).

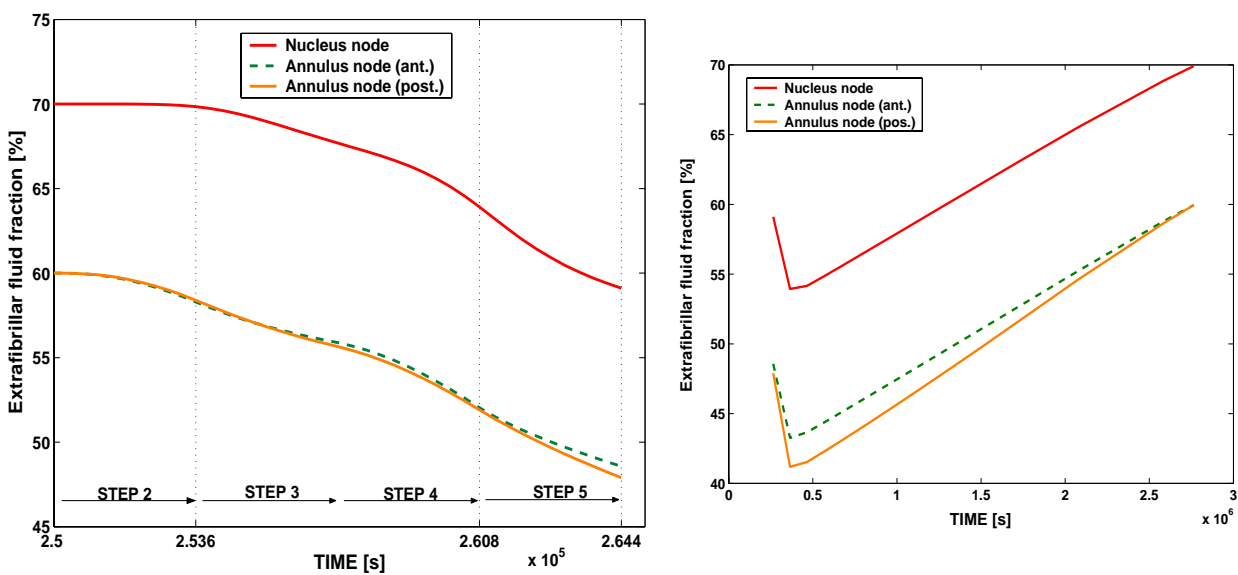


Figure 3.3: The extrafibrillar fluid fraction on different nodes (black dots in Figure 3.2) from the anterior to the posterior side in the nucleus and annulus during step 2 (start loading) to step 6 (fully unloaded). The left figure shows the loading steps 2-5, with a time scale of 3600s for each step, while step 6 (right figure) simulates a resting period; in with the fluid is regained after load removal.

The disc generated an intradiscal pressure of 0.18MPa in the nucleus pulposus after step 1 (Figure 3.4 left). The different loading steps had the following impact on the pressure: a linear increasing axial load of 500N (over 3600s) rose the intradiscal pressure to 0.56MPa in the nucleus.

During step 3 no load change occurred and the load was kept constant, which slightly decreased pressure in the center of the nucleus. A linear increasing axial load (step 4) of 1000N (over 3600s) enlarged the pressure to a maximum of 0.70MPa in the nucleus (Figure 3.4 right).

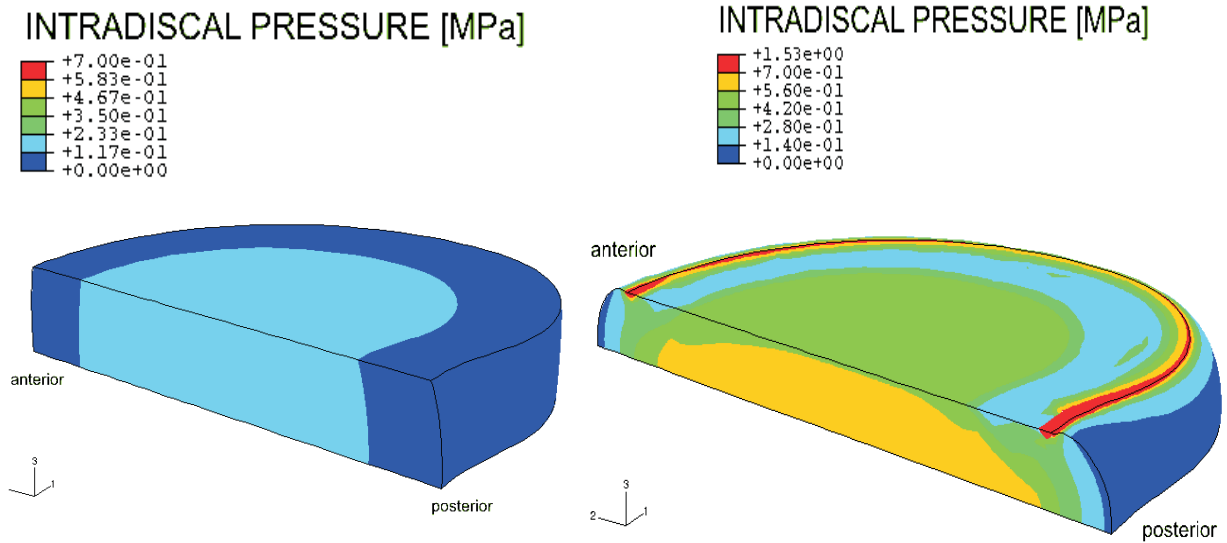


Figure 3.4: Color plot of unloaded model (left) and axially loaded model with 1000N (right) showing the intradiscal pressure. The highest noticeable pressure (ca. 0.7MPa) starts from the transversal plane to the top plate on the medial sagittal plane with a concentration in the center of the nucleus. The pressure in the inner annulus neighboring the nucleus also increased.

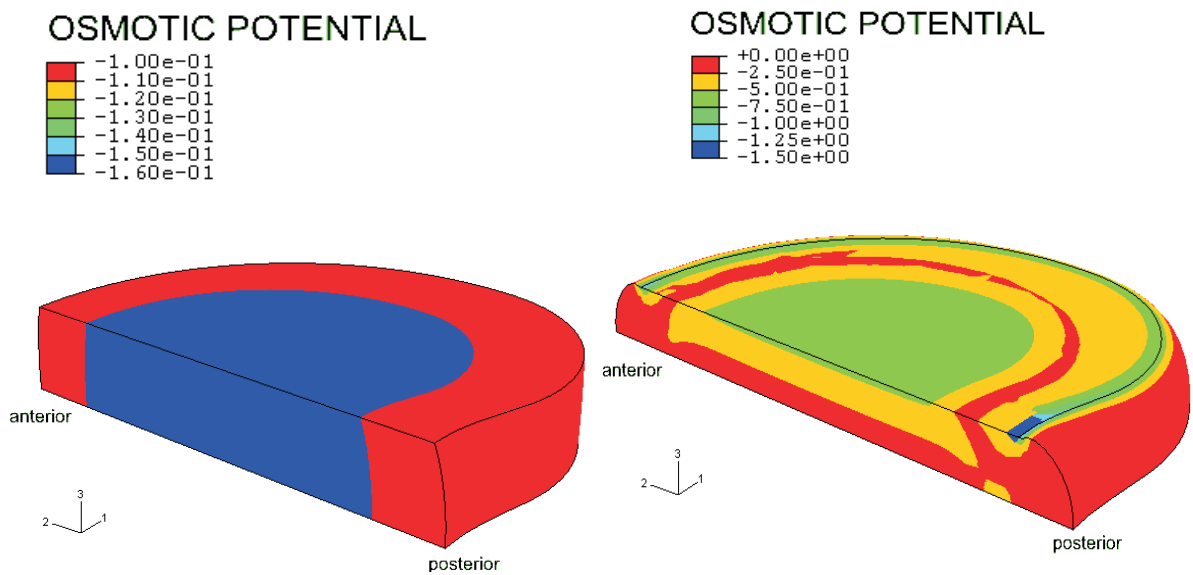


Figure 3.5: Color plot of an unloaded model (left) and an axially loaded model with 1000N (right), showing the osmotic potential (the negative of the osmotic pressure). After swelling, during the first step, osmotic pressure is highest in the nucleus pulposus, while the osmotic pressure in the annulus is about 40% lower. After loading, the osmotic pressure rises first close to the outflow boundaries. When the fluid is pressed out, the fixed charge density concentration increases, which results in an increase of osmotic pressure.

After swelling, during the first step, the osmotic pressure was highest in the nucleus pulposus. The osmotic pressure in the annulus was about 40% lower and was distributed evenly from the anterior to posterior side (Figure 3.5 left). Loading the disc changed the osmotic pressure distribution as follows: the osmotic pressure rose sharply at the outflow boundaries. When the fluid was pressed out, the fixed charge density concentration rose correspondingly, that resulted in an increase of osmotic pressure (Figure 3.5 right). As time proceeded and the load was maintained, the high osmotic pressure region spreads away from the outflow boundary.

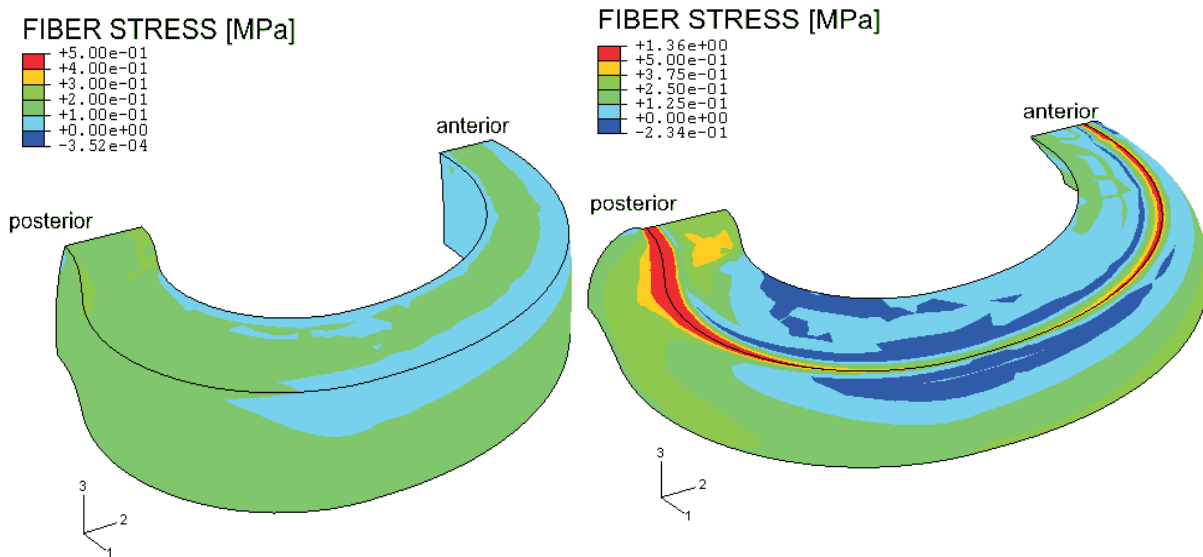


Figure 3.6: Color plot of an unloaded model (left) and an axial loaded model with 1000N (right) showing the fiber stress in one family of fibers. While the model was unloaded during the constrained swelling (step1), a prestressing of the collagen fibers was observed. The fiber stress in the nucleus was set to zero, thus, the nucleus was not plotted here.

The color plots in Figure 3.6 show the stresses for one family of fibers. The impact of the tissue swelling tendency on the collagen fibers can clearly be seen after step 1. A prestressing of the collagen fiber is noticed without any external loading. Stresses are high on the outward bulging of the disc starting from the posterior and anterior side and decreasing slightly towards the lateral side of the annulus. Stress concentrates posteriorly and anteriorly on the top plate of the model, while the area of high stress is much larger on the posterolateral side than on the anterior side. Much lower stresses were observed in the nucleus since the model only implements fibers in the annulus.

3.5 Discussion

Because intervertebral disc cells are sensitive towards osmotic pressure and hydrostatic pressure changes, the primary aim of our work was to predict these quantities. For the first time, in this chapter a novel 3D FE model of the disc is described in detail. This model is a very useful tool to simulate finite deformations 3D osmotic viscoelasticity of the swelling intervertebral disc.

The computed axial stress profiles reproduced the main features of stress profiles, in particular the characteristic posterior and anterior stress peaks, which were observed experimentally by McNally et al. [74]. Stress profilometry measurements in intact disc post mortem by McNally et al. [74] revealed that stresses in the nucleus were nearly constant, whereas high peaks of compressive stress were found on the posterior and anterior side of the annulus. The posterior side experienced the highest compressive stress peaks in the experimental [4,74] as well as in the numerical results (Figure 3.7). The comparison of the stress profile showed that the computed stress peaks were larger than the experimental measured stress peaks. One of the reasons could be that the model does not account for a transition zone between annulus and nucleus, which resulted in a discontinuity of the material parameters. Another reason for this could be the choice of material parameters for the non-fibrillar matrix and the fibrillar matrix. The non-fibrillar matrix properties were based on literature data of the intervertebral disc, while the fibrillar matrix properties were from validated articular cartilage properties [126,128].

These peaks may partly explain the prevalence of postero-lateral herniation in humans [28,73]. The non-homogenous stress distribution observed experimentally and numerically, questions the plane stress assumption by Iatridis et al. [48] in their simulations of the PEACE model. The plane stress assumption requires the total stress to be homogeneous while the present simulation clearly demonstrated gradients in total stress in the outer annulus region (Figure 3.7).

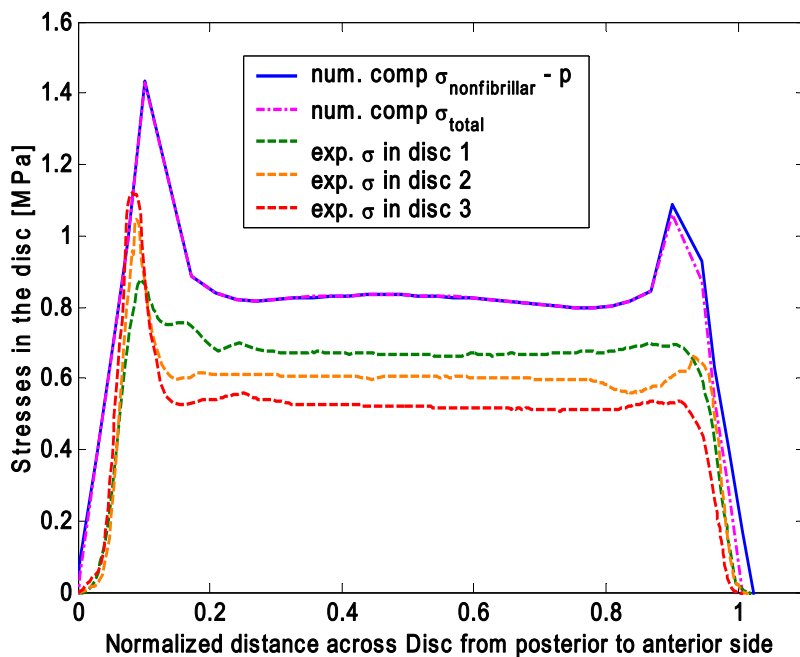


Figure 3.7: Comparison of experimental stress results from McNally and coworkers [74] of human disc with the numerical predictions of compressive (comp) stress from the presented model. For the total stress (σ_{total}) and the nonfibrillar matrix stress ($\sigma_{nonfibrillar}$) minus the hydrostatic pressure (p), stress peaks are seen on the posterior and anterior side of the annulus, while nearly constant stresses are noticed in the nucleus.

Unlike previous models [6,65,99] our model took the intradiscal pressure in the unloaded state to be non-zero, and its predictions showed that it maintained a finite value even after hours of loading. This finding was in agreement with the pressures measured *in vivo* by Nachemson [79] and Wilke et al. [122]. The high intradiscal pressure along the edge of the vertebrae may be un-physiological (Figure 3.4). The same holds for the high osmotic pressure along the edge of the vertebrae (Figure 3.5). These findings may be due to the rigid body behavior of the vertebrae in the model which, according to Brinckmann et al. [15] and Iatridis et al. [49], is not realistic.

During constrained swelling - the first step of our simulation - an increase in intradiscal pressure was observed, which led to prestressing of the collagen fibers even before load was applied; neglecting this effect underestimates the stresses and strains in the collagen structure. This prestress has been considered by others; one approach for considering the prestressing of the annulus fibers is through the implementation of a stress offset (σ_{offset}), as done by Iatridis and coworkers [50]. Their *in vitro* experimental findings were consistent with the *in vivo* experimental results of subjects in the supine position [79,122] as these findings indicated the presence of residual stresses in the unloaded disc. Huyghe et al. [44] found significant offset stresses in confined compression and swelling *in vitro* of canine annulus tissue.

The present numerical analysis, in contrast to Iatridis et al. [50], does not include a priori-offset stress: it computes the prestressing from physical principles of osmosis and experimentally quantified material parameters. This high osmotic pressure in the unloaded disc is achieved in the model by reducing the hypertonic external salt concentration to a physiological salt concentration. These changes result in swelling (Step 1), which is constrained by sandwiching the disc between two vertebral bodies; a hydrostatic pressure of 0.2MPa arises in the nucleus pulposus (Figure 3.4), and the fluid content increases to almost 70-72% (Figure 3.3).

Recent experimental results demonstrated that disc cell responses are strongly influenced by osmolarity [81]. Therefore, in order to correctly understand the patterns of disc degeneration, the inclusion of the swelling process into the disc model is required.

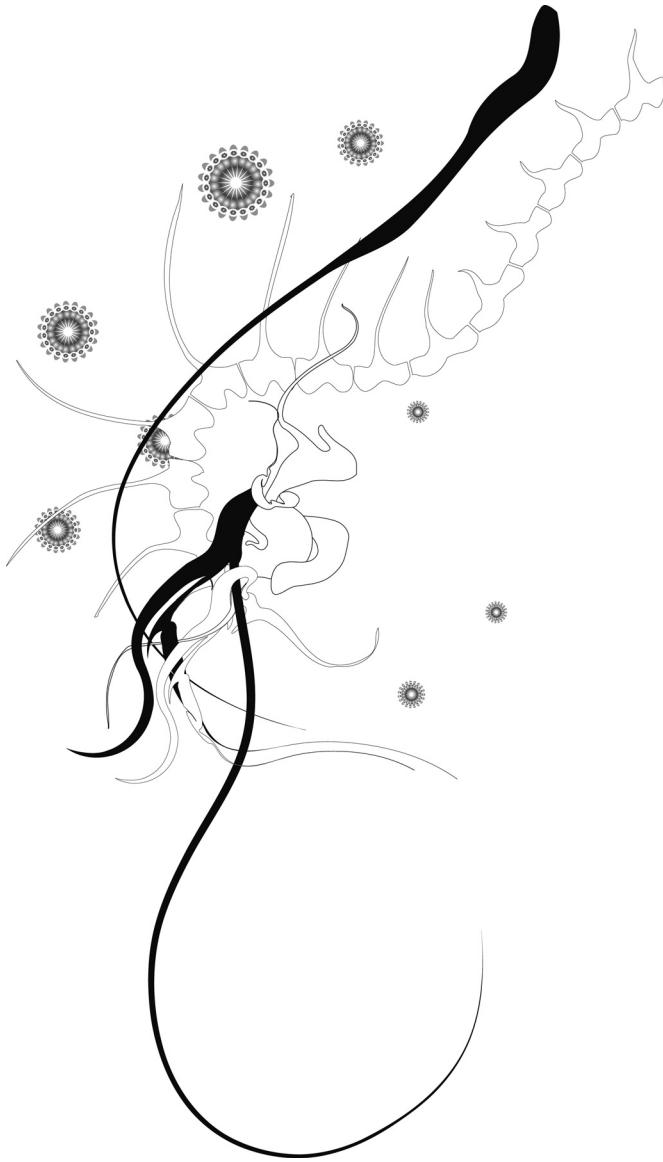
As the collagen fibers are introduced individually into the poroviscoelastic swelling model [126], separate predictions of stresses in the collagen fibers and in the matrix are possible. The total stress of the tissue is the sum of the effective stress in the ground matrix (solid) plus the fiber stresses minus the hydrostatic pressure (Equation 3.5 & 3.6). The computed stresses are defined per unit area of disc tissue. To evaluate the fiber stresses per unit area of fiber, the computed stresses have to be divided by the fiber volume fraction, resulting in much higher values.

As the model explicitly includes swelling, properties evaluated for biphasic or monophasic models [7,29] only give indirect clues for the elastic properties to be substituted into the model. Because the contribution of the proteoglycans to the aggregate modulus is mostly integrated into the model through osmosis, the value of the model parameters should be closer to the trypsin treated values than the non-trypsin treated values.

The Young's modulus of the nucleus pulposus was chosen to be 0.15MPa. Together with the Poisson ratio of 0.17, this resulted in an aggregate modulus of 0.16MPa. Perie et al. [84] measured aggregate moduli of nucleus pulposus and found 0.04 ± 0.02 MPa for

trypsin treated nucleus pulposus and 0.58 ± 0.12 MPa for non-trypsin treated. It has been shown that the permeability [54,84] for the nucleus and annulus are different. For simplicity, we assume homogenous hydraulic permeability. Maroudas et al. [69] presented swelling data showing that intrafibrillar water content is modulated by the extrafibrillar osmotic pressure. For simplicity this effect has not been integrated into our disc model.

The volume and fluid content of the disc depend on the loading condition. These conditions lead to an outward bulging of the outer annulus. The largest noticeable deformations were on the posterior side of the model. Observed strains exceed locally up to 20%, hence justifying the need for a finite deformation analysis.



Chapter 4

Intra and extrafibrillar fluid exchange in the disc

The content of this chapter is based on an article in *Journal of Orthopaedic Research*, Oct (10): 1317-24: "Are disc pressure, stress and osmolarity affected by intra and extrafibrillar fluid exchange?"

Y. Schroeder
S. Sivan
W. Wilson
Y. Merkher
J.M. Huyghe
A. Maroudas
F.P. T. Baaijens

4.1 Introduction

The mechanical properties of the intervertebral disc are regulated by its biochemical composition. With ageing and degeneration the water content of the disc decreases which highly influences the mechanical properties. The annulus fibrosus (AF) consists of collagen, which provides tensile strength, and proteoglycans (PG's), which due to their strong swelling ability [41,107,110] ensure tissue hydration. The swelling propensity in the nucleus is even more pronounced. As discussed in chapter 3 the initial osmovoelastical 3D finite element (FE) model [95] demonstrated that the inclusion of osmotic forces significantly affect stress distribution in the human disc, which is in agreement with earlier work [48]. The initial model predicts intradiscal pressures in the order of 0.1-0.2MPa in unloaded discs, which is in agreement with experimental measurements [122].

Osmotic forces have a major impact on crack opening and propagation [129] and on cellular responses [22,82,97]. In particular, osmosis provides an understanding on why fissures in the degenerating disc are so poorly related to external mechanical load [115]. Although osmotic pressures are an order of magnitude lower than external mechanical load, decreasing osmosis in the degenerated disc does cause local stress concentration which might cause crack propagation [47]. Wognum et al. [129] demonstrated, by means of two intervertebral disc models, that the high osmolarity in a healthy disc protects the disc against patency and propagation of cracks. The mechanism underlying this protective effect is best understood in the context of Starling's law. This law states that the driving force of fluid flow from the crack to the medium is governed by the gradient of the chemical potential of water. The chemical potential is the difference between hydrostatic pressure and osmotic pressure ($=\text{gas constant times absolute temperature times osmolarity}$). A crack in a healthy young disc is surrounded by high osmotic pressure tissue, causing the fluid to leave the crack and the crack to close. Degeneration of the tissue causes the osmotic pressure of the tissue to decrease, due to loss of proteoglycans (PG's), leading the fluid into the crack. Therefore, patent cracks are observed in the degenerated disc. Wognum et al. [129] did not account for intrafibrillar water in either of their models.

Changes in water content of the disc are controlled primarily by the difference between the externally applied pressure and the disc's swelling pressure. The latter depends mainly on effective stress and the fixed charge density (FCD), which in turn depends on PG content. This swelling tendency is magnified by the partial shielding of the water by the collagen [107]. PG's, due to their size, cannot penetrate the intrafibrillar space (Figure 4.1). Hence, to predict the osmotic pressure of the disc from its PG content, the latter must be determined on the basis of the extrafibrillar water (EFW) only [100,108]. Sivan et al. [100] used low-angle X-ray scattering and osmotic stress techniques to determine the lateral packing of the collagen molecules in the annular fibrosus of young and old human intervertebral disc. They found that the lateral packing, and hence the intrafibrillar water content, depends on age, external osmotic pressure, and location in the tissue. Subtracting intrafibrillar water (IFW) from total hydration yields the amount of extrafibrillar water, from which the accurate fixed charge density of the tissue can be estimated.

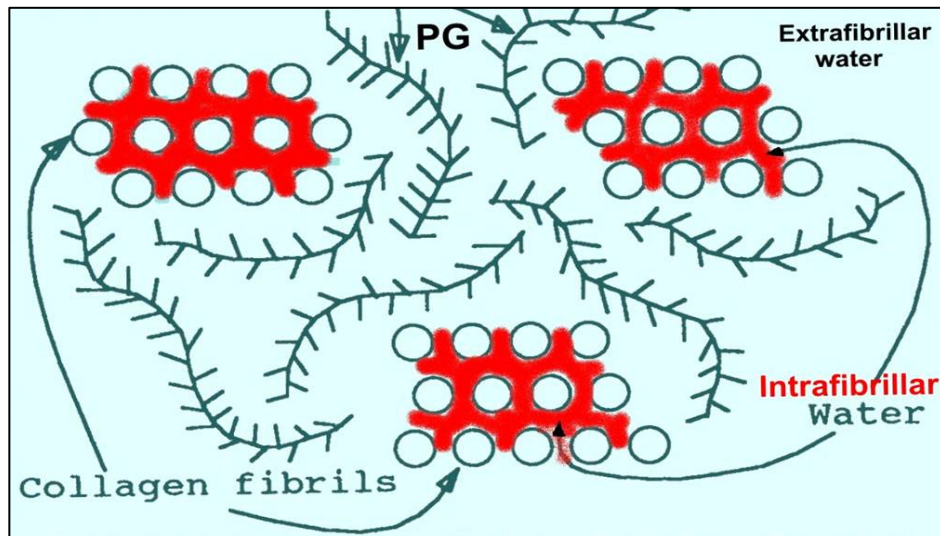


Figure 4.1: Schematic drawing of extracellular matrix with differentiating the total water content of the tissue into intrafibrillar and extrafibrillar water (adapted from Urban & McMullin [108], personal communication).

Huyghe & Janssen [45] integrated the concepts of intrafibrillar water as proposed by Maroudas and Bannan [68] for articular cartilage, and Urban and McMullin [108] for nucleus pulposus intervertebral disc, into the Mixture Theory. The resulting set of partial differential equations is a generalization of the earlier quadriphasic model [44], and was used by Huyghe et al. [43] for the analysis of one-dimensional swelling and compression experiments of canine annuli fibrosi samples. Wilson et al. [124] simplified the equations of Huyghe & Janssen [45] by assuming the ionic constituents to be in equilibrium with the physiological boundary conditions. They showed that the depth dependence of the stress-strain curve of articular cartilage is predicted solely from the depth dependence of the composition of the tissue. In this analysis, the intrafibrillar water was a key element.

As the stress state of the intervertebral disc is essentially triaxial, a 3D FE model was mandatory for this study. Hence, we extended the initial 3D osmoviscoelastic FE model of the disc (chapter 3) [95] to account for the IFW content and for the solid fraction dependency, to study the effects of water differentiation on the intradiscal pressure and stress distribution throughout the tissue. This was done along the lines of Wilson et al. [123,124].

4.2 Material and Methods

The initial 3D osmoviscoelastic FE model of the disc (chapter 3) [95] was extended to include the intrafibrillar water dependency. Additionally, the material properties were made directly dependent on the tissue composition. This relationship was the same for all areas of the disc, that is, the same for annulus and nucleus. Hence, the difference in composition of annulus versus nucleus caused the material properties of both tissues to differ. A brief overview of the most important adaptations for this specific study is given below, because the adaptations of the fibril-reinforced poroviscoelastic FE model are thoroughly described elsewhere [124].

4.2.1 Rule of Mixtures

In the previous chapter [95] we used the following description for the effective stress σ_e

$$\sigma_e = \sigma_{nf} + \sum_{i=1}^{totf} \sigma_f^i, \quad (4.1)$$

where σ_{nf} is the stress in the non-fibrillar matrix, and σ_f^i the fibril stress in the i^{th} fibril with respect to the global coordinate system. We assumed that the fibril network is smeared out over the non-fibrillar matrix, ensuring that the fibrillar component – and in particular the fiber orientation - is independent from the coarseness of the finite element mesh (chapter 3) [95]. To account for the distinct volumes of the different components, the present model included the solid fraction dependency according to the rule of mixtures.

This rule is based on the following assumptions: (i) a finite number of components is present in each infinitesimal volume of the composite material; (ii) each component contributes to the total material behavior in the same proportion as its volumetric participation; (iii) all components have the same strains. When the rule of mixtures is used, the effective stress becomes [124]:

$$\sigma_e = \left(1 - \sum_{i=1}^{totf} \rho_c^i\right) \sigma_{nf} + \sum_{i=1}^{totf} \rho_c^i \sigma_f^i, \quad (4.2)$$

with ρ_c^i the volume fraction of the collagen fibrils in the i^{th} direction with respect to the total volume of the solid matrix. Because the solid is assumed incompressible, the relative fractions of the fibrillar and non-fibrillar matrix remain constant.

With Equation (4.2) the total tissue stress becomes [124]:

$$\sigma_{tot} = -\mu^f \mathbf{I} + n_{s,0} \left(\left(1 - \sum_{i=1}^{totf} \rho_c^i\right) \sigma_{nf} + \sum_{i=1}^{totf} \rho_c^i \sigma_f^i \right) - \Delta \pi \mathbf{I}, \quad (4.3)$$

where μ^f is the water chemical potential, $\Delta\pi$ the osmotic pressure gradient, σ_{nf} the stress in the non-fibrillar matrix, $n_{s,0}$ the initial solid volume (in the unloaded and non-swollen state), and σ_f^i the fibril stress in the i^{th} fibril with respect to the global coordinate system.

As described in chapter 3, the model distinguishes between an elastic non-fibrillar solid matrix, a fibrillar matrix and an osmotically prestressed extrafibrillar fluid [95]. The non-fibrillar solid matrix is described through a modified Neo-Hookean law, while the fibrillar matrix accounts for the viscoelastic properties of the collagen fibers [123,124].

4.2.2 Osmotic swelling

Because we assumed the ion concentrations to be in equilibrium at all times, the biphasic swelling theory [125] is applicable to describe the swelling behavior. The osmotic pressure gradient is then given by

$$\Delta\pi = \phi_{int} RT \left(\sqrt{c_F^2 + 4 \frac{(\gamma_{ext}^{\pm})^2}{(\gamma_{int}^{\pm})^2} c_{ext}^2} \right) - 2\phi_{ext} RT c_{ext} \quad (4.4)$$

with c_{ext} the external salt concentration and c_F the FCD per unit total water volume. The osmotic (ϕ_{int} , ϕ_{ext}) and activity coefficients (γ_{in} , γ_{ext}) are implemented as proposed by Huyghe et al. [43]. Note that the current FCD is a function of the volumetric deformation (J) of the tissue as [126]

$$c_F = c_{F,0} \frac{n_{f,0}}{n_{f,0} - 1 + J} \quad (4.5)$$

Inclusion of intra- and extrafibrillar water

When the distinction between intrafibrillar and extrafibrillar water is taken into account, the effective FCD should be expressed as mEq fixed charges per ml extrafibrillar water. Hence, the effective FCD becomes

$$c_{F,exf} = \frac{n_f c_F}{n_{exf}} \quad (4.6)$$

According to Urban and McMullin [109] and Maroudas et al. [69] the amount of extrafibrillar water is then given by

$$n_{exf,m} = n_{f,m} - n_{inf,m} = n_{f,m} - \phi_{ci} \rho_{c,tot,m}, \quad (4.7)$$

where $n_{f,m}$ and $n_{inf,m}$ are the mass fraction of total and intrafibrillar water, respectively, ϕ_{ci} a parameter that defined the mass intrafibrillar water per collagen mass, and $\rho_{c,tot,m}$ is the collagen mass fraction with respect to the total wet weight, which is given by

$$\rho_{c,tot,m} = (1 - n_{f,m}) \sum_{i=1}^{toif} \rho_c^i \quad (4.8)$$

The osmotic pressure gradient $\Delta\pi$ from Equation (4.4) is then given by

$$\Delta\pi = \phi_{int} RT \sqrt{c_{F,exf}^2 + 4 \frac{\gamma_{ext}^{\pm 2}}{\gamma_{int}^{\pm 2}} c_{ext}^2} - 2\phi_{ext} RT c_{ext} \quad (4.9)$$

Permeability

When accounting for the fact that only the extrafibrillar fluid can flow out of the tissue, the permeability becomes

$$k = k_0 \left(\frac{1 - n_{exf,0}}{1 - n_{exf}} \right)^M, \quad (4.10)$$

where k_0 is the initial permeability, M a positive constant, $n_{exf,0}$ the initial extrafibrillar fluid fraction and n_{exf} the current extrafibrillar fluid fraction.

4.2.3 Finite element model

The FE mesh was based on a simplified geometry of a human lumbar disc (L₄/L₅) (Figure 4.2) [95]. Because symmetry about the transversal and sagittal plane was assumed, the mesh was reduced to 1/4 of the size of the disc.

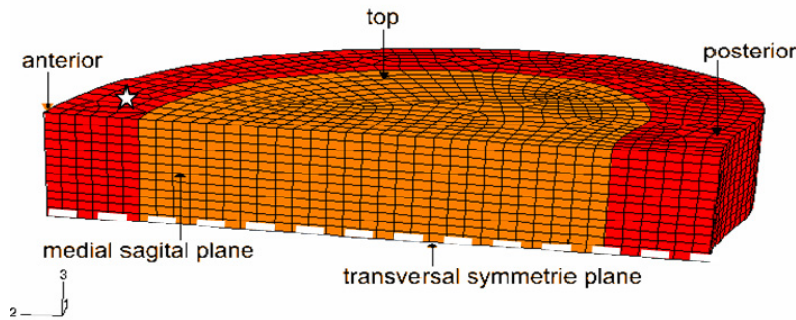


Figure 4.2: Finite element mesh of 1/4 of an IVD with differentiation in nucleus (light) and annulus (dark) regions in the stress-free state, with selected node (white star) and node path (white dashed line) for comparison.

The same boundary conditions and loading steps were applied, as previously described in chapter 3 [95]. During the first step the initial mesh was equilibrated with a hypertonic salt solution. Hence, the disc was brought into its physiological unloaded state in equilibrium with a physiological salt solution, while the disc was gripped between the two vertebrae. The vertebrae were assumed infinitely stiff. This restrained the disc from swelling freely and allowed the disc to develop its turgor. In steps 2 to 4, the disc was axially loaded over a time of 3600s each and step 6 again simulated the physiological unloaded state. The magnitudes of load (500N → 1000N) were the same as used in the study of chapter 3 [95].

The material properties of the non-fibrillar matrix were chosen from literature [95], while the fibrillar matrix properties were based on validated articular cartilage properties [126] as described in more detail in the previous chapter 3. To account for the effects of the material properties choice especially for the fibrillar matrix, an additional computation was included with an increase of the fiber stiffness. Because the material properties were directly dependent on the tissue composition, the composition shown in Table 4.1 was used for human intervertebral disc. In comparison to the applied composition in chapter 3, this composition data was obtained from the same samples as used for the IFW measurements and not taken from literature. Hence, for this study the composition data (Table 4.1) was updated.

Table 4.1: Applied composition for all simulations taken from experimental data of human disc tissue [100, unpublished data of Sivan et al.].

Composition parameters	Annulus	Nucleus
Fixed charge density [mE/ml]	0.15	0.3
Fluid fraction [% wet weight]	77	82.5
Collagen content [% dry weight]	48	0.9

Intrafibrillar water

In the previous chapter, we used a correction factor to account for the influence of intrafibrillar water [95], based on the work of Urban and McMullin [108] on the swelling pressure of nuclei pulposi of human intervertebral discs. They showed that the amount of IFW is approximately 1.33g water per g collagen, for such a low collagen-containing tissue as the nucleus pulposus.

Sivan et al. [100] presented data on the amount of the IFW for a much higher collagen-containing tissue, that is, annulus fibrosus. According to their data, applied load markedly influences IFW content and the accurate fixed charge density. To evaluate the influence of IFW content on intradiscal pressures and stresses, 2 simulations were performed assuming:

1. the IFW content to be zero

2. the IFW content to be varying.

To include the dependency of φ_{ci} on the applied osmotic pressure gradient $\Delta\pi$ in Equation (4.7) for nucleus and annulus tissue separately, the following equations were implemented:

- for human annulus tissue:
$$\varphi_{ci} = 0.5931e^{0.3696\Delta\pi} + 0.9222, \quad (4.11)$$

- for human nucleus tissue:
$$\varphi_{ci} = 0.4794e^{0.3218\Delta\pi} + 0.7410. \quad (4.12)$$

These curves were obtained by fitting an exponential function to the data of Sivan et al. [100, unpublished data of Sivan et al.] (Figure 4.3).

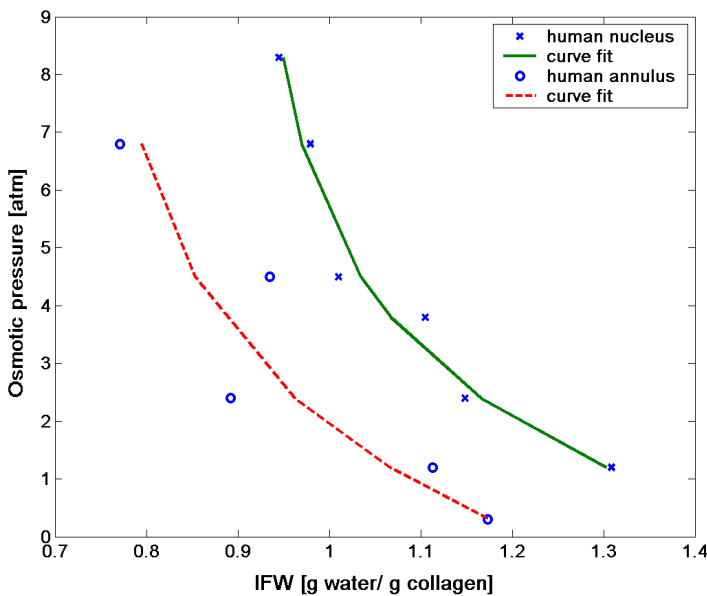


Figure 4.3: To account for the intrafibrillar water (IFW) dependency on the applied osmotic pressure an exponential fit for human annulus and nucleus tissue was implemented [100, unpublished data Sivan et al.].

4.3 Results

For better evaluation of osmolarity changes during different loading steps at specific positions, a node in the anterior annulus region was selected (Figure 4.2). With an increase in axial load (500N → 1000N), the discrepancies in the osmolarity estimations for all simulations increased (Figure 4.4). After applying 1000N, the osmolarity in the first simulation (IFW=0) was 234mOsm. For the second simulation, the osmolarity increased to about 273mOsm at the same location. Relative to the osmolarity of blood (150 mOsm), this was an increase of 46% $[(273-234) / (234-150)]$. Additionally, a specific node path was chosen, crossing the disc from posterior to anterior side, to visualize the intradiscal pressure and stress profiles throughout the disc (Figure 4.2).

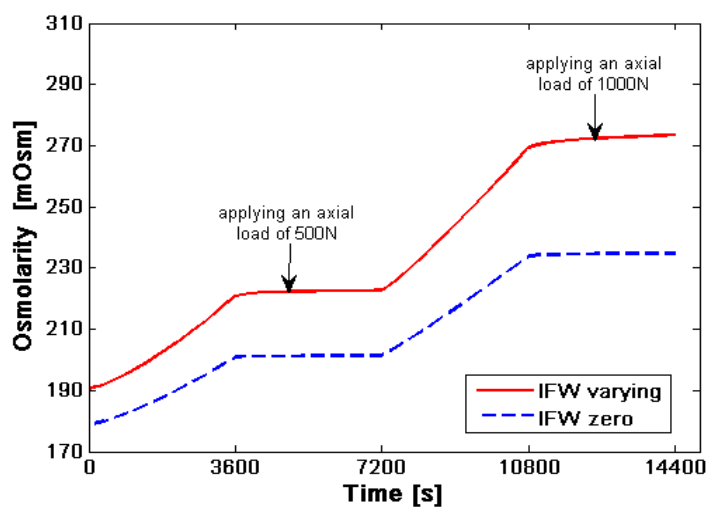


Figure 4.4: Osmolarity changes for comparing simulations with and without accounting for IFW content under different loading steps for one point on anterior side of annulus (Figure 4.2).

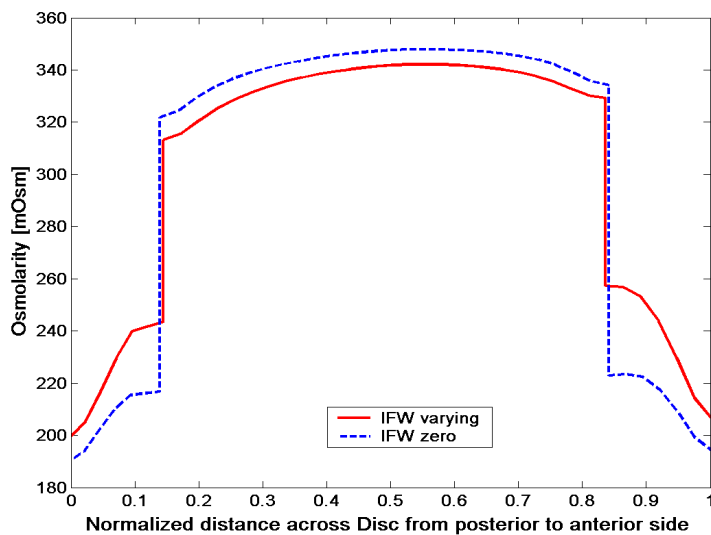


Figure 4.5: Osmolarity profile from posterior to anterior annulus, comparing simulations with and without accounting for IFW content (with a load of 1000N).

Neglecting the intrafibrillar water content led to an underestimation of the osmolarity in the annulus and – to a lesser extent – to an overestimation of the osmolarity in the nucleus (Figure 4.5).

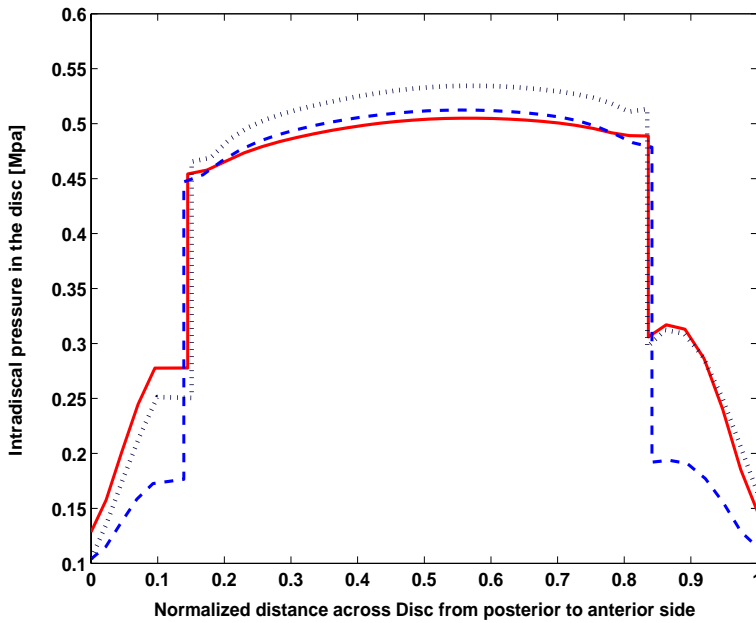


Figure 4.6: *Intradiscal pressure profile from posterior to anterior annulus, comparing simulations with and without accounting for IFW content (with a load of 1000N);*
 Continuous line: *IFW varying with standard fiber stiffness;*
 Dashed line: *IFW zero;*
 Dotted line: *IFW varying with tenfold increase of fiber stiffness.*

The intradiscal pressure was calculated as the sum of the chemical potential and the osmotic pressure (Figure 4.6). No clear difference in the intradiscal pressure for the nucleus region was calculated. The varying IFW content boosts the intradiscal pressure estimations in the annulus region significantly. The highest difference (about 10%) occurred were close to the nucleus region (inner annulus), while it decreased towards the outer annulus. This result was not affected when the fiber stiffness was increased by a factor 10.

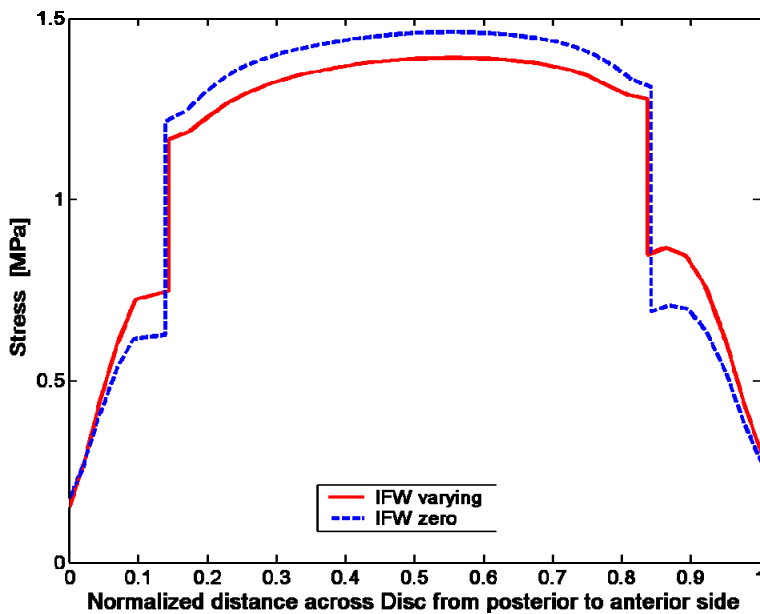


Figure 4.7: *Effective stress profile from posterior to anterior annulus, comparing simulations with and without accounting for IFW content (with a load of 1000N).*

The effective stress was computed as the sum of the total matrix stress plus the solid fraction n_s in the loading direction of the model. When IFW content was not taken into account, a slight under estimation of the effective stresses in the annulus was found (Figure 4.7) and an even stronger underestimation of the pressure. In the nucleus region, however, not accounting for the IFW effect led to an overestimation of the effective stresses (Figure 4.7).

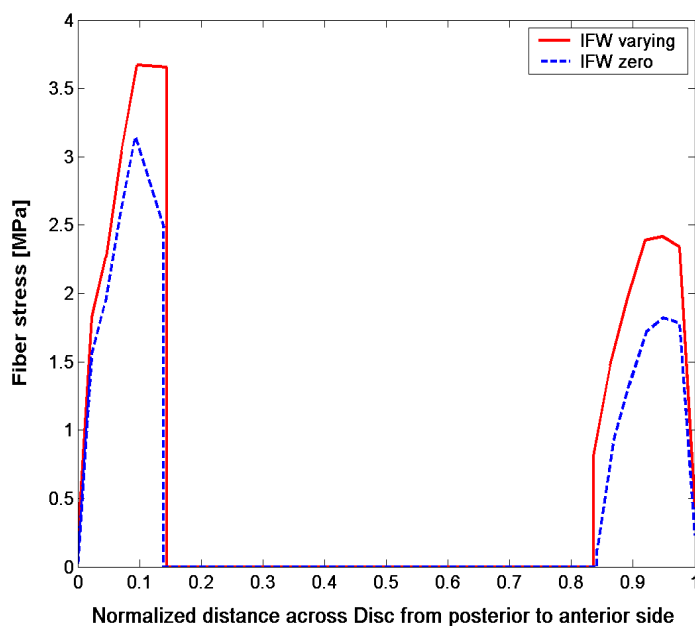


Figure 4.8: Fibril stress profile (plotted for one fiber family) from posterior to anterior annulus, comparing simulations with and without accounting for IFW content (with a load of 1000N)

The fiber stress depends on the collagen fraction and density. In Figure 4.8, only the profiles for one fiber family and direction were plotted. Neglecting the intrafibrillar water influence led to an underestimation of the fiber stresses by up to 20% in the annulus.

4.4 Discussion

The present model is the first finite element model of the disc that accounts for intra-extrafibrillar fluid exchange within the disc. The results show that the intra-extrafibrillar fluid exchange has a substantial effect on the intradiscal pressure, the osmolarity, the axial effective stress distribution and the fiber stress within the disc.

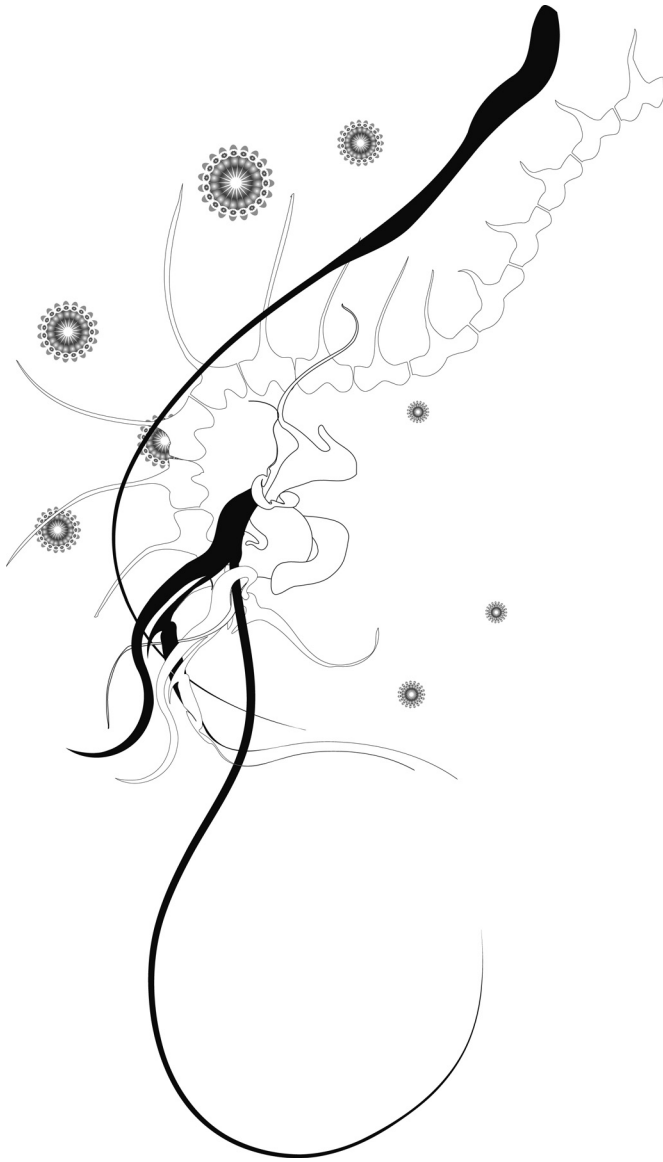
Different repercussions were calculated for the nucleus, with low collagen content, and the annulus with high and oriented collagen content. While intradiscal pressure was more than doubled in the inner annulus, the intradiscal pressure in the nucleus hardly changed. The osmolarity increased in the annulus while it decreased in the nucleus. The axial effective stress profile indicated a redistribution of the load from nucleus to annulus.

The uncertainty of the values of material parameters calls for cautious interpretation of the results. The present calculations indicate that IFW is an important factor in the relative roles of nucleus and annulus in the load bearing capacity of the human disc. Even a tenfold increase in the fiber stiffness did not alter the trend of the results. In the annular region, the IFW effect enhances the disc osmolarity relative to the crack osmolarity substantially, increasing thereby the protecting effect of the high osmolarity within the annulus against patency and against propagation of cracks. The affinity of collagen for water draws water out of the extrafibrillar space, while in turn the water affinity of the counter ions in the extrafibrillar space draws water out of the crack. This dual mechanism keeps micro cracks in the annulus tightly closed. This indicates that IFW may have an important protecting role against herniation. The lower fixed charge density of the annulus relative to that of the nucleus is compensated by the higher intrafibrillar water content.

The stress and pressure profiles for the annulus region showed a strong dependency on the inclusion of the IFW content. The osmolarity and the intradiscal pressure in the annulus were underestimated when the IFW content was neglected. The same effect was noticeable for the effective stresses and the fibril stresses. An additional interesting effect was noticed by comparing the effective stress profiles; neglecting the IFW content leads to an underestimation of the effective stress in the annulus. In the nucleus region on the other hand, an overestimation of the effective stress even with a low collagen content of about 0.9% per dry weight was noticed. This discrepancy might be explained through a load shift from nucleus towards annulus.

The numerical simulations emphasized the importance of including the IFW content for intradiscal pressure and stresses estimation, as the results showed that the intradiscal pressure profile was clearly influenced by the intrafibrillar water. The intrafibrillar water was especially of importance in the collagen-rich annulus fibrosus, because up to 30% of the total fluid may be IFW [101] which influences the swelling and load bearing properties of the disc.

Limitations of this study were the set of material properties chosen for the non-fibrillar and fibrillar matrix in the model. However, our previous results showed that while the model is allowed to equilibrate to 0.15 M NaCl during the first step, the disc model develops an intradiscal pressure of about 0.2MPa [95]. The intradiscal pressure of the model is consistent with measurements of Wilke et al. [122] for intradiscal pressure in a supine position for human discs.



Chapter 5

Material properties and osmotic viscoelastic constitutive law

The content of this chapter is based on an article in *Journal of Orthopaedic Research* (accepted):
“Experimental and Model Determination of Human Intervertebral Disc Osmotic Viscoelasticity”

Y. Schroeder
D. M. Elliott
W. Wilson
F.P.T. Baaijens
J.M. Huyghe

5.1 Introduction

Finite element (FE) models have become an important tool to study load distribution in the healthy and degenerated disc. However, model predictions require accurate constitutive models and material properties [14]. As the mechanical properties of the intervertebral disc are regulated by its biochemical composition and fiber-reinforced structure, the constitutive law describing this complex tissue requires careful consideration [51]. The annulus fibrosus (AF) consists of collagen, which provide tensile strength, and proteoglycans (PG's), which due to their strong swelling ability [41] provide the tissue hydration [107,110]. This swelling tendency is amplified by the partial shielding of the water by the collagen [107]. A high intradiscal pressure in the nucleus is the consequence of the swelling propensity. This intradiscal pressure is balanced by (1) the external load and (2) tensile stresses in the dense collagen fiber structure of the annulus. We previously presented an initial 3D osmovoelastoc model [93,95] which accounts for the interdependency of the swelling ability and the collagen pre-stressing. The initial model predicts intradiscal pressures in the order of 0.1-0.2MPa in unloaded discs, which is in agreement with *in vivo* experimental measurements of Wilke et al. [121] (chapter 3). However, lack of experimental data to determine some of the model parameters limits the applicability of this model.

While numerous studies have investigated the annulus fibrosus compressive [10,26,34,42,50] and tensile properties [1,27,30,34,102], specific conditions required to determine model parameters for the osmovoelastoc model are not available. In compression, previous studies have quantified the load distribution and shift between fibrillar matrix and solid matrix of the annulus. However, in these studies the initial conditions of the swelling behavior before the stress-relaxation experiments, as required for our model have not been established. In tension, previous studies have quantified the annulus elastic behavior [7,27,29,102] or the collagen failure criteria [119] and the viscoelastic nature of the sheep annulus [59] and of collagen type I [98]. However, human annulus nonlinear viscoelastic stress-relaxation behaviors have not been quantified. Unlike the annulus, experimental measurements of compressive properties of the nucleus pulposus tissue have been very limited as the handling of the tissue is hampered by its swelling. Recent confined compression studies, however, have presented biphasic material properties for the nucleus pulposus [53,84].

Therefore, the objective of this study was (1) to complement the existing material testing in the literature with confined compression and tensile stress-relaxation tests on human annulus fibrosus and (2) to use this data, together with existing nucleus pulposus compression data to tune an osmovoelastoc material constitutive law.

5.2 Material and Method

5.2.1 Experiment

Human lumbar annulus fibrosus tissue was tested in confined compression and uniaxial tension. Non-degenerated discs ($n=3$), classified as grade 2 on the Thompson scale were obtained from spines (L1/L2 & L3/L4, age 45-51) [53]. For the nucleus, we used data from a previously published study on human tissue kindly provided to us by Johannessen and Elliott [53]. For each separate experiment, 3 samples from different human disc were chosen. From these datasets, in each experiment the mean values were taken as the average of the 3 specimens at each time interval and the range i.e. maximum and minimum values were obtained.

Confined compression experiment

Confined compression properties of the annulus were measured under the same protocol as previously described for the nucleus pulposus [53]. Briefly, frozen excised tissue samples from the outer annulus were microtomed to ensure uniform thickness and a circular punch was used to prepare uniform cylindrical test samples. Samples were placed in confining chamber and allowed to equilibrate in 0.15M PBS for 5 min, and the compression force was recorded. This was followed by a 3 hours isometric swelling test (1% strain) to define the initial stress state. In addition to this, a 2-hour confined compression (5% strain) and relaxation experiment was used to perform the model fit on.

Tensile Test

To quantify the nonlinear viscoelastic stress-relaxation behavior of human annulus tissue, the following loading protocol was developed. As explained by Guerin and Elliott [37,38] uniform rectangular, circumferentially oriented samples were prepared from the outer annulus for this study. Briefly, frozen excised outer lateral annulus samples were microtomed to ensure uniform thickness and a custom-designed parallel edge razor die was used to obtain rectangular samples. The rectangular annulus samples were placed in custom-designed grips and allowed to equilibrate for 900s in a 0.15M PBS bath at room temperature. The circumferential direction of the sample coincided with the loading direction. The sample was preconditioned up to 10% maximum strain (20 cycles@1%/s), then a defined force ($<0.1N$) was applied and held constant for 900s to define the reference state. This was then followed by a 2% strain ramp (@1%/s) and a relaxation period of 900s. The strain and relaxation increments were repeated for 6% and 10% maximum strain. To fit the constitutive law, data from the higher strain range (6% and 10% strain) was selected.

5.2.2 Finite element Model

The initial 3D osmoviscoelastic FE model [93,95] describes the disc tissue as a biphasic material, consisting of a porous solid matrix saturated with water. Additionally, the material properties are made directly dependent on the tissue composition. This relationship is the same for all areas of the disc, i.e. the same for annulus and nucleus. Hence, the difference in composition of annulus versus nucleus causes the material properties of both tissues to differ. The model is composed of the following constitutive structures: an elastic non-fibrillar solid matrix (σ_{nf}), a 3D viscoelastic collagen fiber structure (σ_f), and an osmotically pre-stressed permeable extrafibrillar fluid. Hence, the total tissue stress (σ_{tot}) is the sum of these three constituents [124]:

$$\sigma_{tot} = n_{s,0} \left(\underbrace{\left(1 - \sum_{i=1}^{totf} \rho_c^i \right)}_{non-fibrillar} \sigma_{nf} + \underbrace{\sum_{i=1}^{totf} \rho_c^i \sigma_f^i}_{fibrillar} \right) - \underbrace{\Delta\pi - \mu^f}_{fluid} \mathbf{I}, \quad (5.1)$$

where σ_{nf} is the stress in the non-fibrillar matrix, $n_{s,0}$ the initial solid volume fraction, ρ_c the fibril density, σ_f^i the fibril stress in the i^{th} fibril with respect to the global coordinate system, $totf$ the total amount of fibers, μ^f is the water chemical potential and with $\Delta\pi$ the osmotic pressure relative to the external physiological salt solution. The initial solid volume fraction $n_{s,0}$ and the fibril density ρ_c are different at different locations in the disc. The constitutive law describing σ_{nf} is independent of the location in the disc. For example, σ_{nf} is the same for annulus and nucleus.

Elastic non-fibrillar solid matrix

The solid matrix is presumed to become incompressible when the solid fraction comes close to 1 and to be fully compressible when the solid fraction comes close to 0 [124]. Hence, the behavior of the non-fibrillar solid matrix is described through the following modified Neo-Hookean law [123,124]

$$\sigma_{nf} = -\frac{1}{6} \frac{\ln(J)}{J} G_m \mathbf{I} \left[-1 + \frac{3(J + n_{s,0})}{(-J + n_{s,0})} + \frac{3 \ln(J) J n_{s,0}}{(-J + n_{s,0})^2} \right] + \frac{G_m}{J} (\mathbf{F} \cdot \mathbf{F}^T - J^{2/3} \mathbf{I}), \quad (5.2)$$

where G_m is the shear modulus and J is the determinant of the deformation tensor \mathbf{F} . The first term of Equation 5.2 is a modification relative to the first term of Equation (3.1) of chapter 3 [95], as it assures that the tissue compressibility vanishes as J approaches $n_{s,0}$, e.g. the fluid is fully expelled.

3D viscoelastic collagen fiber structure

The viscoelastic behavior of the collagen fibers is represented through a Zener model [93,95]: consisting of a linear spring parallel to a nonlinear spring in series with a linear dashpot. Assuming that the fibrils only resist tension, the stresses in the viscoelastic fibrils are given by:

$$\sigma_f = -\frac{\eta}{2\sqrt{(\sigma_f - E_0 \varepsilon_f)E_\varepsilon}} \dot{\sigma}_f + E_0 \varepsilon_f + \left(\eta + \frac{\eta E_0}{2\sqrt{(\sigma_f - E_0 \varepsilon_f)E_\varepsilon}} \right) \dot{\varepsilon}_f, \quad (5.3)$$

where σ_f and ε_f are the fibril stress and strain, respectively. E_0 is the parallel stiffness and E_ε is the serial stiffness constants and η is a damping coefficient. The strain is defined with respect to an initial stress-free state. However, Equation (5.3) differs slightly from Equation (3.3) in chapter 3 [95] as it has been corrected after a closer examination. For a detailed explanation the reader is referred to Wilson et al. [128]. Equation (5.3) is identical throughout the annulus.

The disc collagen fiber structure is a complex combination of larger collagen fibrils, arranged in concentric lamellae with alternating fiber orientation and smaller fibrils structures, e.g. minor collagen, elastin or collagen crosslinks [21,39,70,91,103,131]. For simplicity in the previous chapters (chapter 3 & 4) the fiber orientation is assumed to be ± 30 degrees to the transversal plane described through primary fibers only [93,95] However, for this curve fitting procedure a fiber angle of ± 20 degrees to the y-axis is chosen to reduce slack of the collagen fibers, which also lies within the experimental range shown by Guerin and Elliott [38].

Osmotically prestressed fluid

The fluid is partially intrafibrillar and partially extrafibrillar. We assume the intrafibrillar permeability to be negligible compared to the extrafibrillar permeability. Therefore, the model includes a strain-dependent hydraulic extrafibrillar permeability (k) [93] which accounts for the intrafibrillar water differentiation as previously explained in [123]

$$k = k_0 \left(\frac{1 - n_{exf,0}}{1 - n_{exf}} \right)^M, \quad (5.4)$$

where k_0 is the initial permeability, M a positive constant, $n_{exf,0}$ the initial extrafibrillar fluid fraction and n_{exf} the current extrafibrillar fluid fraction.

Because we assume the ion concentrations to be in equilibrium at all times, the biphasic swelling theory [125] is applicable to describe the swelling behavior. Hence, the osmotic pressure gradient is then given by:

$$\Delta \pi = \phi_{int} RT \sqrt{c_{F,exf}^2 + 4 \frac{\gamma_{ext}^{\pm 2}}{\gamma_{int}^{\pm 2}} c_{ext}^2} - 2\phi_{ext} RT c_{ext}, \quad (5.5)$$

with c_{ext} the external salt concentration and the fixed charge density (FCD) is based on the extra-fibrillar fluid fraction $c_{F,exf}$, is then given by

$$c_{F,exf} = \frac{n_f c_F}{n_{exf}} \quad (5.6)$$

With n_f the total fluid fraction, n_{exf} the extra-fibrillar fluid fraction and c_F the normal FCD in mEq per ml total fluid. The osmotic (ϕ_{int} , ϕ_{ext}) and activity coefficients (γ_{int} , γ_{ext}) are implemented as proposed by Huyghe et al. [43]. The composition is accounted through the fixed charge density in Equation (5.5).

5.2.3 Determination of the material properties

The material properties G_m , k_o , M , E_o , E_c and η , were determined by fitting the model to the average experimental data from confined compression experiments of nucleus and annulus tissue, as well as uniaxial tensile tests in circumferential direction of the annulus. For the nucleus, we used data from a previously published study on human tissue [54]. The fitting of the confined compression experiments determined primarily the shear modulus (G_m) of the non-fibrillar matrix, the initial permeability (k_o) and the positive constant (M) of the model. While the fitting of the annulus fibrosus tensile tests determined primarily the material parameters of the fibrillar matrix (E_o , E_c , η).

The curve fitting procedures were performed iteratively, using a multidimensional unconstrained nonlinear minimization procedure available in Matlab Version 5.3 (The MathWorks Inc.). From within this Matlab procedure, ABAQUS was called to simulate the different experiments. The output from ABAQUS was then transferred to Matlab, after which the objective function was determined as:

$$f = \underbrace{\frac{1}{n} \sum_{i=1}^n \left(\frac{F_{EXP}^i - F_{FEM}^i}{F_{EXP}^i} \right)^2}_{\text{confined compression}} + \underbrace{\frac{1}{m} \sum_{i=1}^m \left(\frac{F_{EXP}^i - F_{FEM}^i}{F_{EXP}^i} \right)^2}_{\text{annulus}} + \underbrace{\frac{1}{o} \sum_{i=1}^o \left(\frac{F_{EXP}^i - F_{FEM}^i}{F_{EXP}^i} \right)^2}_{\text{6\%}} + \underbrace{\frac{1}{p} \sum_{i=1}^p \left(\frac{F_{EXP}^i - F_{FEM}^i}{F_{EXP}^i} \right)^2}_{\text{10\%}} + \underbrace{\frac{1}{p} \sum_{i=1}^p \left(\frac{F_{EXP}^i - F_{FEM}^i}{F_{EXP}^i} \right)^2}_{\text{tensile test}}, \quad (5.7)$$

where F_{FEM} are the reaction forces of the model simulations and F_{EXP} are the reaction forces of the 4 experiments and $n=9188$, $m=9188$, $o=225$, $p=257$ are the number of data points. The iteration process was started with the following initial values for normal disc tissue for $G_m=0.903$ MPa and $M=1.399$, these values were taken from Wilson et al. [123]. However, for the initial permeability we used $k_o = 5.0 \times 10^{-16}$ m⁴/Ns as presented in table 3.2 of chapter 3 [95] and for the fibrillar matrix initial guess we used the following values ($E_o=3.370$ MPa; $E_c=380.8$ MPa, and $\eta=1.532 \times 10^3$ MPa-s) as presented in table 3.2 of chapter 3 [95].

5.2.4 Curve fitting procedure

In view of the fact that the material properties directly depend on the tissue composition, the following human intervertebral disc composition data were selected for the curve fitting procedure. Because no biochemical analysis of the samples was performed in this study, the same composition data as described in chapter 4 were applied. Thus, the annulus was simulated with a collagen content of 60% per dry weight and with a fluid fraction of 77% per wet weight at a fixed charge density (FCD) of 0.15 mE/ml [100,102]. The composition of the nucleus was as follows; a collagen content of 0.9% per dry weight, a fluid fraction of 82.5% per wet weight and with a FCD of 0.3mE/ml [unpublished data by Sivan et al.].

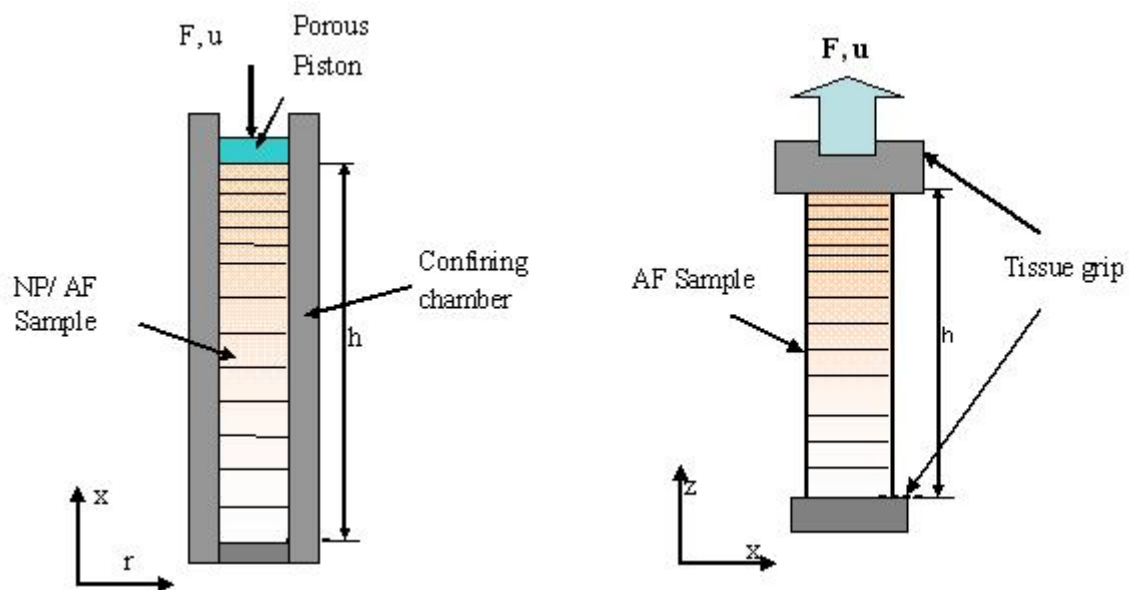


Figure 5.1: a)

Schematic drawing of mesh used for confined compression fitting procedure; mesh dimensions correspond with average sample dimensions for annulus plugs (Height x Diameter=2.793 x 2.5mm).

b)

Schematic drawing of mesh used for uniaxial tensile fitting procedure; mesh dimensions correspond with average sample dimensions for rectangular circumferential annulus samples (Height x Width=7.5 x 2.95mm).

Each model parameter determination included an initial step in which the model equilibrated with a physiological salt solution of 0.15M, before the different loading protocols were applied. For more details on this subject the reader is referred to chapter 3 [95]. Figure 5.1 a) shows the schematic drawings of the mesh used in the confined compression experiment of the nucleus and annulus sample, while Figure 5.1 b) shows the mesh used for the tensile test simulations. The mesh dimensions were averaged for all nucleus and annulus samples. This was done for each experiment separately.

Model solution for confined compression experiments

For nucleus pulposus tissue data provided by Johannessen and Elliott [54] were used. During the simulation, the reaction force was computed while the same loading protocol was applied. The simulation was limited to an axisymmetric model, using an axisymmetric FE mesh, consisting of a single column of 84 axisymmetric pore pressure elements (CAX4P). The nodal displacements at the bottom plane were confined in z direction. The displacement of all nodes was confined in radial direction. At the top of the model, zero pore pressure was prescribed, i.e. fluid flowed in and out freely. All other surfaces were assumed to be impermeable.

For annulus fibrosus tissue in confined compression as measured here, a simplified 2D finite element mesh was used for this simulation, consisting of a single column of 84 pore pressure elements (CPE4P). However, since a 2D fiber structure was included in the annulus model, the fibers were oriented ± 20 degrees to the z axis. This assumption of a simplified 2D fiber representation was based on the sample (orientation) and the loading protocol, as only axially loaded and axially oriented samples for the confined compression experiment were used. Thus, the collagen fibers were all under compression and hence hardly contributed to the axial stiffness of the sample.

The nodal displacements at the bottom plane were confined in z direction. The displacements of all nodes were confined in x direction. At the top of the model, zero pore pressure was prescribed, i.e. fluid flowed in and out freely. All other surfaces were assumed to be impermeable. Again, the same loading protocol as for the nucleus was used, the mesh was axially compressed by 5% strain followed by a relaxation period. During this process, the axial reaction forces were computed.

Model solution for uniaxial tensile test of annulus

The fitting of the viscoelastic properties was performed on a data set from the 6% and 10% maximum strain ramp and relaxation increments. We selected these two increments from a higher strain range, because the non-linear viscoelastic response of the collagen fibers was dependent on the strain range [119]. For these simulations, a simplified 3D mesh was used, consisting of one column of 84 3D 8-node pore pressure brick elements (C3D8P), with the same fiber orientation (± 20 degrees to the z axis) as described in the 2D model. The boundary conditions were as follows: the nodal displacements at the bottom plane were confined in z direction, the nodal displacements on the left plane were confined in x and y direction. As the tensile test was done in a 0.15M PBS bath, zero pore pressure was prescribed at all surfaces. The mesh was axially elongated by 6% strain after which a relaxation period of 15min followed. The simulation was then repeated for 10% strain. During both simulations the axial reaction force was computed and fitted.

5.3 Results

For the confined compression experiment of the nucleus, the reaction force was in good agreement with the average value of the experimental range (Figure 5.2). Yet, the descending part of the curve was underestimated. The coefficient of determination (R^2) for this fit was 0.96. The confined compression of annulus showed good conformity of the reaction force during the 2h relaxation. However, the reaction force was overestimated during the ramp portion of the experiment (Figure 5.3).

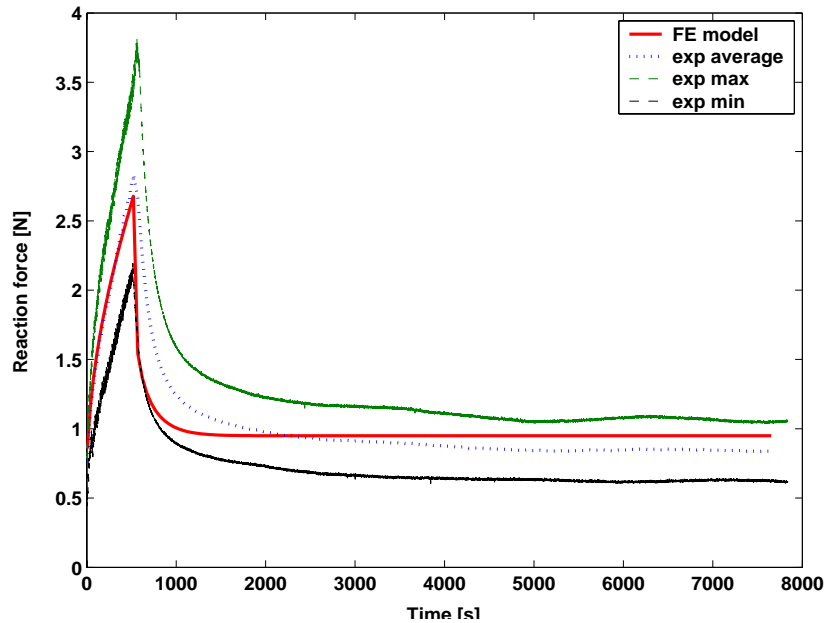


Figure 5.2: Comparison of experimental reaction force from confined compression experiment and FE model fit for nucleus tissue.

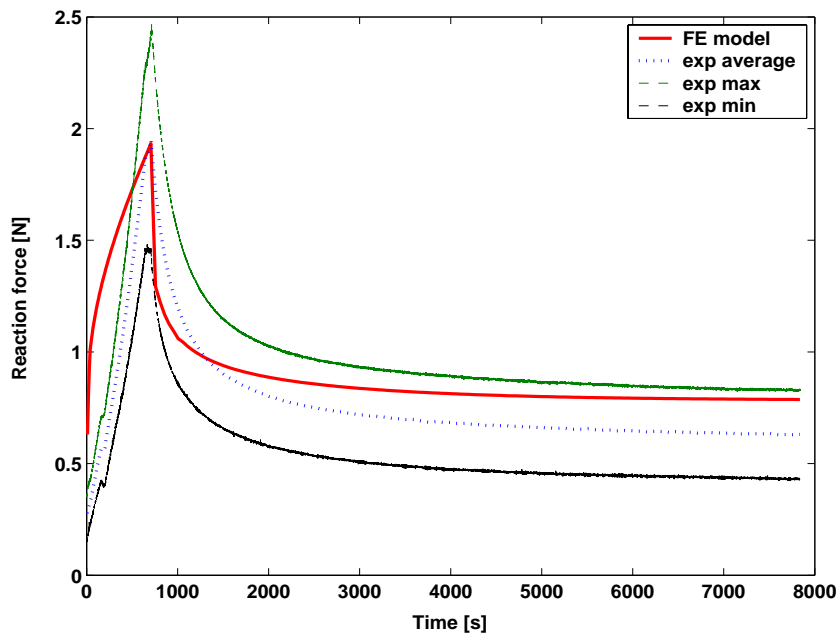


Figure 5.3: Comparison of experimental reaction force from confined compression experiment and FE model fit for annulus tissue.

Because these discrepancies did not allow a full fit, we included the computed reaction force into the minimization procedure only after the strain ramp. The coefficient of determination (R^2) for this second fit was 0.93. Consequently, we obtained the following

material parameters $G_m=1.233\text{MPa}$; $M=1.566$ and $k_o=0.654\times 10^{-16} \text{ m}^4/\text{Ns}$ to describe the compressive behavior of normal human intervertebral disc tissue.

To clarify once more, the material properties used here were directly dependent on the tissue composition, which were included in the model during parameter determination through the values of the initial solid volume fraction ($n_{s,o}$) and the extra- fibrillar fluid fraction (n_{ex}). The relationship applied here, was the same for all areas of the disc, i.e. the same for annulus and nucleus. Hence, the difference in composition of annulus versus nucleus caused the material properties of both tissues to differ.

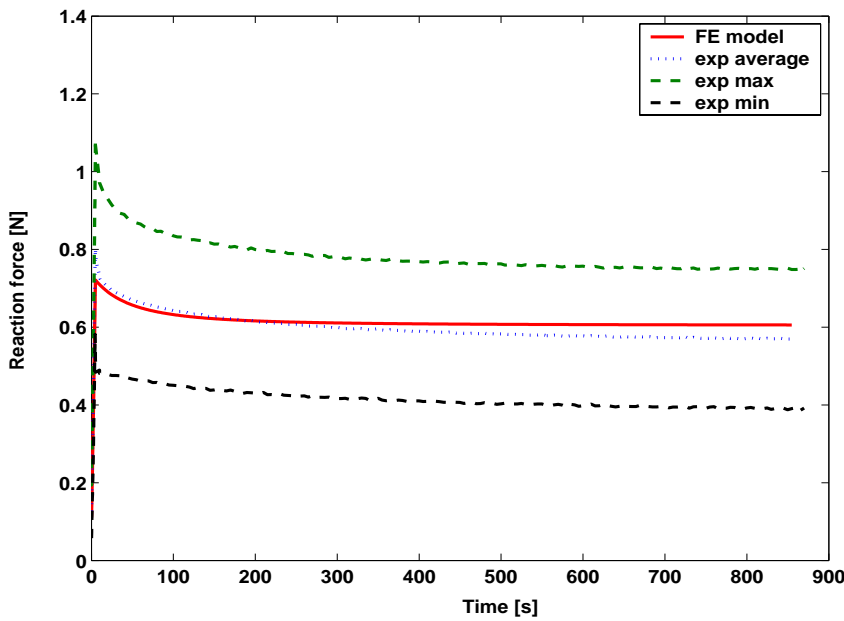


Figure 5.4: Comparison of experimental reaction force from uniaxial tensile test with 6% strain along with FE model fit for annulus tissue.

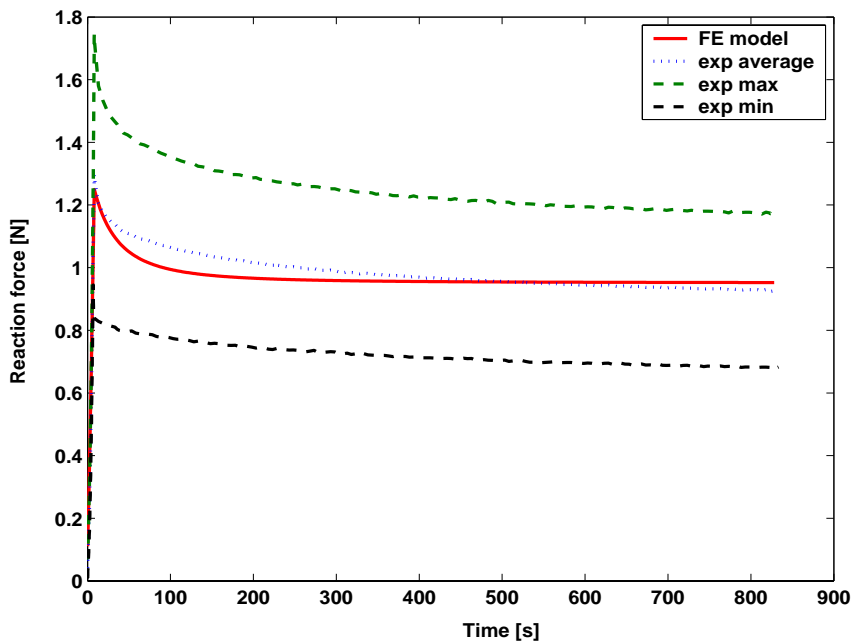


Figure 5.5: Comparison of experimental reaction force from uniaxial tensile test with 10% strain along with FE model fit for annulus tissue.

The coefficients of determination (R^2) for the two simulations, tensile test with 6% strain and 10% maximum strain, were 0.95 and 0.88, respectively. The computed reaction forces for the tensile test with 6% and 10% strain were in good agreement with the average experimental values (Figure 5.4 & 5.5). As a result, we obtained the following fiber material parameters $E_o=77.0\text{MPa}$; $E_c=500\text{MPa}$ and $\eta=1.8\times 10^3\text{MPa}\cdot\text{s}$ to describe the viscoelastic behavior of the annulus collagen fibers.

5.4 Discussion

The purpose of this study was (1) to complement the existing material data in the literature to describe the non-linear viscoelastic behavior of the annulus and (2) to combine these new tensile data with existing data on compressive properties of the annulus and nucleus to tune an osmoviscoelastic material law for the human intervertebral disc. The tensile data underlined the viscoelastic behavior of human annulus tissue. The compressive properties, defined through confined compression experiments of nucleus [54] and annulus tissue, combined with the viscoelastic properties of the annulus were applicable for adjusting the osmoviscoelastic material law.

The osmoviscoelastic FE model of the disc used for this curve fitting procedure showed good conformity with the experimental data (Figure 5.2 & 5.3) for the confined compression relaxation of the nucleus and annulus. However, in the first half of the ramp phase of the confined compression, the computed reaction force was overestimated by the model. This was only seen in the annulus simulation, not in the nucleus. The reason for this overestimation is unclear. A possible explanation could be the permeability change under structural compaction in the annulus and the simplified fiber structure. Secondly, in the confined compression experiments of the nucleus (Figure 5.2) the descending part of the model curve was underestimated in comparison to the average experimental value, which suggests that the time constant was underestimated in the model solution.

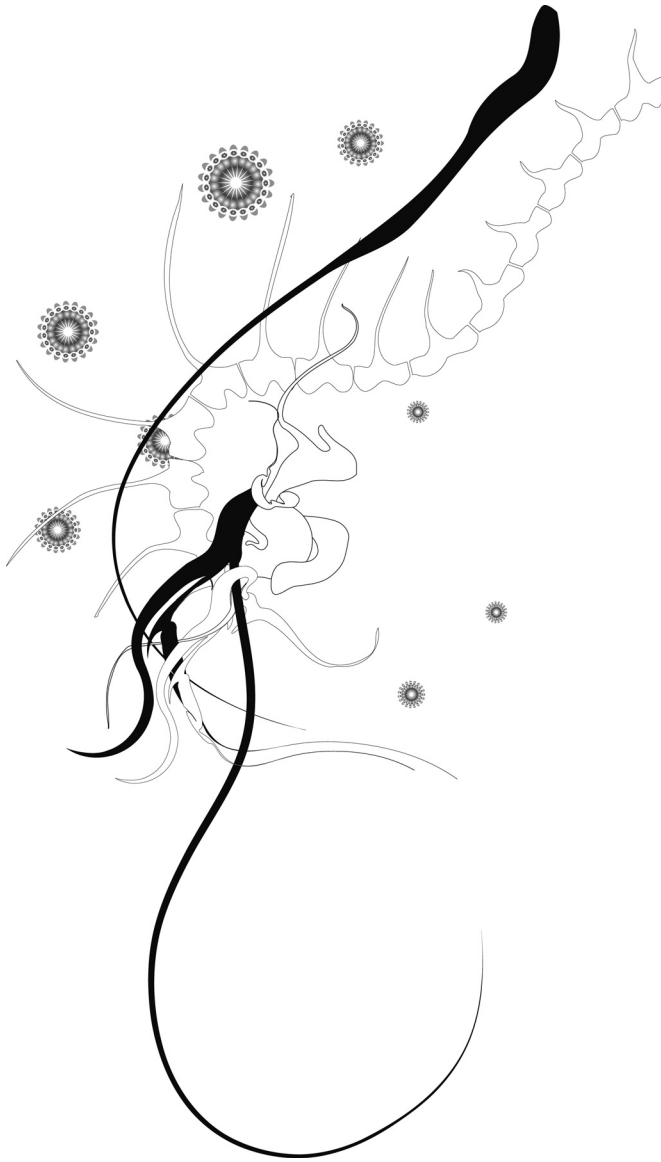
In addition, the fits of both tensile test simulations were in good agreement with the average experimental values and emphasized the need for a viscoelastic material law for the annulus collagen fibers (Figure 5.4 & 5.5). The conformity of the numerical and experimental fits showed that the Zener model was a good approach to describe the viscoelastic behavior of the annulus collagen fibers in the strain range of 6% to 10 %.

There were some limitations in this study. The number of samples used in the experimental tests was. For G_m , k_o and M , which apply both to annulus and nucleus, we had $n=6$. For E_o , E_c and η we had $n=3$. However, directly using experimental data to determine model parameters as applied here is still an advantage over most disc finite element models, which simply utilized average data from the literature. The characterization of an anisotropic, nonlinear multi-component material like the intervertebral disc is an iterative procedure. Different aspects of the material law are coming to expression in different experiments. One model should fit all the data of the different experiments. Our approach here is purposely not to do a thorough detailed analysis of each experiment type separately, but rather to verify trends of the response of

the model to different types of loading. For this reason, we chose not to do just 1 type of experiment, but rather to fit simultaneously for a collection of different experiments. The consequence of this is that each experiment is done only on 3 samples. The set of data points, however, remains very large, because we have results as a function of time, and we require the model to fit the data during a window in time small. Additionally, it is also recommendable to further verify the model with other objective functions. However, this is beyond the scope of the present study.

The average tissue properties measured in compression were $G_m=1.233\text{MPa}$; $M=1.566$; $k_o=0.654\times 10^{-16}\text{m}^4/\text{Ns}$ and in tension were $E_o=77.0\text{MPa}$; $E_e=500\text{MPa}$ and $\eta=1.8\times 10^3\text{MPa}\cdot\text{s}$. The hydraulic permeability was similar to previous reports [10, 27,50], supporting the use of these experiments to determine model parameters. Second, there was some divergence of the average experimental and numerical results (Figure 5.3). This divergence may be explained by the composition and the fiber orientation; as the composition and the fiber angle used in the curve fitting procedure were not measured directly, but chosen from literature [38,100,102].

To conclude, the osmovoelastic material constitutive law and the experimental data enabled us to describe the fiber and non-fiber properties of the human disc. The osmovoelastic constitutive material law emphasized the interdependency of the strong swelling ability of the tissue and the viscoelastic nature of the collagen fibers. This is especially of importance for numerical models to further study the load sharing behavior with regard to disc degeneration and regeneration.



Chapter 6

Evaluation of the 3D FE osmoviscoelastic disc model with experimental data from literature

The content of this chapter is based on a manuscript which will be submitted to the Journal of Orthopaedic Research “Evaluation of the 3D FE osmoviscoelastic disc model with experimental data from literature.”

Y. Schroeder
J. M. Huyghe

6.1 Introduction

Back pain is a frequently occurring complaint in adults, having a relatively large impact on the European economy as it often partially incapacitates the patient [83]. Intervertebral discs are believed to be a key element of back pain. Apart from providing flexibility to the spine, intervertebral discs have a mechanical role in absorbing and transmitting loads through the spine. Furthermore, load-induced intra-tissue physical conditions are believed to play a role in the progression of disc degeneration [97]. As measurements in living humans are complex, finite element (FE) models have become an important tool to study load distribution in healthy and degenerated discs. The disc is subjected to a combination of elastic, viscous and osmotic forces, but the latter has mostly been neglected in previous 3D FE models. For example, in the fiber-reinforced disc tissue, there is interdependency between swelling of its proteoglycan (PG) ground substance and the tensile stresses in its collagen structure, but this has not been accounted for [106]. Furthermore, the total amount of water in the tissue is divided into intrafibrillar water (IFW) and extrafibrillar water (EFW). IFW is present in the intrafibrillar space within the collagen fibers and is, therefore, not accessible to the PG's, which reside in the extrafibrillar compartment. Experimental results have shown that both gene expression of cells in the intervertebral disc and propagation of cracks are affected by changes in osmotic pressure [101,129], which must be determined on the basis of the extrafibrillar water (EFW) only [108]. Hence, quantification of intra- and extrafibrillar fluid exchange and its effect on osmolarity of disc tissue is important for determining the physical conditions of disc tissue and its role in disc degeneration and failure [93].

In an initial osmoviscoelastic FE model (chapter 3) [95], the interdependency of swelling and collagen pre-stressing was modeled. It predicted intradiscal pressures on the order of 0.1-0.2MPa in unloaded discs, in agreement with *in vivo* experimental measurements of Wilke et al. [121]. In the initial disc model, a correction factor was used to account for the influence of IFW (chapter 3) [95], based on the seminal work of Urban and McMullin [108] for a low collagen containing tissue such as the nucleus pulposus. However, this was recently shown not to be the case for the annulus which has much higher collagen content. The data of Sivan et al. [100] demonstrated that IFW is sensitive to the applied load which can alter significantly the fixed charged density. Consequently, the initial FE model of the disc was extended to include the intra and extrafibrillar water differentiation (chapter 4) [93] and exhibited that the intradiscal pressure profile was clearly influenced by the IFW content [93]. Unfortunately, lack of experimental data to determine some of the model parameters limited the applicability of the model.

In addition to osmotic effects, mechanical properties of the intervertebral disc are complex. The composite behavior of disc tissue is regulated by its biochemical composition and fiber-reinforced structure [14,51]. The anisotropic, nonlinear behavior of a multi-component material like the intervertebral disc can only be assessed through a variety of experiments. Hence, data from several different experiments was simultaneously fitted to a simple FE model to calculate the material law for the disc (chapter 5) [94]. As part of this study experimental data for the material properties of the disc published in literature, was complemented with further tensile tests on human annulus fibrosus. Furthermore, the existing data on compression of non-degenerated

human annulus and nucleus tissue together with the new tensile data was used to tune an osmoviscoelastic material constitutive law [94]. Model solutions for the different experiments were acquired through fitting data from results obtained with simplified 2D/3D meshes. The simplified osmoviscoelastic FE model of the disc used for this curve fitting procedure showed good conformity with the experimental data for the confined compression relaxation of the nucleus and annulus sample, and, additionally, the model solutions for the tensile tests were in good agreement with the average experimental values.

The aim of the present study is to incorporate the osmoviscoelastic constitutive law and the obtained material properties into a full 3D osmoviscoelastic FE disc model and to validate the model on the basis of experimental data of whole discs (radial bulging, height change and intradiscal pressure) from literature [16,17,40].

6.2 Material and Methods

6.2.1 Finite element model

The 3D osmoviscoelastic FE model [93,95] describes the disc tissue as a biphasic material, consisting of a porous solid matrix saturated with water. The material properties are made directly dependent on the tissue composition. The relationship between composition and material properties is the same for all areas of the disc, i.e. the same for annulus and nucleus. Hence, the difference in composition of annulus versus nucleus causes the material properties of both tissues to differ. The total tissue stress (σ_{tot}) is the sum of 3 terms, an elastic term from the non-fibrillar solid *matrix* (σ_{nf}), a 3D viscoelastic term from the collagen fiber structure (σ_f), and an osmotic term from the permeating extrafibrillar fluid [123]:

$$\sigma_{tot} = n_{s,0} \left(\underbrace{\left(1 - \sum_{i=1}^{totf} \rho_c^i \right) \sigma_{nf}}_{\text{non-fibrillar}} + \underbrace{\sum_{i=1}^{totf} \rho_c^i \sigma_f^i}_{\text{fibrillar}} \right) - \underbrace{\Delta\pi \mathbf{I} - \mu^f \mathbf{I}}_{\text{fluid}}, \quad (6.1)$$

with $n_{s,0}$ the initial solid volume fraction, σ_f^i the fibril stress in the i^{th} fibril with respect to the global coordinate system, $totf$ the total amount of fibers, with ρ_c the fibril density, μ^f is the water chemical potential and with $\Delta\pi$ the osmotic pressure relative to the external physiological salt solution. The initial solid volume fraction $n_{s,0}$, and the fibril density ρ_c are different at different locations in the disc. The constitutive law describing σ_{nf} is independent of the location in the disc. For example, σ_{nf} is the same for annulus and nucleus. The osmotic pressure gradient $\Delta\pi$ is then given by

$$\Delta\pi = \phi_{int} RT \sqrt{c_{F,exf}^2 + 4 \frac{\gamma_{ext}^{\pm 2}}{\gamma_{int}^{\pm 2}} c_{ext}^2 - 2\phi_{ext} RT c_{ext}}, \quad (6.2)$$

with c_{ext} the external salt concentration and $c_{F,ext}$ the FCD per extrafibrillar water. The osmotic (ϕ_{int} , ϕ_{ext}) and activity coefficients (γ_{int} , γ_{ext}) are implemented as proposed by Huyghe et al. [43].

Elastic non-fibrillar solid matrix

The solid matrix is presumed to become incompressible when the solid volume fraction comes close to 1 and to be fully compressible when the solid fraction comes close to 0 [123]. Hence, the behavior of the non-fibrillar solid matrix is described through the following modified Neo-Hookean law [123],

$$\boldsymbol{\sigma}_{nf} = -\frac{1}{6} \frac{\ln(J)}{J} G_m \mathbf{I} \left[-1 + \frac{3(J + n_{s,0})}{(-J + n_{s,0})} + \frac{3 \ln(J) J n_{s,0}}{(-J + n_{s,0})^2} \right] + \frac{G_m}{J} (\mathbf{F} \cdot \mathbf{F}^T - J^{2/3} \mathbf{I}), \quad (6.3)$$

where G_m is the shear modulus and J is the determinant of the deformation tensor \mathbf{F} .

3D viscoelastic collagen fiber structure

The viscoelastic behavior of the collagen fibers is represented through a Zener model [93,95], consisting of a linear spring parallel to a nonlinear spring in series with a linear dashpot. Assuming that the fibrils only resist tension, the stresses in the viscoelastic fibrils are given by:

$$\sigma_f = -\frac{\eta}{2\sqrt{(\sigma_f^i - E_0 \varepsilon_f^i) E_\varepsilon}} \dot{\sigma}_f^i + E_0 \varepsilon_f^i + \left(\eta + \frac{\eta E_0}{2\sqrt{(\sigma_f^i - E_0 \varepsilon_f^i) E_\varepsilon}} \right) \dot{\varepsilon}_f^i, \quad (6.4)$$

where σ_f and ε_f are the fibril stress and strain, respectively. E_0 is the parallel stiffness and E_ε is the serial stiffness constants and η is a damping coefficient. The strain is defined with respect to an initial stress-free state.

The disc collagen fiber structure is a complex combination of larger collagen fibrils, arranged in concentric lamellae with alternating fiber orientation and smaller fibrils structures, e.g. minor collagen, elastin or collagen crosslinks [21,39,70,91,103,131]. For simplicity in our previous studies the fiber orientation is assumed to be ± 30 degrees to the transversal plane described through primary fibers only (chapter 3 & 4) [93,95].

In the present analysis, this description of the 3D-collagen network is supplemented with a second, more advanced approach. In this second more complex approach secondary fibers are incorporated into the full 3D FE disc model to account for smaller fibril structures. Thus, at each integration point it is assumed that there are 2 primary (± 30 degrees) and 13 secondary fibril directions. It is assumed that the orientation of the secondary fibrils is random. The network of secondary fibrils is represented by a homogeneous 3D network of fibrils, running in the x-, y- and z-directions, and in all directions with angles of 45 degrees with respect to the x-, y-, and z-axes. These secondary fibrils are relatively short and account for extra matrix stiffness in the

associated direction. The density of the primary fibrils is assumed to be higher than of the secondary fibrils. The fibril densities are embedded as:

$$\begin{aligned} \rho_c &= \frac{C}{2C+13} \quad \text{for the primary fibrils} \\ \rho_c &= \frac{1}{2C+13} \quad \text{for the secondary fibrils} \end{aligned}, \quad (6.5)$$

with C a positive constant larger than 1 [126].

Osmotically prestressed fluid

The fluid is partially intrafibrillar and partially extrafibrillar. We assume that the intra-extrafibrillar fluid-ion exchange is so fast that at all times the intrafibrillar compartment is in equilibrium with the extrafibrillar compartment. Intrafibrillar hydraulic permeability is assumed to be negligible compared to the extrafibrillar hydraulic permeability. Therefore, the model includes a strain-dependent hydraulic extrafibrillar permeability (k) [93]

$$k = k_0 \left(\frac{1 - n_{exf,0}}{1 - n_{exf}} \right)^M, \quad (6.6)$$

where k_0 is the initial permeability, M a positive constant, $n_{exf,0}$ the initial extrafibrillar fluid fraction and n_{exf} the current extrafibrillar fluid fraction. In this case, k_0 and M are the same for all areas in the disc.

6.2.2 Material properties

The 3D FE mesh was based on a simplified geometry of a human lumbar disc (L4/L5) [95]. Because symmetry about the transversal and sagittal plane was assumed, the mesh was reduced to 1/4 of the size of the disc (Figure 6.1) [95].

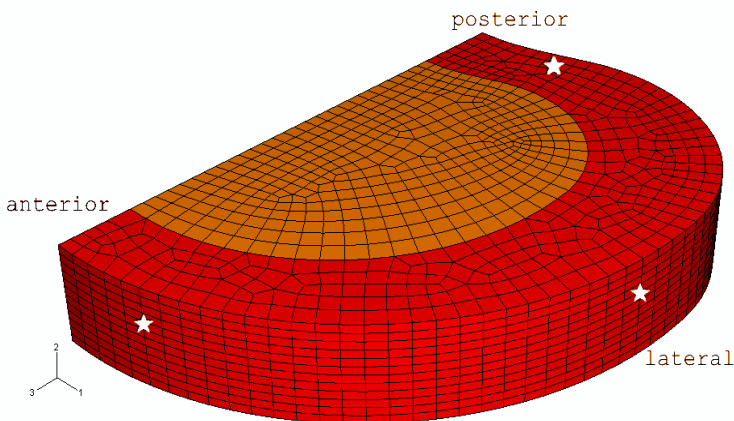


Figure 6.1: Finite element mesh of 1/4 of an intervertebral disc with differentiation in nucleus (light) and annulus (dark) regions in the stress-free state, with selected nodes (white stars) on anterior, posterior and lateral side for comparison (Table 6.3 & 6.4).

The fiber and non-fiber properties of the disc were derived from the osmovoelastoc constitutive law and experimental data as previously described in chapter 5 [94]. Hence, the following parameters were used: the compressive material properties of normal disc tissue are $G_m=1.23\text{MPa}$, $M=1.57$, and $k_o=0.65\times 10^{-16}\text{ m}^4/\text{Ns}$; while the tensile fiber material parameters were $E_o=77.0\text{MPa}$; $E_e=500\text{MPa}$ and $\eta=1.8\times 10^3\text{MPa}\cdot\text{s}$ [94].

In view of the fact that the material properties directly depend on the tissue composition, the following human intervertebral disc composition data were selected for the study. Because no biochemical analysis of the samples was performed, the same composition data as described in chapter 4 & 5 were applied. Thus, the annulus was simulated with a collagen content of 60% per dry weight and with a fluid fraction of 77% per wet weight at a fixed charge density (FCD) of 0.15mE/ml [100,102]. The nucleus had a collagen content of 0.9% per dry weight, a fluid fraction of 82.5% per wet weight and a FCD of 0.3mE per ml extrafibrillar water [unpublished data by Sivan et al.].

6.2.3 Boundary conditions

The same boundary conditions were applied, as previously described in chapter 3 [95]. Briefly, during the first step the initial mesh was equilibrated with a hypertonic salt solution (0.15M). Hence, the disc was brought into its physiological unloaded state in equilibrium with a physiological salt solution, while the disc was gripped between the two vertebrae. The vertebrae were assumed infinitely stiff. This restrained the disc from swelling freely and allowed the disc to develop its turgor. Afterwards, different loading protocols (Table 6.1) to simulate the two experiments were applied to the model.

Table 6.1 To allow comparison of the different data sets, two loading protocols are used in this study.

	Loading protocol 1 (Compare to Brinckmann et al. [16, 17])	Loading protocol 2 (Compare to Heuer et al. [40])
Step 1	Initial swelling	Initial swelling
Step 2	Axial load from 0 to 1000N over 360s	Axial load from 0 to 500N over 360s
Step 3	Constant axial load of 1000N over 1800s	Constant axial load of 500N over 900s
Step 4	Decreasing axial load from 1000N to 300N over 360s	Decreasing axial load from 500N to 0N over 360s

The first loading protocol was that from the studies of Brinckmann and coworkers [16,17]. As the geometry and size of the full 3D osmovoelastoc FE disc model was similar to the average size of L4/L5 human disc measurements by Brinckmann & Grootenboer [16], data from these discs were selected for comparison in this study. The main focus of their study was to evaluate the relationship between the amount of removed disc tissue and the subsequent change of disc height, radial bulging and intradiscal pressure. In particular, the intradiscal pressure measurements of intact human specimen were of interest for our

study. Table 2 from the paper of Brinckmann & Grootenboer [16] presents an overview of intradiscal pressure of intact human disc dependent on axial loading. Thus, for the L4/L5 disc level an axial load of 300N resulted in an intradiscal pressure range of 0.23-0.46MPa and an axial load of 1000N resulted in an intradiscal pressure range of 0.73-1.38MPa [16].

In a similar study, Brinckmann & Horst [17] measured the geometrical changes of the disc under different loading conditions. They found that a reduction of an axial load from 1000N to 300N resulted in a decrease of the radial bulge of about 0.2mm and led to a disc height increase of 0.33mm. Note, the experimental results of Brinckmann & Horst [17] presented an average data set obtained from measurements of different disc levels and stages.

A recently published study by Heuer et al. [40] was simulated by the second loading protocol. The main focus of this study was the time dependent deformation behavior of the disc under compressive load. Heuer and coworkers performed measurements on human L4/L5 disc under 500N compression load and the deformations of the disc were recorded with a laser scanner [40]. Hence, the recorded experimental data were used to compare the overall behavior of the 3D disc model. An axial load of 500N resulted in an intradiscal pressure range of 0.36-0.53MPa and an immediate disc height reduction of 1.14mm. They also found that radial bulging was largest in the anterolateral and anterior region. Furthermore, their results indicated the largest creep behavior of about 0.1mm on the posterolateral region.

6.2.4 Model adaptations

During validation of the full 3D FE disc model with the geometry and intradiscal pressure data from the literature, 4 adaptations to the model were explored, e.g. material parameters and collagen structure (Table 6.2).

Table 6.2 A detailed overview of the different model adaptations which were explored during validation process.

Model adaptations	Material properties		Fiber structure
	non- fibrillar	fibrillar	
0	$G_m=1.23 \text{ MPa}$ $M=1.57$ $k_o=0.65 \times 10^{-16} \text{ m}^4/\text{Ns}$	$E_o=77.0 \text{ MPa}$ $E_\varepsilon=500 \text{ MPa}$ $\eta=1.8 \times 10^3 \text{ MPa}\cdot\text{s}$	primary fibers
1	5x G_m	same as above	same as above
2	5x G_m	same as above	primary and secondary fibers
3	1.5x G_m	same as above	primary and secondary fibers

In comparison to base model, 0, the shear stiffness (G_m) was increased 5 times for model adaptation 1 to ensure convergence and reduce the anisotropy of the model. In adaptation 2, a higher shear stiffness and secondary fibrils (see paragraph 3D viscoelastic collagen fiber structure) were included to account for smaller fibril structures and to reduce the deformability of the 3D disc model. However, as the increase of shear

stiffness ($5 \times G_m$) for model adaptation 1 was an initial guess, the shear stiffness was reduced to a more reasonable value ($1.5 \times G_m$) for model adaptation 3. To assure that the chosen values for G_m were acceptable, the material law simulations for the confined compression experiments of nucleus and annulus as described in chapter 5 [94] were repeated.

6.3 Results

Results - comparing disc deformations

For evaluation of geometry changes during different loading steps, nodes in the anterior, posterior and lateral annulus region were selected (Figure 6.1). Results for the disc deformation of model adaptations 1-3 were presented in more detail with the data of Brinckmann & Horst [17] and Heuer et al. [40] in Table 6.3 & Table 6.4. For the base model with only primary fibers and the material parameters taken directly from the earlier material law fit, no results were available because the model did not converge to a solution for either loading protocol.

Table 6.3: Results of disc deformations for step 4 of loading protocol 1.

Disc deformation Step4 (1000N → 300N)	Model adaptation 1	Model adaptation 2	Model adaptation 3	Brinckmann et al. [17] (Averaged)
Height change	0.628	0.576	0.701	0.33mm
Radial bulging				
Anterior	-0.5mm	-0.28mm	-0.15mm	
Posterior	-0.7mm	-0.5mm	-0.48mm	
Lateral	-0.3mm	-0.37mm	-0.38mm	
(Averaged)	-0.5mm	-0.38mm	-0.34mm	-0.2mm

Table 6.4: Results of disc deformations for Step 2 & 3 of loading protocol 2.

Disc deformation Step 2 (0N → 500N)	Model adaptation 1	Model adaptation 2	Model adaptation 3	Heuer et al. [40]
Height change	-0.57mm	-0.52mm	-0.87mm	-(1.00-1.35mm)
Radial bulging				
Anterior	0.48mm	0.38mm	0.61mm	(0.46-1.34mm)
Posterior	0.55mm	0.51mm	0.85mm	(0.24-0.9mm)
lateral	0.54mm	0.47mm	0.68mm	(0.10-1.09mm)
Disc deformation Step 3 (500N over 900s) Radial bulging Averaged				
	0.15 mm	0.15 mm	0.1 mm	0.1mm
Height change	-0.2mm	-0.2mm	-0.32mm	-0.16
Total height change	-0.77	-0.72	1.19	-(1.08-1.57)

The average radial bulging for step 4 of loading protocol 1 was smallest for model adaptation 3 and largest for model adaptation 1 (Table 6.3). The load reduction for model adaptation 3 resulted in a decrease of the radial deformation of 0.32mm. On the other hand the height change (increase) was largest for model adaptation 3 and lowest for model adaptation 1. For model adaptation 3 the height increased by 0.7mm for step 4. The computed height change was a factor 2 higher than what Brinckmann and Horst [17] measured. The computed decrease in radial bulging was also slightly higher than what was measured experimentally by Brinckmann and Horst [17] (Table 6.3).

As for step 2 (load increase) of loading protocol 2, the radial bulging increased from model adaptation 1 towards model adaptation 3. The same behavior was noticed for the height change; it increased gradually with the model adaptations from 1 to 3. Comparing experimental measurements of Heuer et al. [40] with the computed results of step 2 from model adaptation 3 showed that the model slightly underestimates the height change (reduction), but the computed radial deformations for all nodes lay well within the experimental range. Step 3 of loading protocol 2 focused on the creep behavior of the model. The computed average radial deformation was in agreement with the experimental data of Heuer et al. [40]. However, the computed height reduction was slightly overestimated by the model (Table 6.4).

Results - comparing intradiscal pressure

Results for the computed intradiscal pressure of model adaptation 1-3 for loading protocol 1 were presented in more detail with the data from Brinckmann and Grootenboer [16] in Table 6.5. For the base model with only primary fibers and the material parameters taken directly from the earlier material law fit, no results were available because the model did not converge to a solution for either loading protocol.

Table 6.5 Results of intradiscal pressure for Step 2 & 4 of loading protocol 1 in the nucleus region.

Intradiscal pressure Averaged for the nucleus region	Model solution 2	Model solution 3	Model solution 4	Brinckmann et al. [16] (Averaged)
Step2 (0N →1000N)	0.6-1.2MPa	0.6-1.2MPa	0.6-1.0MPa	(0.73-1.38 M Pa)
Step4 (1000N →300N)	0.2MPa	0.2MPa	0.2MPa	(0.23-0.46MPa)

An intradiscal pressure of 0.4-1.2MPa for 500N was noticed in the nucleus region for model adaptation 1 & 2. Similar results were seen for model adaptation 3; an intradiscal pressure of 0.4-1.0MPa for 500N was noticed in the nucleus region (Figure 6.2). The computed intradiscal pressure value (0.4-1.0MPa) for 500N axial load for model adaptations 1-3 was in agreement with the experimental range (0.36-0.53MPa) of intradiscal pressure measurements for L4/L5 human disc by Heuer and coworkers [40]. The computed results for loading protocol 1 were also in good agreement with the experimental range measured by Brinckmann and Grootenboer [16] (Table 6.5).

Intradiscal pressure

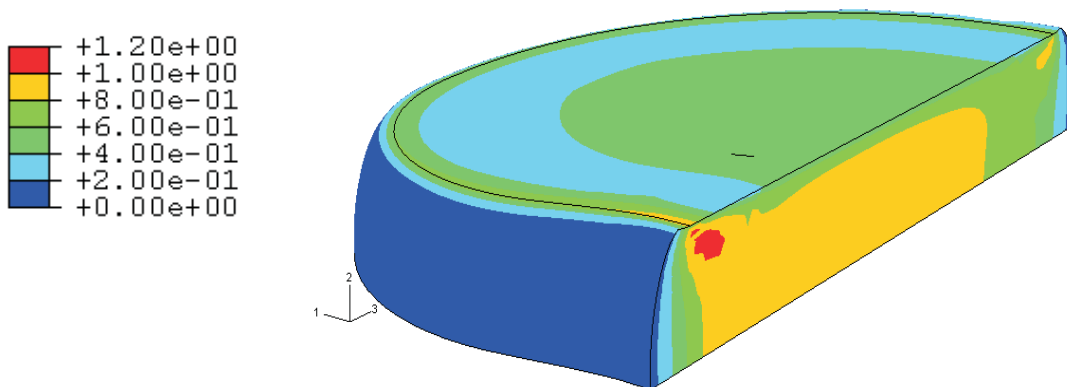


Figure 6.2: Color plot of an axially loaded model with 500N for 360s (step 2 of loading protocol 2) showing the intradiscal pressure. The highest noticeable pressure (ca. 0.8MPa) started from the transversal plane to the top plate on the medial sagittal plane with a concentration in the center of the nucleus. The pressure in the inner annulus neighboring the nucleus also increased.

Results – material law simulations for model adaptation 1-3

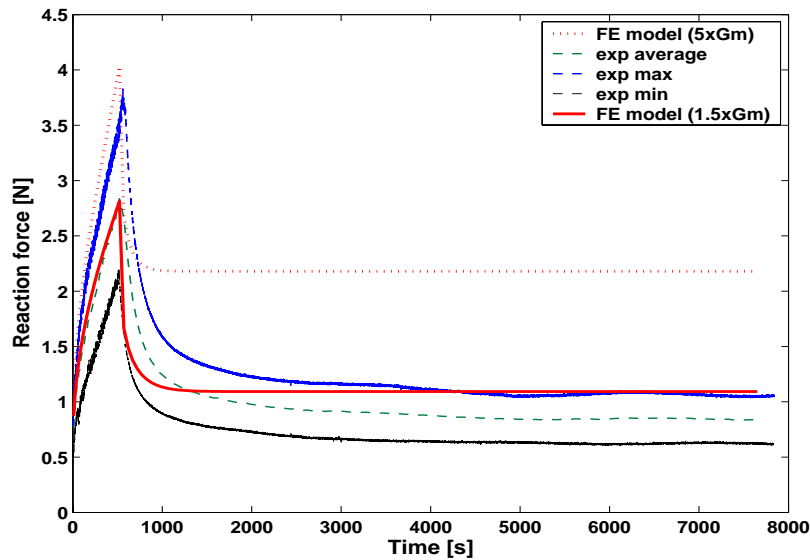


Figure 6.3: Comparison of experimental reaction forces from confined compression experiment [94] and FE model simulations of nucleus samples for model adaptation 1-3.

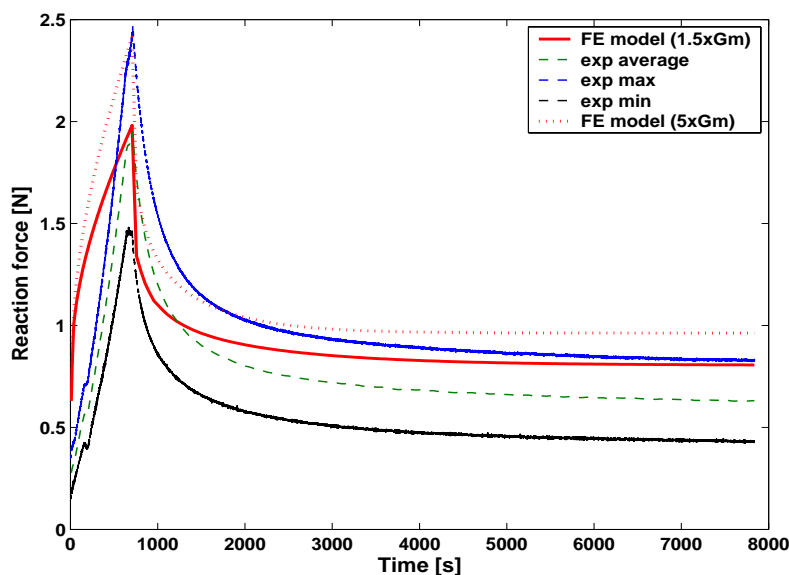


Figure 6.4: Comparison of experimental reaction forces from confined compression experiment [94] and FE model simulations of annulus samples for model adaptation 1-3.

Simulations of the material law fit for the confined compression experiments of nucleus and annulus samples [94] were repeated with the new values for the shear stiffness from model adaptation 3 ($1.5xG_m$) and for model adaptation 1&2 ($5xG_m$). For the confined compression experiment of the nucleus of model adaptation 3 ($1.5xG_m$), the reaction force lay within the experimental range (Figure 6.3). Yet, the descending part of the curve was underestimated. The reaction force during the 2h relaxation of the confined compression of the annulus was also in agreement with the experimental range. However the reaction force was overestimated during the ramp portion of the experiment (Figure 6.4). Because these discrepancies did not allow a full fit, we included the computed reaction force into the minimization procedure only after the strain ramp. As for model adaptation 1&2, figure 6.3 & 6.4 show clearly that the increase of G_m ($5xG_m$) was not in agreement with the experimental data.

6.4 Discussion

To further quantify the overall behavior of the model, the osmoviscoelastic constitutive law and the derived material properties [94] were used in our full 3D FE disc model. Simulations with the above described model adaptations (material property sets and fiber structures, Table 6.2) were performed under different axial loading conditions (Table 6.1). Different loading protocols allowed the comparison of the overall model behavior to two data sets, firstly data from Brinckmann and coworkers [16,17] and secondly data from Heuer et al. [40]. In particular, the computed intradiscal pressures, the radial deformations and the height changes were compared to experimental data.

The base model with only primary fibers and the material parameters taken directly from the earlier material law [94] did not converge to a solution for either loading protocol. Stiffening of the model was necessary. As shown for model adaptation 1 & 2, stiffening of the non-fibrillar component resulted in convergence, but underestimated the relaxation during confined compression (Figure 6.3 & 6.4). Hence, a different model adaptation was necessary. Only by accounting for the secondary fibers (model adaptation 3) the model fitted the experiments of isolated samples as well as measurements done on whole disc.

Heuer and coworkers performed measurements on human L4/L5 disc under 500N compression load and the deformations of the disc were recorded with a laser scanner [40]. Hence, the recorded experimental data were used to compare the overall behavior of the 3D disc model. The model deformations from model adaptation 3 with the second loading protocol were in agreement with the experimental data of Heuer et al. [40]. In detail for step 2, the model bulging on the anterior side lay well within the experimental range (0.46-1.34), also the posterior and lateral deformations lay well within the experimental range measured by Heuer et al. [40]. As for the height reduction (0.87mm) the model behavior was in a reasonable range of the experimental data (1.0 -1.35mm). The creep behavior of the model in step 3 was overestimated in comparison to the mean value given by Heuer et al. [40]. However, the total disc height reduction after step 3 lay well within the experimental range given (1.08-1.57mm).

In a similar study Brinckmann & Horst measured the geometrical changes of the disc under different loading conditions [17]. They found that a reduction of an axial load from 1000N to 300N resulted in a decrease of the radial bulge of about 0.2mm. In comparison the model showed under the same loading conditions a decrease in radial deformation of about 0.34mm on average for model adaptation 3.

The model deformations from model adaptation 3 with the first loading protocol were in reasonable agreement with the experimental data. However, the deformations were overestimated by the model. A possible explanation could be the simplified vertebrae of the disc model. The current 3D mesh does not take into account the convex curvature of the endplate and assumes the vertebra to be infinitely stiff. Hence, the rigid body behavior of the vertebra, which was not realistic [15,49,66], resulted in larger radial deformations of the model than experimentally measured by Brinckmann & Horst [17]. However, Brinckmann et al. [15] stated in a study concerning the endplate deformations that the axial inward bulge of the endplates is of the same order of magnitude as the

mean radial bulge of the disc, thus the choice of vertebral boundary conditions may explain the overestimation of the bulging.

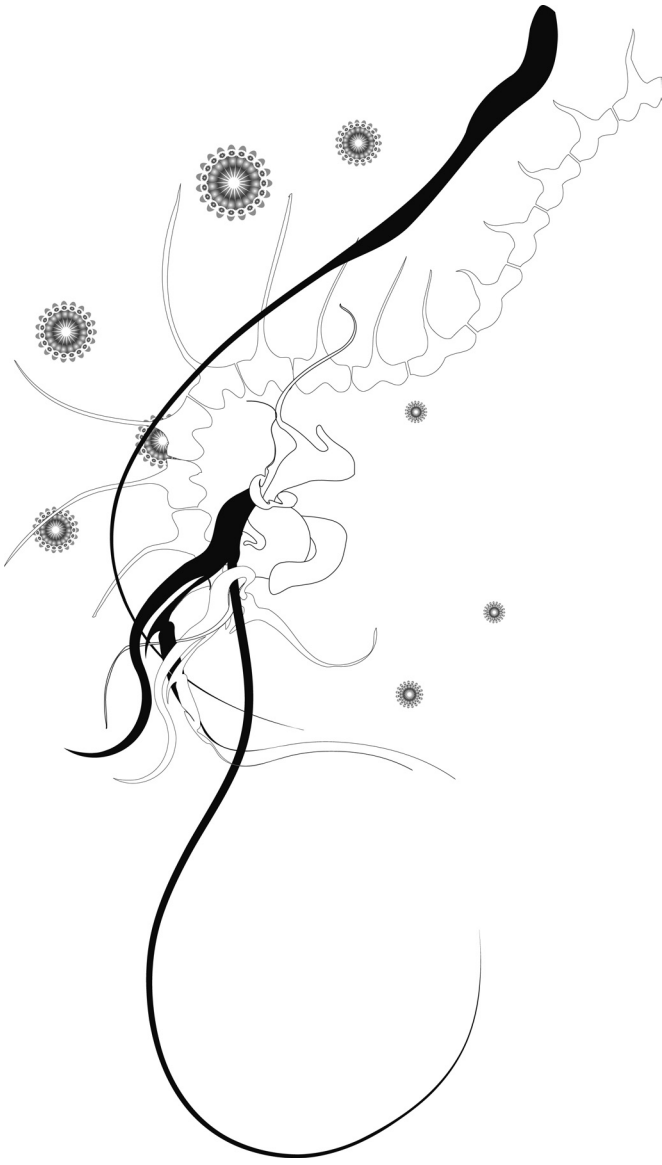
The computed intradiscal pressure value (0.8-1.2MPa) for 1000N was in good agreement with the experimental range (0.93-1.38MPa) of intradiscal pressure measurements for L₄/L₅ human disc by Brinckmann and Grootenboer [16] for model adaptation 3. As for the seconded loading protocol, the computed intradiscal pressure value (0.4-0.8MPa) for 500N axial load was in reasonable agreement to intradiscal measurements (0.36-0.53MPa) of Heuer and coworkers [40].

To summarize, model adaptation 3 accounted for the secondary fiber structure, showed reasonable conformity with the experimental data of whole discs for intradiscal pressure, height change and radial bulging. Moreover, the slight increase of the shear stiffness was also within the experimental range of the earlier material law for isolated samples as presented in chapter 5 [94]. On the other hand, Figure 6.3 & 6.4 clearly indicated that the assumption of higher shear stiffness ($5xG_m$), as done in model adaptation 1 & 2, was not in agreement with the experimental range of the compression data for nucleus and annulus tissue [94].

Thus, only an increase of shear stiffness, as done in model adaptation 1 was not a valid approach to assure convergence of the model. The inclusion of the secondary fiber structure, however, firstly reduced the average radial bulging, while maintaining convergence of the model.

Evaluation of the model with two different data sets, using different measurement techniques and accuracy calls for cautious interpretation of the results. For example, in comparison to the experimental measurements of Brinckmann and Horst [17] the model deformations were still slightly overestimated. This emphasizes the development of a more realistic 3D FE mesh, especially the inclusion of the convex curvature of the endplate and their deformability [15,49,66]. However, good conformity was seen between the experimental bulging data of Heuer et al. [40] and the overall bulging behavior of the model. Conversely, the creep behavior as measured by Heuer et al. [40] was overestimated by the model and therefore, the viscoelastic behavior of the annulus and the fluid flow need to be evaluated more closely, as both are time dependent. Differences in measurement values of the two studies may be explained through differences in their measurement methods. For example, in the study of Brinckmann and Horst [17], a linear potentiometer transducer was used, which touched the disc, to measure changes of the disc contour. However, for the study of Heuer et al. [40], a different approach was applied: deformations of the disc were recorded with a laser scanner. Thus, no contact between sample and measurement device existed.

In conclusion, the base model with only primary fibers and the material parameters taken directly from the earlier material law fit did not converge to a solution for either loading protocol [94]. However, model adaptation 3 converged, while accounting for primary and secondary fibers. Moreover the validation process showed that model adaptation 3 was in reasonable agreement with the experimental data of whole discs from Brinckmann and coworkers [16,17], Heuer et al. [40] and that the material law was also within the experimental range [94] of isolated samples.



Chapter 7

General discussion & conclusion

7.1 Introduction

Multidisciplinary approaches, such as the EURODISC project, focused on analyzing the biochemistry, cell biology and mechanical properties of the disc and relating those findings to genetic studies. As part of this project, the research presented in this thesis has focused on the development of a finite element (FE) model that accounts firstly for the interdependency between swelling and the collagen structure (chapter 3) and secondly, incorporated important experimental findings on intra-extrafibrillar water exchange from other partners of the EURODISC project (chapter 4). Relaxation, confined compression and cyclic loading experiments were conducted to quantify model parameters and were integrated into an osmovoelastoc constitutive law (chapter 5) which in turn was built into the 3D disc model.

In this chapter, the most important findings of the individual studies are summarized and the full 3D osmovoelastoc model in its current state discussed. Also, further improvements and essential applications of the model with regard to disc degeneration are presented.

7.2 Development of a 3D osmovoelastoc FE model of the disc

The intervertebral disc is continuously exposed to mechanical loads –also during resting periods. Even breathing causes measurable changes in intradiscal pressure [79,122]. The disc is subjected to a combination of elastic, viscous and osmotic forces [41,81,82]; the latter being mostly neglected in previous 3D FE models. Also, the interdependency between the swelling tendency of the disc tissue and the tensile stresses in its collagen structure has not been taken into account thus far. Therefore, we developed a FE model that accounts and further defines osmotic forces with regard to the stress distribution within the disc.

Prestressing of fibers due to swelling

This thesis presents a model which computes the prestressing of the collagen fiber structure in the disc from physical principles of osmosis and experimentally quantified material parameters and does not include *a priori* offset stress, as seen in other finite element approaches [50].

Briefly, the model achieved a high intradiscal pressure in the unloaded disc by reducing the hypertonic external salt concentration around the stress-free disc model to a physiological salt concentration. These changes resulted in swelling (step 1), which was constrained by sandwiching the disc between two vertebral bodies. Hence, during constrained swelling - step 1 of all simulations - an increase in intradiscal pressure was observed which led to prestressing of the collagen fibers even before load was applied.

Consequently, neglecting this effect underestimated the stresses and strains in the collagen structure. This has been numerically quantified in the study presented in chapter 3 [95]. The necessity of accounting for this effect was also demonstrated experimentally by Urban and Maroudas [106].

Intrafibrillar water influences stress and pressure estimations in the disc

The model presented in this thesis is the first finite element model of the intervertebral disc that takes into account the intra-extrafibrillar fluid exchange within the disc [93]. An evaluation study was performed, which appraised the importance of including the intrafibrillar water (IFW) content in intradiscal pressure and stress estimations, as the intradiscal pressure profile was clearly influenced by the intrafibrillar water (chapter 4 [93]).

The intrafibrillar water seems especially important in the collagen-rich annulus fibrosus, as up to 30% of the total fluid may be IFW [101]. This amount of IFW influences the swelling and load bearing properties of the disc. Quantification of intra- and extrafibrillar fluid exchange are physiologically relevant, since gene expression of cells and propagation of cracks in the intervertebral disc are affected by changes in extrafibrillar osmolarity [22,82, 97, 129].

Fiber structure - larger collagen fibrils & smaller fibril structures

For simplicity, in our earlier studies the fiber orientation was assumed to be ± 30 degrees to the transversal plane [93, 95] (chapter 3-5). However, the disc collagen fiber structure is a complex combination of larger collagen fibrils, arranged in concentric lamellae with alternating fiber orientation and smaller fibrils structures, e.g. minor collagen, elastin or collagen crosslinks [21,39,70,91,103,131].

Therefore, this description of the 3D-collagen network was supplemented later with a second, more advanced approach (chapter 6). In this second, more complex approach, secondary fibers were incorporated into the full 3D osmoviscoelastic FE disc model to account for smaller fibril structures. The orientation of these secondary fibrils was assumed to be random.

7.2.1 Constitutive law and material parameter determination

FE models have become an important tool to study load distribution in the healthy and degenerated disc. However, model predictions require accurate constitutive laws and material properties. Seeing that the mechanical properties of the intervertebral disc are regulated by both its biochemical composition and fiber-reinforced structure, the constitutive law used to describe this complex tissue requires careful consideration.

Osmoviscoelastic material law for human disc tissue

Tensile tests on human tissue were performed to measure the non-linear viscoelastic behavior of the annulus, and were found to be complimentary to the already existing material data in the literature. The tensile data underlined the viscoelastic behavior of human annulus tissue.

The compressive properties, defined through confined compression experiments of nucleus [54] and annulus tissue (chapter 5) [94], combined with the viscoelastic properties of the annulus were used to adjust the osmoviscoelastic material law.

The presented osmovoelastoc constitutive material law emphasized the inter-dependency of the strong swelling ability of the tissue and the viscoelastic nature of the collagen fibers. This is especially relevant in a study of the load sharing behavior with regard to disc degeneration and regeneration.

Fiber and non-fiber properties of the human disc

The characterization of an anisotropic, nonlinear multi-component material like the intervertebral disc is an iterative procedure. Different aspects of the material law are coming to expression in different experiments. One model should fit all the data of the different experiments. Our approach was purposely not to do a detailed thorough analysis of each experiment type separately, but rather to verify trends of the response of the model to different types of loading. For this reason, we chose not to do just 1 type of experiment, but rather to fit simultaneously for a collection of different experiments. Thus, the big advantage of this approach compared to most others is, that here model parameters could be determined directly using experimental data, while in most cases averaged data from literature is utilized.

While numerous studies have investigated the compressive and tensile properties of the annulus fibrosus, specific conditions required to determine model parameters for an osmovoelastoc model were not available. Hence, the osmovoelastoc material constitutive law and the experimental data (compressive properties: defined through confined compression experiments of nucleus [54] and annulus tissue; viscoelastic properties: defined through own tensile test of annulus samples (chapter 5) [94]) were used to describe the fiber and non-fiber properties of the human disc. The compressive material properties of normal disc tissue were $G_m=1.23\text{MPa}$, $M=1.57$ and $k_o=0.65\times 10^{-16}\text{m}^4/\text{Ns}$; the tensile fiber material parameters were $E_o=77.0\text{MPa}$; $E_e=500\text{MPa}$, and $\eta=1.8\times 10^3\text{MPa}\cdot\text{s}$.

7.2.2 Evaluation of the full 3D osmovoelastoc FE model

The development of a FE model is based on a mathematical approximation method, therefore verifications and validating the numerical model with experimental data is essential. Thus, justifying the authors choices in the development process of the disc model to focus more on the constitutive law rather than accounting for the geometric features through a more detailed FE mesh.

Radial bulging and creep behavior of the model

The osmovoelastoc material law tuned by the experiments on relaxation, tensile cyclic loading and confined compression, was implemented into the 3D model. The bulging and creep behavior of the resulting disc model was confronted with experiments of whole discs from the literature. From this comparison, it appeared that a refinement of the osmovoelastoc model was necessary. Thus, the simplified fiber structure from earlier studies was extended with a more complex secondary fiber structure, which reduced the deformability of the model, while maintaining a correct reproduction of the experiments in confined compression, relaxation and tensile stiffness. Furthermore, to ensure

convergence of the highly non-linear simulations, the shear stiffness of the elastic non-fibrillar matrix was increased slightly, which was still in reasonable agreement with the experimental data (confined compression experiments of chapter 6 [94]).

Evaluation of the model with two different data sets, using different measurement techniques and accuracy calls for cautious interpretation of the results. For example, in comparison to the experimental measurements of Brinckmann and coworkers [16,17] the model deformations were still slightly overestimated. This emphasizes to develop a more realistic 3D FE mesh, especially accounting for the convex curvature of the endplate and their deformability [15,49,66]. However, good conformity was seen between the experimental bulging data of Heuer et al. [40] and the overall bulging behavior of the model. Conversely, the creep behavior as measured by Heuer et al. [40] was overestimated by the model and therefore the viscoelastic behavior of the annulus and the fluid flow need to be evaluated more closely, as both are time dependent. Differences in measurement values of the two studies may be explained through differences in their measurement methods. For example, in the study of Brinckmann and Horst [17] a linear potentiometer transducer was used, which touched the disc, to measure changes of the disc contour. However, for the study of Heuer et al. [40] a different approach was applied, deformations of the disc were recorded with a laser scanner. Thus, no contact between sample and measurement device existed.

7.3 Relevance of this FE model and future adaptations

The close networking within the EURODISC project allowed the incorporation of very recent scientific findings into the development process of the FE model. For example, the relevance of water differentiation (intra- and extrafibrillar water) on osmotic forces was experimentally proven by our co-workers from Israel (Sivan et al. [100]), while the cell sensitivity towards osmolarity was experimentally shown by the group from Ulm (Neidlinger-Wilke et al. [81]). The puzzling epidemiological finding of yet another research group on EURODISC (Videman et al. [115]), that disc degeneration is poorly correlated with mechanical loading of the disc, is another indication that the osmotic events in a disc may be more relevant to the fissuring of the degenerating disc than the external mechanical load [129]. These findings and others directly influenced the objectives and outcome of this thesis.

The key role of osmotic prestressing and intrafibrillar water in the protection of the disc against fissuring has important clinical implications. First, it may explain the limited success associated with ergotherapeutic and physiotherapeutic programs to prevent disc degeneration [19,20,24]. Second, the mechanism of osmotic prestressing and intrafibrillar water may be used directly in the design of the artificial intervertebral disc [46,120].

7.3.1 Applications through collaborations with other ‘disc groups’

It is striking that the development of the present model has fostered a large number of collaborations with many groups throughout the world. This fact is probably directly related to the interest that the model has awaked within the scientific community.

Unpublished data on human intradiscal stress profiles, generously provided by Prof. Donal McNally (University of Nottingham, UK) were very instrumental for the development process of the model and led to an interesting discussion on how the model can be useful to study disc herniation.

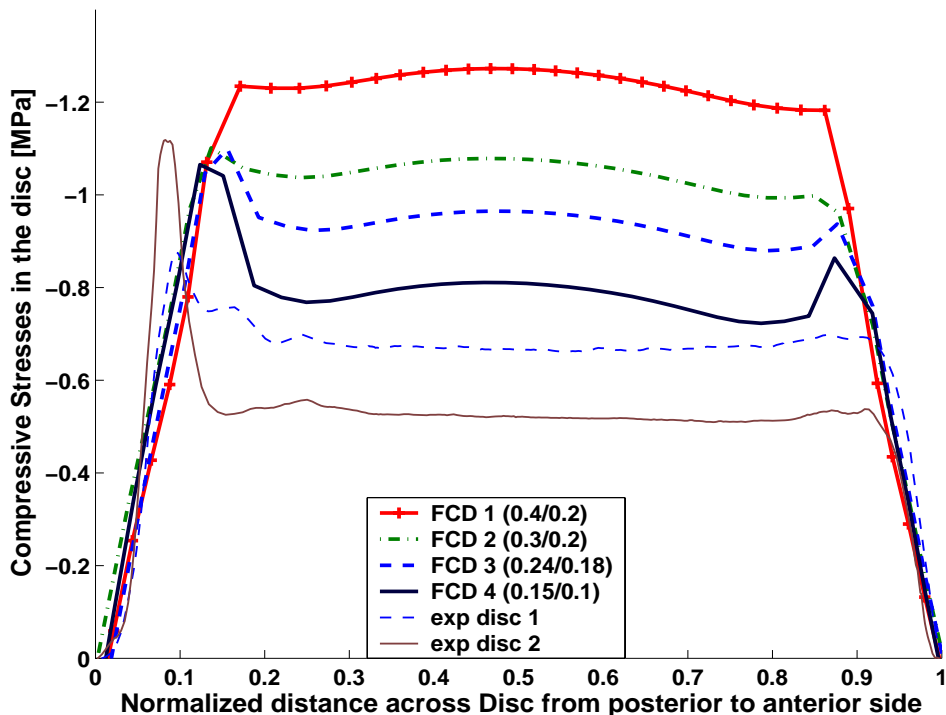


Figure 7.1: Both experimental [74] and numerical data show sharp peaks of axial stress in the posterior annulus and lower peaks in the anterior annulus. The occurrence of the peaks in the numerical simulation depends on the level of FCD in the disc. Decreasing the FCD shows clearly the development of stress peaks in the annulus. A uniform stiffness is seen in the nucleus region.

In an earlier study (chapter 3), we have shown that the computed axial stress profiles reproduced the main features of stress profiles, in particular the characteristic posterior and anterior stress peaks, which were observed experimentally by McNally et al. [74]. The stresses in the nucleus were nearly constant, whereas high peaks of compressive stress were found on the posterior and anterior side of the annulus. The posterior side experienced the highest compressive stress peaks in both the experimental [4,74] as well as the numerical results. These peaks may explain the prevalence of postero-lateral herniation in human intervertebral discs.

Thus, the collaboration with the group of Prof. Donal McNally from the University of Nottingham, allows studying different parameters and their effects on the stress distribution in the disc tissue. In particular, the FE model and the experimental data are used to validate the following objective: ‘is the loss of swelling behavior (fixed charge density) a reason for stress peaks in the annulus’.

Preliminary results of the ongoing sensitivity study [92] suggested that the development of these peaks depends partly on the amount of fixed charges, which influences the swelling capacity of the disc tissue. Hence, an increase of the stress peaks was noticed when the swelling ability of the tissue was reduced (Figure 7.1). This indicates a load shift from nucleus towards the annulus and may explain the prevalence of disc herniation in the age range of 30 to 50 years old, as this is the age when the disc degeneration is particularly fast and when the peaks are most likely to develop.

Since data on material properties of human intervertebral disc tissue are limited, the cooperation with the group of Prof. Dawn Elliott (University of Pennsylvania, USA) was very useful for determining the fiber and non-fiber properties of the model from human disc tissue (chapter 5). During a short visit in her lab, the author was able to perform confined swelling experiments on human annulus fibrosus tissue. Together with their previously published data on confined swelling properties of human nucleus tissue [54] these experimental results of the annulus complemented the already existing data on human nucleus tissue to provide a set of fiber and non-fiber properties for the model. Furthermore, the close collaboration led to the development of an experimental protocol to further define the viscoelastic properties of the annulus. Parts of the results are presented here and were directly used to determine the fiber properties of the model. As an ongoing study, currently more experiments are scheduled to address the remaining objectives (e.g. importance of strain rate dependency for viscoelastic material law). The outcome will amongst others be used to validate the question if further defining the viscoelastic material law influences the creep behavior of the model. Creep deformations (loss of water) are physiological and reversible. However, a distinction between creep deformations and non-reversible deformations occurring from mechanical damage is not easy. Hence, quantification of the creep behavior of the tissue is needed. Furthermore, this is of interest for failure mechanisms studies in biological tissue, as mechanical loading should be applied in a physiologically-reasonable timescale.

Another interesting application was established through the collaboration with the group of Prof. Theo Smit (Free University of Amsterdam, NL), as the osmotic viscoelastic FE model is used to study the flow-related mechanisms of nutrition of the intervertebral disc. In particular, the model helps to improve the understanding and verification of recent *in vitro* results on the diurnal change under loading [111]. Currently, simulations are performed under different axial loading to compute the fluid flow, e.g. out- and inflow, and compare them to experimental measurements [111].

As the swelling properties of the disc are very important to its mechanical behavior, studies of the cellular responses in their natural environment are essential. A recent study of the group of Prof. James Iatridis (University of Vermont, USA) underlined this

important issue, as their paper showed that the mechanical properties of the pericellular matrix differs with the experimental technique used to measure these properties [77]. Another experimental study [49,66] of this group showed the importance of including the endplates into the modeling processes for understanding the load distribution in the disc. Again, the close collaboration with this group allows interesting discussions on how the model can be improved and validated, as experimental data is generously provided and shared. Thus, it is emphasized to develop a more realistic 3D FE mesh, that accounts for the convex curvature of the endplates and their deformability [15, 49,66] .

7.3.2 Future adaptations to improve the model application

Because of the complex tissue structure, especially the interdependency of the swelling and the collagen structure, it is important to include both the organization and reorganization of the collagen fibers, which are directed by the mechanical conditions, into the model [25]. To further study the effect of ageing and degeneration on the bone remodeling process of the adjusting vertebra, the bone remodeling process should be included in the model [90] Experimental data using immunofluorescent co-localization of different types of collagen in the collagen structure can be used as input for this part of modeling. Western-blot analysis can be applied to quantify the contents of the different collagen subtypes as well as their relative susceptibility to degeneration.

The mechanical function of the disc is regulated by its biochemical composition. As the cell density is very low in the intervertebral disc, the environment of the disc cells, responsible for its composition and integrity, is mainly influenced through loading. The degree of change in the extra cellular environment most likely depends on the magnitude, duration and type of loading. Existing data from Jill Urban and her group [96,105] showed that pH level and the O₂ consumption highly influence cellular responses to loading. Because of the avascularity of the disc tissue, these parameters are likely to be disturbed over prolonged periods. Compression tests at different O₂ levels and pH, using indicators for both hypoxia and acidosis at the cellular level will provide input on the effects of changes in those parameters. Therefore, the model could be extended on the microscopic level to account for changes of pH, oxygen as well as glucose turnover.

7.4 Conclusion

To be able to understand the mechanisms of disc degeneration (and regeneration), identifying the pathways by which the cells sense their environment as well as their reaction in order to maintain this environment is paramount. Thus, a multidisciplinary approach is needed to solve the complex questions surrounding degeneration and regeneration processes of the intervertebral disc. The close collaboration of our group with major groups in this field of research creates the possibility in agreeing jointly on a line of experiments and to verify relevant extensions and applications (clinical relevance) of the osmoviscoelastic FE model for the future. Such cooperation is needed since the amount of single studies will be too much for one lab.

Reference

- [1] Acaroglu ER, Iatridis JC, Setton LA, et al. 1995. Degeneration and aging affect the tensile behavior of human lumbar anulus fibrosus. *Spine* 20: 2690-701.
- [2] Adams MA, Bogduk N, Burton AK, Dolan P. *The Biomechanics of Back Pain*. Elsevier Science 2004
- [3] Adams MA, McMillan DW, Green TP, Dolan P. 1996. Sustained loading generates stress concentrations in lumbar intervertebral discs. *Spine* 21: 434-8.
- [4] Adams MA, McNally DS, Dolan P. 1996. 'Stress' distributions inside intervertebral discs. The effects of age and degeneration. *J Bone Joint Surg Br* 78: 965-72.
- [5] Antoniou J, Steffen T, Nelson F, et al. 1996. The human lumbar intervertebral disc - Evidence for changes in the biosynthesis and denaturation of the extracellular matrix with growth, maturation, ageing, and degeneration. *Journal of Clinical Investigation* 98: 996-1003.
- [6] Argoubi M, Shirazi-Adl A. 1996. Poroelastic creep response analysis of a lumbar motion segment in compression. *J Biomech* 29: 1331-9.
- [7] Bass EC, Ashford FA, Segal MR, Lotz JC. 2004. Biaxial testing of human annulus fibrosus and its implications for a constitutive formulation. *Ann Biomed Eng* 32: 1231-42.
- [8] Battie MC, Videman T, Gibbons LE, et al. 1995. Determinants of lumbar disc degeneration - A study relating lifetime exposures and magnetic resonance imaging findings in identical twins. *Spine* 20: 2601-12.
- [9] Battie MC, Videman T, Parent E. 2004. Lumbar disc degeneration: epidemiology and genetic influences. *Spine* 29: 2679-90.
- [10] Best BA, Guilak F, Setton LA, et al. 1994. Compressive mechanical properties of the human anulus fibrosus and their relationship to biochemical composition. *Spine* 19: 212-21.
- [11] Best BA, Guilak F, Weidenbaum M, Mow VC. 1989. Compressive stiffness and permability of intervertebral disc tissue: Variations with radial position, region and level. In *Adv in Bioengineering BED-Vol 15*: 73-4.
- [12] Biot MA. 1972. Theory of finite Deformations of porous solids. *Indiana University Mathematical Journal* 21: 597-620.
- [13] Boos N, Weissbach S, Rohrbach H, et al. 2002. Classification of age-related changes in lumbar intervertebral discs. *Spine* 27: 2631-44.
- [14] Bowden A. Finite Element Modeling of the Spine. In: SM Kurtz, AA Edidin. *Spine Technology Handbook*. Elsevier Academic Press 2006
- [15] Brinckmann P, Frobin W, Hierholzer E, Horst M. 1983. Deformation of the vertebral end-plate under axial loading of the spine. *Spine* 8: 851-6.
- [16] Brinckmann P, Grootenboer H. 1991. Change of disk height, radial disk bulge, and intradiscal pressure from discectomy - an invitro investigation on human lumbar disks. *Spine* 16: 641-6.
- [17] Brinckmann P, Horst M. 1985. The influence of vertebral body fracture, intradiscal injection and partial discectomy on the radial bulge and height of human lumbar disks. *Journal of Biomechanics* 18: 546.

- [18] Buckwalter JA. 1995. Aging and degeneration of the human intervertebral disc. *Spine* 20: 1307-14.
- [19] Burton AK. 1997. Back injury and work loss - Biomechanical and psychosocial influences. *Spine* 22: 2575-80.
- [20] Burton AK, Balague F, Cardon G, et al. 2006. Chapter 2 - European guidelines for prevention in low back pain. *European Spine Journal* 15: S136-S168.
- [21] Cassidy JJ, Hiltner A, Baer E. 1989. Hierarchical structure of the intervertebral disc. *Connect Tissue Res* 23: 75-88.
- [22] Chen J, Baer AE, Paik PY, et al. 2002. Matrix protein gene expression in intervertebral disc cells subjected to altered osmolarity. *Biochem Biophys Res Commun* 293: 932-8.
- [23] Cheung JT, Zhang M, Chow DH. 2003. Biomechanical responses of the intervertebral joints to static and vibrational loading: a finite element study. *Clin Biomech (Bristol , Avon)* 18: 790-9.
- [24] Dishman RK, Oldenburg B, O'Neal H, Shephard RJ. 1998. Worksite physical activity interventions. *American Journal of Preventive Medicine* 15: 344-61.
- [25] Driessen NJ, Bouten CV, Baaijens FP. 2005. A structural constitutive model for collagenous cardiovascular tissues incorporating the angular fiber distribution. *J Biomech Eng* 127: 494-503.
- [26] Drost MR, Willems P, Snijders H, et al. 1995. Confined compression of canine annulus fibrosus under chemical and mechanical loading. *J Biomech Eng* 117: 390-6.
- [27] Ebara S, Iatridis JC, Setton LA, et al. 1996. Tensile properties of nondegenerate human lumbar annulus fibrosus. *Spine* 21: 452-61.
- [28] Edwards WT, Ordway NR, Zheng Y, et al. 2001. Peak stresses observed in the posterior lateral annulus. *Spine* 26: 1753-9.
- [29] Elliott DM, Setton LA. 2000. A linear material model for fiber-induced anisotropy of the annulus fibrosus. *J Biomech Eng* 122: 173-9.
- [30] Elliott DM, Setton LA. 2001. Anisotropic and inhomogeneous tensile behavior of the human annulus fibrosus: experimental measurement and material model predictions. *J Biomech Eng* 123: 256-63.
- [31] Eyre DR, Matsui Y, Wu JJ. 2002. Collagen polymorphisms of the intervertebral disc. *Biochem Soc Trans* 30: 844-8.
- [32] Freemont AJ, Peacock TE, Goupille P, et al. 1997. Nerve ingrowth into diseased intervertebral disc in chronic back pain. *Lancet* 350: 178-81.
- [33] Frijns AJH, Huyghe JM, Janssen JD. 1997. A validation of the quadriphasic mixture theory for intervertebral disc tissue. *International Journal of Engineering Science* 35: 1419-29.
- [34] Galante JO. 1967. Tensile properties of the human lumbar annulus fibrosus. *Acta Orthop Scand Suppl*-91.
- [35] Gruber HE, Hanley EN. 1998. Analysis of aging and degeneration of the human intervertebral disc - Comparison of surgical specimens with normal controls. *Spine* 23: 751-7.

- [36] Gruber HE, Hanley EN, Jr. 2002. Ultrastructure of the human intervertebral disc during aging and degeneration: comparison of surgical and control specimens. *Spine* 27: 798-805.
- [37] Guerin HA, Elliott DM. 2005. The role of fiber-matrix interactions in a nonlinear fiber-reinforced strain energy model of tendon. *J Biomech Eng* 127: 345-50.
- [38] Guerin HA, Elliott DM. 2006. Degeneration affects the fiber reorientation of human annulus fibrosus under tensile load. *J Biomech* 39: 1410-8.
- [39] Guerin HL, Elliott DM. 2006. Quantifying the contributions of structure to annulus fibrosus mechanical function using a nonlinear, anisotropic, hyperelastic model. *J Orthop Res* 25: 508-16.
- [40] Heuer F, Schmitt H, Schmidt H, et al. 2007. Creep associated changes in intervertebral disc bulging obtained with a laser scanning device. *Clin Biomech (Bristol , Avon)* 22: 737-44.
- [41] Houben GB, Drost MR, Huyghe JM, et al. 1997. Nonhomogeneous permeability of canine anulus fibrosus. *Spine* 22: 7-16.
- [42] Huyghe JM, Drost MR. 2004. Uniaxial tensile testing of canine annulus fibrosus tissue under changing salt concentrations. *Biorheology* 41: 255-61.
- [43] Huyghe JM, Houben GB, Drost MR, van Donkelaar CC. 2003. An ionised/non-ionised dual porosity model of intervertebral disc tissue. *Biomech Model Mechanobiol* 2: 3-19.
- [44] Huyghe JM, Janssen JD. 1997. Quadriphasic mechanics of swelling incompressible porous media. *International Journal of Engineering Science* 35: 793-802.
- [45] Huyghe JM, Janssen JD. 1999. Thermo-chemo-electro-mechanical formulation of saturated charged porous solids. *Transport in Porous Media* 34: 129-41.
- [46] Huyghe JM, van Donkelaar CC, Wijlaars MW, et al. Prothesis made of a fiber-reinforced hydrogel, method of manufacturing the prothesis and use thereof. NL: 2005
- [47] Huyghe JM, Wognum S, Baaijens FPT. 2006. Untitled - Point of view - Response. *Spine* 31: E527.
- [48] Iatridis JC, Laible JP, Krag MH. 2003. Influence of fixed charge density magnitude and distribution on the intervertebral disc: applications of a poroelastic and chemical electric (PEACE) model. *J Biomech Eng* 125: 12-24.
- [49] Iatridis JC, MacLean JJ, Owen J.P. 2005. Role of endplates in contributing to compression behaviors of motion segments and intervertebral discs. *ECM VI/SRN I: Spinal Motion Segment: From Basic Science to Clinical Application*. Davos Conference Proceeding
- [50] Iatridis JC, Setton LA, Foster RJ, et al. 1998. Degeneration affects the anisotropic and nonlinear behaviors of human anulus fibrosus in compression. *J Biomech* 31: 535-44.
- [51] Iatridis JC, Weidenbaum M, Setton LA, Mow VC. 1996. Is the nucleus pulposus a solid or a fluid? Mechanical behaviors of the nucleus pulposus of the human intervertebral disc. *Spine* 21: 1174-84.
- [52] Ishihara H, McNally DS, Urban JP, Hall AC. 1996. Effects of hydrostatic pressure on matrix synthesis in different regions of the intervertebral disk. *J Appl Physiol* 80: 839-46.

- [53] Johannessen W, Elliott DM. 2005. Effects of degeneration on the biphasic material properties of human nucleus pulposus in confined compression. *Spine* 30: E724-E729.
- [54] Johannessen W, Elliott DM. 2005. Swelling dominates function of human nucleus pulposus even with degeneration. *Transactions Orthop Res Soc: Vol. 30*, p185, Washington, D.C.. Conference Proceeding
- [55] Johnson WE, Sivan S, Wright KT, et al. 2006. Human intervertebral disc cells promote nerve growth over substrata of human intervertebral disc aggrecan. *Spine* 31: 1187-93.
- [56] Johnson WEB, Caterson B, Eisenstein SM, et al. 2002. Human intervertebral disc aggrecan inhibits nerve growth in vitro. *Arthritis and Rheumatism* 46: 2658-64.
- [57] Johnson WEB, Eisenstein SM, Roberts S. 2001. Cell cluster formation in degenerate lumbar intervertebral discs is associated with increased disc cell proliferation. *Connective Tissue Research* 42: 197-207.
- [58] Johnson WEB, Sivan S, Wright KT, et al. 2006. Human intervertebral disc cells promote nerve growth over substrata of human intervertebral disc aggrecan. *Spine* 31: 1187-93.
- [59] Kasra M, Parnianpour M, Shirazi-Adl A, et al. 2004. Effect of strain rate on tensile properties of sheep disc anulus fibrosus. *Technol Health Care* 12: 333-42.
- [60] KAUPPILA LI. 1995. Ingrowth of blood-vessels in disc degeneration - angiographic and histological studies of cadaveric spines. *Journal of Bone and Joint Surgery-American Volume* 77A: 26-31.
- [61] Kurtz SM, Edidin AA. *Spine Technology Handbook*. 1 ed. Elsevier Academic Press 2006
- [62] Lai WM, Hou JS, Mow VC. 1991. A triphasic theory for the swelling and deformation behaviors of articular-cartilage. *Journal of Biomechanical Engineering-Transactions of the Asme* 113: 245-58.
- [63] Lanir Y. 1987. Biorheology and fluid flux in swelling tissues, II. Analysis of unconfined compressive response of transversely isotropic cartilage disc. *Biorheology* 24: 189-205.
- [64] Lanir Y. 1987. Biorheology and fluid flux in swelling tissues. I. Bicomponent theory for small deformations, including concentration effects. *Biorheology* 24: 173-87.
- [65] Lee KK, Teo EC. 2004. Poroelastic analysis of lumbar spinal stability in combined compression and anterior shear. *J Spinal Disord Tech* 17: 429-38.
- [66] MacLean JJ, Owen JP, Iatridis JC. 2007. Role of endplates in contributing to compression behaviors of motion segments and intervertebral discs. *Journal of Biomechanics* 40: 55-63.
- [67] Marchand F, Ahmed AM. 1990. Investigation of the laminate structure of lumbar disc anulus fibrosus. *Spine* 15: 402-10.
- [68] Maroudas A, Bannan C. 1981. Measurement of swelling pressure in cartilage and comparison with the osmotic pressure of constituent proteoglycans. *Biorheology* 18: 619-32.
- [69] Maroudas A, Wachtel E, Grushko G, et al. 1991. The effect of osmotic and mechanical pressures on water partitioning in articular cartilage. *Biochim Biophys Acta* 1073: 285-94.

- [70] Matcher SJ, Winlove CP, Gangnus SV. 2004. The collagen structure of bovine intervertebral disc studied using polarization-sensitive optical coherence tomography 131. *Phys Med Biol* 49: 1295-306.
- [71] McNally DS, Adams MA. 1992. Internal intervertebral-disk mechanics as revealed by stress profilometry. *Spine* 17: 66-73.
- [72] McNally DS, Adams MA, Goodship AE. 1992. Development and validation of a new transducer for intradiscal pressure measurement. *Journal of Biomedical Engineering* 14: 495-8.
- [73] McNally DS, Adams MA, Goodship AE. 1993. Can intervertebral disc prolapse be predicted by disc mechanics? *Spine* 18: 1525-30.
- [74] McNally DS, McKinlay K. 2005. Personal communication.
- [75] McNally DS, Shackelford IM, Goodship AE, Mulholland RC. 1996. In vivo stress measurement can predict pain on discography. *Spine* 21: 2580-7.
- [76] Melrose J, Roberts S, Smith S, et al. 2002. Increased nerve and blood vessel ingrowth associated with proteoglycan depletion in an ovine anular lesion model of experimental disc degeneration. *Spine* 27: 1278-85.
- [77] Michalek AJ, Iatridis JC. 2006. A numerical study to determine pericellular matrix modulus and evaluate its effects on the micromechanical environment of chondrocytes. *J Biomech*
- [78] Mow VC, Kuei SC, Lai WM, Armstrong CG. 1980. Biphasic creep and stress relaxation of articular cartilage in compression? Theory and experiments. *J Biomech Eng* 102: 73-84.
- [79] Nachemson A., Morris J. 1963. Lumbar discometry. Lumbar intradiscal pressure measurements in vivo. *Lancet* 1: 1140-2.
- [80] Natarajan RN, Williams JR, Andersson GB. 2004. Recent advances in analytical modeling of lumbar disc degeneration. *Spine* 29: 2733-41.
- [81] Neidlinger-Wilke C., Wuertz K., Claes L, Urban JP. Osmolarity influences disc cell gene expressions in response to mechanical stimulation and at unloaded culture conditions. 14 ed. *European Spine Journal* 2005
- [82] Neidlinger-Wilke C, Wurtz K, Urban JP, et al. 2006. Regulation of gene expression in intervertebral disc cells by low and high hydrostatic pressure. *Eur Spine J* 15 Suppl 15: 372-8.
- [83] Op De Beeck R., Hermans D. Research on work-related low back disorders. European Agency for Safety and Health at work 2000
- [84] Perie D, Iatridis JC, Demers CN, et al. 2005. Assessment of compressive modulus, hydraulic permeability and matrix content of trypsin-treated nucleus pulposus using quantitative MRI. *J Biomech* 38: 2164-74.
- [85] Pollintine P, Dolan P, Tobias JH, Adams MA. 2004. Intervertebral disc degeneration can lead to "stress-shielding" of the anterior vertebral body - A cause of osteoporotic vertebral fracture? *Spine* 29: 774-82.
- [86] Pollintine P, Tobias JH, McNally DS, et al. 2002. Intervertebral disc degeneration increases load-bearing by the neural arch and reduces BMD in the anterior vertebral body. *Journal of Bone and Mineral Research* 17: S178.

- [87] Roberts S, Caterson B, Menage J, et al. 2000. Matrix metalloproteinases and aggrecanase - Their role in disorders of the human intervertebral disc. *Spine* 25: 3005-13.
- [88] Roberts S, Evans H, Trivedi J, Menage J. 2006. Histology and pathology of the human intervertebral disc. *Journal of Bone and Joint Surgery-American Volume* 88A: 10-4.
- [89] Roberts S, Urban JPG, Evans H, Eisenstein SM. 1996. Transport properties of the human cartilage endplate in relation to its composition and calcification. *Spine* 21: 415-20.
- [90] Ruimerman R, Hilbers P, van Rietbergen B, Huiskes R. 2005. A theoretical framework for strain-related trabecular bone maintenance and adaptation. *J Biomech* 38: 931-41.
- [91] Schollmeier G, Lahr-Eigen R, Lewandrowski KU. 2000. Observations on fiber-forming collagens in the annulus fibrosus. *Spine* 25: 2736-41.
- [92] Schroeder Y., McNally DS, McKinlay K, et al. 2005. Comparison of experimental and numerical stress profiles in disc show similar stress peaks; why? ECM VI/SRN I: Spinal Motion Segment: From Basic Science to Clinical Application. Davos Conference Proceeding
- [93] Schroeder Y., Sivan S, Wilson W, et al. 2007. Are disc pressure, stress and osmolarity affected by intra and extrafibrillar fluid exchange? *J Orthop Res* 10:1317-24
- [94] Schroeder Y, Elliott DM, Wilson W, et al. 2007. Experimental and model determination of human intervertebral disc osmotic viscoelasticity. *J Orthop Res* (accepted):
- [95] Schroeder Y, Wilson W, Huyghe JM, Baaijens FP. 2006. Osmotic viscoelastic finite element model of the intervertebral disc. *Eur Spine J* 15 Suppl 15: 361-71.
- [96] Selard E, Shirazi-Adl A, Urban JP. 2003. Finite element study of nutrient diffusion in the human intervertebral disc. *Spine* 28: 1945-53.
- [97] Setton LA, Chen J. 2006. Mechanobiology of the intervertebral disc and relevance to disc degeneration. *J Bone Joint Surg Am* 88 Suppl 2: 52-7.
- [98] Silver FH, Ebrahimi A, Snowhill PB. 2002. Viscoelastic properties of self-assembled type I collagen fibers: molecular basis of elastic and viscous behaviors. *Connect Tissue Res* 43: 569-80.
- [99] Simon BR, Wu JS, Carlton MW, et al. 1985. Poroelastic dynamic structural models of rhesus spinal motion segments. *Spine* 10: 494-507.
- [100] Sivan S, Merkher Y, Wachtel E, et al. 2006. Correlation of swelling pressure and intrafibrillar water in young and aged human intervertebral discs. *J Orthop Res* 24: 1292-8.
- [101] Sivan S, Neidlinger-Wilke C, Wurtz K, et al. 2006. Diurnal fluid expression and activity of intervertebral disc cells. *Biorheology* 43: 283-91.
- [102] Skaggs DL, Weidenbaum M, Iatridis JC, et al. 1994. Regional variation in tensile properties and biochemical composition of the human lumbar annulus fibrosus. *Spine* 19: 1310-9.

- [103] Smith LJ, Fazzalari NL. 2006. Regional variations in the density and arrangement of elastic fibres in the annulus fibrosus of the human lumbar disc. *Journal of Anatomy* 209: 359-67.
- [104] Sun DD, Leong KW. 2004. A nonlinear hyperelastic mixture theory model for anisotropy, transport, and swelling of annulus fibrosus. *Ann Biomed Eng* 32: 92-102.
- [105] Urban JP. 2002. The role of the physicochemical environment in determining disc cell behaviour. *Biochem Soc Trans* 30: 858-64.
- [106] Urban JP, Maroudas A. 1981. Swelling of the intervertebral disc in vitro. *Connect Tissue Res* 9: 1-10.
- [107] Urban JP, Maroudas A, Bayliss MT, Dillon J. 1979. Swelling pressures of proteoglycans at the concentrations found in cartilaginous tissues. *Biorheology* 16: 447-64.
- [108] Urban JP, McMullin JF. 1985. Swelling pressure of the intervertebral disc: influence of proteoglycan and collagen contents. *Biorheology* 22: 145-57.
- [109] Urban JP, McMullin JF. 1988. Swelling pressure of the lumbar intervertebral discs: influence of age, spinal level, composition, and degeneration. *Spine* 13: 179-87.
- [110] Urban JP, Roberts S. 2003. Degeneration of the intervertebral disc. *Arthritis Res Ther* 5: 120-30.
- [111] van der Veen AJ, Mullender M, Smit TH, et al. 2005. Flow-related mechanics of the intervertebral disc: the validity of an in vitro model. *Spine* 30: E534-E539.
- [112] van der Voet. 1997. A comparison of finite element codes for the solution of biphasic poroelastic problems. *Proc Inst Mech Eng [H]* 211: 209-11.
- [113] van Loon R, Huyghe JM, Wijlaars MW, Baaijens FPT. 2003. 3D FE implementation of an incompressible quadriphasic mixture model. *International Journal for Numerical Methods in Engineering* 57: 1243-58.
- [114] Videman T, Battie MC. 1999. Spine update - The influence of occupation on lumbar degeneration. *Spine* 24: 1164-8.
- [115] Videman T, Nurminen M. 2004. The occurrence of anular tears and their relation to lifetime back pain history: A cadaveric study using barium sulfate discography. *Spine* 29: 2668-76.
- [116] Wachtel E, Maroudas A. 1998. The effects of pH and ionic strength on intrafibrillar hydration in articular cartilage. *Biochim Biophys Acta* 1381: 37-48.
- [117] Wagner DR, Lotz JC. 2004. Theoretical model and experimental results for the nonlinear elastic behavior of human annulus fibrosus. *J Orthop Res* 22: 901-9.
- [118] Wang JL, Parnianpour M, Shirazi-Adl A, Engin AE. 2000. Viscoelastic finite-element analysis of a lumbar motion segment in combined compression and sagittal flexion. Effect of loading rate. *Spine* 25: 310-8.
- [119] Wang JL, Parnianpour M, Shirazi-Adl A, Engin AE. 1997. Failure criterion of collagen fiber: Viscoelastic behavior simulated by using load control data. *Theoretical and Applied Fracture Mechanics* 27: 1-12.
- [120] Wijlaars MW, Huyghe JM, van Donkelaar CC. Tissue substitute material. NL: 2005
- [121] Wilke H, Neef P, Hinz B, et al. 2001. Intradiscal pressure together with anthropometric data--a data set for the validation of models. *Clin Biomech (Bristol, Avon)* 16 Suppl 1: S111-S126.

- [122] Wilke HJ, Neef P, Caimi M, et al. 1999. New in vivo measurements of pressures in the intervertebral disc in daily life. *Spine* 24: 755-62.
- [123] Wilson W, Huyghe JM, van Donkelaar CC. 2006. A composition-based cartilage model for the assessment of compositional changes during cartilage damage and adaptation. *Osteoarthritis Cartilage* 14: 554-60.
- [124] Wilson W, Huyghe JM, van Donkelaar CC. 2007. Depth-dependent Compressive Equilibrium Properties of Articular Cartilage Explained by its Composition. *Biomech Model Mechanobiol* 6: 43-53.
- [125] Wilson W, van Donkelaar CC, Huyghe JM. 2005. A comparison between mechano-electrochemical and biphasic swelling theories for soft hydrated tissues. *J Biomech Eng* 127: 158-65.
- [126] Wilson W, van Donkelaar CC, van Rietbergen B, Huiskes R. 2005. A fibril-reinforced poroviscoelastic swelling model for articular cartilage. *J Biomech* 38: 1195-204.
- [127] Wilson W, van Donkelaar CC, van Rietbergen B, et al. 2004. Stresses in the local collagen network of articular cartilage: a poroviscoelastic fibril-reinforced finite element study. *J Biomech* 37: 357-66.
- [128] Wilson W, van Donkelaar CC, van Rietbergen B, et al. 2005. Erratum to "Stress in the local collagen network of articular cartilage: a poroviscoelastic fibril-reinforced finite element study" and "A fibril-reinforced poroviscoelastic swelling model for articular cartilage". *J Biomech* 38: 2138-40.
- [129] Wognum S, Huyghe JM, Baaijens FP. 2006. Influence of osmotic pressure changes on the opening of existing cracks in 2 intervertebral disc models. *Spine* 31: 1783-8.
- [130] Wu JS, Chen JH. 1996. Clarification of the mechanical behaviour of spinal motion segments through a three-dimensional poroelastic mixed finite element model. *Med Eng Phys* 18: 215-24.
- [131] Yu J, Fairbank JC, Roberts S, Urban JP. 2005. The elastic fiber network of the annulus fibrosus of the normal and scoliotic human intervertebral disc. *Spine* 30: 1815-20.

Appendix:

Abaqus has a biphasic model of the form:

$$\text{Momentum balance: } \vec{\nabla} * \boldsymbol{\sigma}_e - \vec{\nabla} p = 0$$

$$\text{Mass balance: } \vec{\nabla} * \dot{\boldsymbol{u}} + \vec{\nabla} \vec{q} = 0$$

$$\text{Darcy's law } \vec{q} = -k \vec{\nabla} p$$

With Dirichlet boundary conditions: $[u] = 0$ and $[p] = 0$,

Here σ_e is the effective stress, p the fluid pressure, \vec{q} the fluid flux, k the permeability and u the displacements.

The swelling behavior through the Donnan osmotic theory was included into the biphasic theory as follows:

$$\text{Mass balance: } \vec{\nabla} * \dot{\boldsymbol{u}}_s - \vec{\nabla} * k \vec{\nabla} (p - \Delta\pi) = 0$$

$$\text{substitution } \vec{\nabla} * \left(\boldsymbol{\sigma}_{non-fibrillar} + \rho_c \sum_{\text{all fibers } i} \sigma_f^i \vec{e}_f^i \vec{e}_f^i \right) - \vec{\nabla} (\mu^f + \Delta\pi) = 0$$

$$\vec{\nabla} * \dot{\boldsymbol{u}}_s - \vec{\nabla} * k \vec{\nabla} \mu^f = 0$$

$$\mu^f = (p - \Delta\pi)$$

Here μ^f is the chemical potential and $\Delta\pi$ is the osmotic pressure given by equation (4) with Dirichlet boundary conditions: $[u] = 0$ and $[\mu^f] = 0$

Acknowledgment

First of all I am very grateful to my supervisors at the Department of Bioengineering, Eindhoven University of Technology. Especially I would like to thank Jacques and Wouter for their endless support and discussions on how to enjoy the challenge and tolerate the ambiguity of research, as well as for making me feel at home in Eindhoven.

My project has been part of EURODISC, a large European project. In Eindhoven the focus has been mostly on the technical part. I am grateful to all the members of the EURODISC project, which assured the balance of mechanics, clinical and biological aspect over the past four years. Thank you, Jill, Sally, Conny, Dimitries, Tapio, Sarit & Alice for sharing your profound knowledge on the intervertebral disc, for giving me the opportunity to learn about disc biology and introducing me to the disc-research community. Furthermore, your guidance and support did not end when the project did. That I am very grateful for, especially during the last month while finishing this thesis. Your guidance, both scientifically and personally, throughout our project meetings and conferences helped me integrate into the scientific community and has led to cooperation with other disc groups. The cooperation with Prof. Donal McNally's group from the University of Nottingham is a good example for this.

Donal, thank you for always taking the time to share your view on disc biomechanics and FE models. Many times, this helped me to put my model problems in the right perspective. Also personally, thank you for making me feel like one of your students, both when visiting Nottingham and on conferences. I haven't forgotten the joint paper yet... Sarrawat, as part of Donal's group I am also very thankful for your support and especially for taking the time to proof read this thesis. I am looking forward to future meetings with you all, both scientifically and personally.

Likewise, I am grateful to Prof. Dawn Elliott and her group from the University of Pennsylvania. Thank you for welcoming me in your lab. During my short stay I learned a lot regarding tissue preparation and experimental disc biomechanics. Again, I am very grateful for your support during the experiments and our joint publication. I really enjoy our scientific discussions, but also the personal discussion regarding my future.

Furthermore, I want to thank Prof. James Iatridis for his support and the interesting discussion on modeling of the disc. Meetings with your group and the openness in sharing data to improve the model are gratefully acknowledged.

The kindness and support I received during the past years contributed largely to completing this thesis and I would like to express my sincere gratitude, to all of you.

*In deinem Leben begenest du vielen Menschen. Aber nur wahre Freunde hinterlassen
Spuren in deinem Herzen.*

Danke, Ulli & Markus, Anne & Santiago. Karin, nochmals danke für das tolle Cover-Design. Katja, Corrine & Emil, Nollaig, Christian, Katharina, Andrea & Reinhard Ihr habt alle ganz besonders dazu beigetragen das ich mich auch in Eindhoven zu Hause fühle. I am very grateful for the support and help of my colleagues, most of all Wouter, Hanna, Famke, Reinout, Peter and Pieter, who also became close friends.

Die letzten Jahre waren ein auf und ab für uns alle, jedoch konnte ich immer auf Eure Liebe und Unterstützung zählen. Danke Mutti und Tante Lilo. Dirk, ich freue mich auf die gemeinsame Zeit mit Dir.

Namaste,

Yvonne Schröder
Eindhoven, November 2007

What is important is to keep learning, to enjoy challenge, and to tolerate ambiguity. In the end there are no certain answers.

Martina Horner

Curriculum Vitae

Yvonne Schroeder was born on May 28, 1977 in Rostock, which is located on the Baltic coast in northeast Germany. After completing her secondary education, Yvonne spent a year abroad in the United States of America to improve her English. On her return to Germany, Yvonne read mechanical engineering at the University of Rostock and graduated in 2003 with a Dipl. Ing. degree (internationally equivalent to a Masters of Science). With a Masters thesis on '*Finite Element Analysis on the Origin of Vertebra Compression Fractures*', Yvonne continued her interest in spinal research and in 2004, undertook a Ph.D. to develop a three-dimensional finite element model of the intervertebral disc to investigate disc degeneration at the Technical University of Eindhoven, in the Netherlands. Since completing her academic studies, Yvonne is currently working in the Orthopaedic Biomechanics department at the TU Eindhoven researching the swelling of elastomeres in collaboration with industry.

Research Interest:

Spine biomechanics, Soft tissue Biomechanics, Finite element modeling, Spinal burst fractures, Intervertebral Disc

Education

Research Fellow

Technical University of Eindhoven,
Eindhoven, Netherlands

Oct 2007 - Oct 2008

Ph.D. in Biomedical Engineering

Technical University of Eindhoven,
Eindhoven, Netherlands

Oct 2003 - Jan 2008

Dipl. Ing. Degree in Mechanical Engineering

(Equivalent to Master of Science)

University of Rostock,
Rostock, Germany

Oct 1996 - Jul 2003
